DOKUZ EYLÜL UNIVERSITY
GRADUATE SCHOOL OF NATURAL AND APPLIED SCIENCES

STABILITY OF SUBMARINE SLOPES

by
Kubilay BAYKAL

October, 2013
İZMİR

STABILITY OF SUBMARINE SLOPES

A Thesis Submitted to the
Graduate School of Natural and Applied Sciences of Dokuz Eylul University
In Partial Fulfillment of the Requirements for the Degree of Master of Science
in Geological Engineering, Applied Geology Program

by
Kubilay BAYKAL

October, 2013
İZMİR

M.Sc THESIS EXAMINATION RESULT FORM

We have read the thesis entitled **"STABILITY OF SUBMARINE SLOPES"** completed by **KUBILAY BAYKAL** under supervision of **PROF. DR. NECDET TÜRK** and we certify that in our opinion it is fully adequate, in scope and in quality, as a thesis for the degree of Master of Science.

Prof. Dr. Necdet TÜRK

Supervisor

Prof. Dr. M. Yalçın Koca

(Jury Member)

Yrd.Doç.Dr. Şenol ÖZYALIN

(Jury Member)

Prof. Dr. Ayşe OKUR

Director

Graduate School of Natural and Applied Sciences

ACKNOWLEDGMENTS

I would like to thank to my supervisor Prof. Dr. Necdet TÜRK, for his help, guidance, criticism and encouragement thought the course of this work.

I would also like to thank to Bora SONUVAR from TRAMOLA INTERNATIONAL APPLIED MARINE RESEARCH LTD., for his help, with suggestions and survey support that he has provided me during the research.

I am especially very grateful to my family for their support.

Kubilay BAYKAL

STABILITY OF SUBMARINE SLOPES

ABSTRACT

In this study, the hydrographic, geological and geotechnical works carried out for "İzmir Bay-Alsancak Port Navigation Channel" and the future dredging works within the scope of İzmir Bay and Alsancak Port Rehabilitation Project are discussed. Within the scope of this study, the surface soil samples (K1-12) are taken from twelve different locations in the study areas on the navigation channel. The geotechnical and geological properties of the soil samples are determined. Hydrographical and oceanographic studies are carried out to reveal the actual 2D and 3D bathymetries of study areas. Furthermore, the inclination and vectors maps are generated. Based on the acquired soil properties and the bathymetric data, slope stability analyses have been performed for the two cross-sectional profiles along the navigation channel, one of which is that the first line and the second one is at the second line. Slide v.6.0 software is used for the slope analysis. The slope stability analyses are carried out for the different seismic loadings (0.12 g and 0.23 g), and the channel depths of 17 m. The seismic accelerations used in the analyses are calculated considering the earthquakes occurred in the past close to study area. In the results of this study, the stability conditions of slopes of navigation channel are demonstrated.

Keywords: Slope, stability, seismic, navigation channel, bathymetry

DENİZALTI ŞEVLERİNİN STABİLİTESİ

ÖZ

Bu çalışma; "İzmir Körfezi-Alsancak Limanı Yaklaşım Kanalı" üzerinde yapılmış olan hidrografik, jeolojik ve jeoteknik çalışmalara ve İzmir Alsancak Limanı İkinci Tevsii projesi kapsamında yapılacak tarama faaliyetlerine değinmektedir. Bu çalışma kapsamında, yaklaşım kanalı üzerinde bulunan çalışma alanları içerisinde 12 farklı noktadan yüzey zemin örnekleri (K1-12) alınmıştır. Alınan zemin örneklerinin jeoteknik ve jeolojik özellikleri belirlenmiştir. Çalışma alanın güncel iki boyutlu ve üç boyutlu batimetri haritalarının ortaya çıkarılması için Hidrografi ve oşinografi çalışmaları yapılmıştır. Ayrıca, eğim ve vektör haritaları da hazırlanmıştır. Elde edilen zemin özellikleri ve batimetrik verilere dayanarak, şev stabilitesi için yaklaşım kanalı boyunca birinci ve ikinci hattan iki adet enine kesit alınmıştır. Şev analizleri için Slide v.6.0 kullanılmıştır. Şev stabilite analizleri farklı sismik yükler (0.12 g ve 0.23 g) ve 17 m kanal derinliği için gerçekleştirilmiştir. Çalışma alanına yakın, geçmişte meydana gelen depremleri göz önüne alarak sismik ivme değerleri hesaplanmıştır. Bu çalışmaların sonucunda, yaklaşım kanalının şevlerinin stabilite koşulları ortaya konmuştur.

Anahtar kelimeler: Şev, stabilite, sismik, yaklaşım kanalı, batimetri

CONTENTS

Page

LIST OF FIGURES

Page

LIST OF TABLES

Page

CHAPTER ONE
INTRODUCTION

1.1 General Considerations

In accordance with the growth in world economy, the demand in marine transportation has been increasing every day. This has been followed by other developments such as increasing demand in container transport, usage of bigger container ships, construction of mega ports, and enhancement of existing ports' capacities.

The rapid increase in container transport is also observed in the ports of our country. Especially, one of the most important international port of our country is Alsancak Port which controls approximately 15-20% of container transport in Turkey.

The shallowest zone of Alsancak navigation channel was identified to be 8.50 by Institute of Marine Sciences and Technology, Dokuz Eylül University [IMST] (1985). This shallowness has been deepened to 10.50 m by means of continuous dredging works from 1985 to the present day. However, the depths in this shallowness do no longer meet today's standard. Such that entries of high-draft vessels to the port are limited because of this shallowness. With the present condition, Alsancak port is not able reply adequately to today's increasing volume of container traffic. General Directorate of State Railways of Republic of Turkey [GDSRRT] has planned to increase the capacity of Alsancak port, by dredging of the existing navigation channel to resolve this problem. Within the scope of this planning, several preliminary studies have been carried out for the navigation channel and the circulation channel by various institutions since 2012 in İzmir bay.

In this study, detailed information about the geotechnical, hydrographic and oceanographic properties of navigation channel is obtained through literature survey, laboratory and field experiments. Furthermore, stability of the side-slopes of the navigation channel which will be generated by the planned dredging works in

Alsancak port is investigated using the information gathered throughout the present study.

The outline of the thesis is as follows, the general descriptions of İzmir-Alsancak port and navigation channel, and the aim of this study is emphasized in this chapter. *The second chapter* presents literature survey about the İzmir bay and Alsancak port-navigation channel. *The third chapter* presents overall information about geological, geotechnical, hydrographic and oceanographic properties of Alsancak navigation channel. *The fourth chapter* summarizes the fundamental causes of seafloor landslides and the trigger mechanisms of the landslides. Also the potential of seafloor landslides for İzmir bay is evaluated in terms of triggering mechanisms. *The fifth chapter* reviews slope stability analysis methods and summarizes the disadvantages and advantages of these methods in slope stability analyses. *The sixth chapter* presents laboratory and field experiments and the results of these studies. *The seventh chapter* presents the results of slope stability analysis carried out with Slide v6.0 (Rockscience) software. The obtained results of these analyses are compared. In the last chapter, the present study is summarized, the appropriate conditions for stability of navigation channel are discussed, and recommended future research agenda for development of the channel is given.

1.2 Study Area

İzmir bay is the biggest bay of Mediterranean and Aegean Seas in the most western coast of Turkey. It has approximately a total area of 200 km^2 and 11.5 billion m^3 water capacity. İzmir bay is investigated geographically in four parts: outer-2, outer-1, middle, and inner bay (Figure 1.1). Navigation channel is located in the inner parts of the İzmir bay.

İzmir-Alsancak navigation channel is a 12870 m long straight line of running along SW-NE direction in İzmir bay. Alsancak navigation channel consists of four parts: first, second, third and turning basin. The approximate lengths of these three regions are respectively as 4420 m., 5500 m., 2955 m., and the diameter of turning basin is 580 meter (see Figure 1.2). The actual coordinates of channel is given in Table 1.1.

Table 1.1 The actual coordinates of Izmir Alsancak navigation channel

Corner Points	Geographic Coordinates (UTM Zone 35N)		Corner Points	Geographic Coordinates (UTM Zone 35N)	
1	38°25'14.88"N	27° 0'52.15"E	**11**	38°26'58.67"N	27° 8'15.63"E
2	38°25'20.67"N	27° 1'24.02"E	**12**	38°26'58.89"N	27° 8'6.85"E
3	38°25'21.38"N	27° 1'29.42"E	**13**	38°26'59.78"N	27° 8'1.67"E
4	38°25'21.17"N	27° 1'33.85"E	**14**	38°25'24.77"N	27° 1'51.46"E
5	38°25'21.20"N	27° 1'38.45"E	**15**	38°25'23.70"N	27° 1'37.39"E
6	38°25'22.31"N	27° 1'52.72"E	**16**	38°25'23.68"N	27° 1'32.93"E
7	38°26'53.81"N	27° 8'3.55"E	**17**	38°25'23.82"N	27° 1'28.37"E
8	38°26'53.10"N	27° 8'17.82"E	**18**	38°25'22.62"N	27° 1'23.56"E
9	38°26'54.33"N	27° 8'35.69"E	**19**	38°25'17.33"N	27° 0'51.32"E
10	38°26'59.57"N	27° 8'33.77"E	**-**	-	-

Dredging activities are planned in the first and third regions, and the turning basin of navigation channel. The first and third regions are risky areas where the dredging activities are planned.

Figure 1.1 The parts of İzmir bay

In this study, the engineering properties of soil are investigated from the point of view of slope stability of navigation channel in the first and third regions (see Figure 1.3).

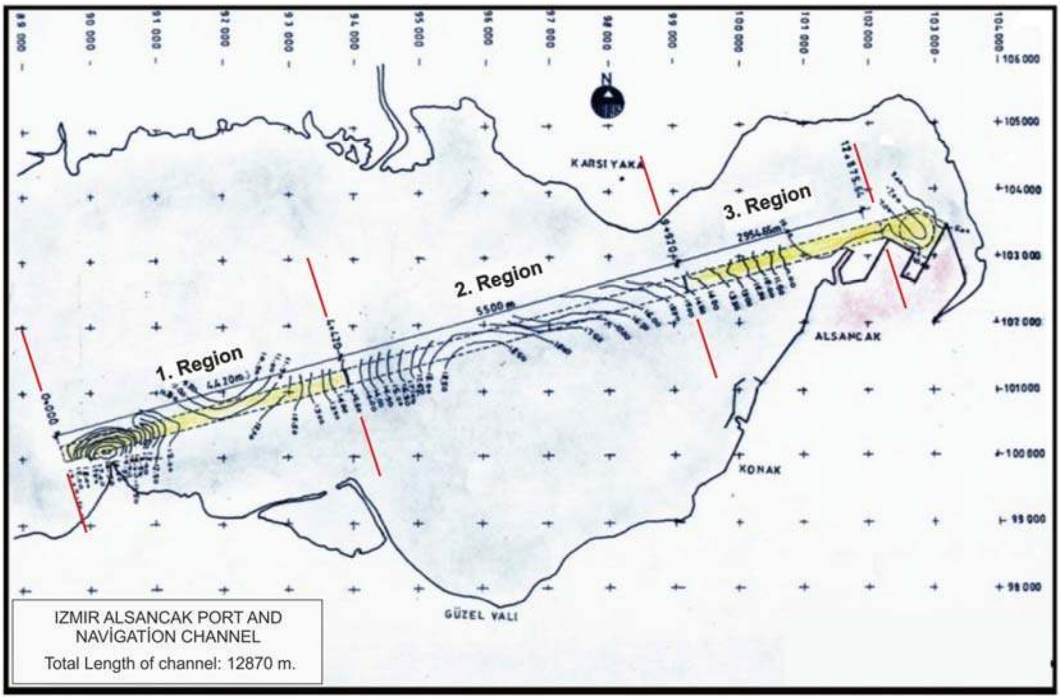

Figure 1.2 The parts of Alsancak navigation channel (Figure was modified from Sonuvar, 2004)

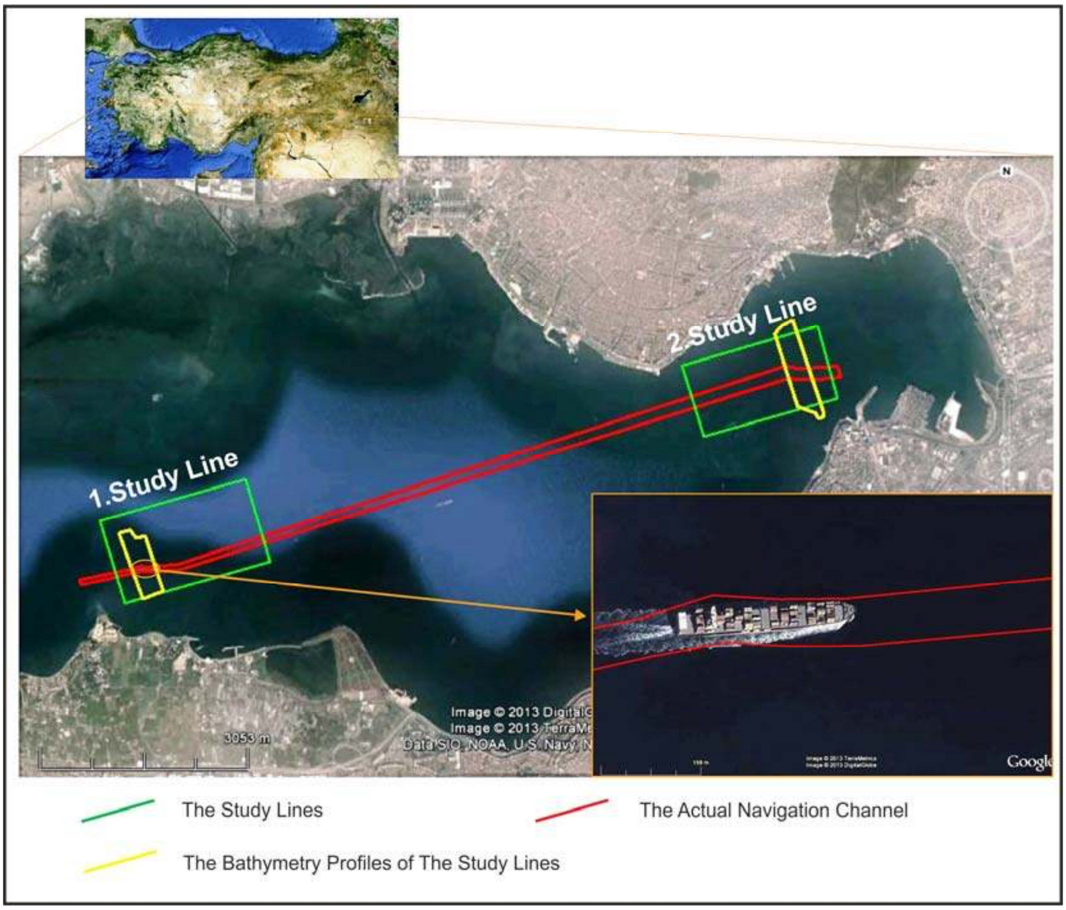

Figure 1.3 Study areas as 1. and 2. line in this work, and the Alsancak port (Google Earth)

1.3 Metarial and Method

Grab Sampler

The required soil samples are taken by using ***grab sampler*** (see Figure 1.4) for laboratory studies and to make the surface sediment distribution map of first and second study lines. The soil samples are taken from 12 different locations on the navigation channel and the north side of İzmir bay.

Figure 1.4 Using grab sampler on this study

Laboratory study

In laboratory studies, the engineering properties of the soil samples of İzmir bay were determined in the Soil Laboratory of Geology Department at the University of Dokuz Eylül according to American Society for Testing and Materials Standards (ASTM). The classification of soil (by sieve analysis and hydrometer tests), total unit weight, specific gravity (G_s), water content (w), atterberg limits and liquidity index, undrained shear strength (by fall cone test) are such properties investigated in the experiments. The laboratory studies have been carried on following the Annual Book of ASTM Standards (Vol.4) (2004) in this works.

Hydrographic and Oceanographic study

The actual bathymetry map was measured with Ecosounder (Hi-Target HD-370), GPS (TopCon GR-500 GPS RTK), (singe beam) transducer and navigation software (HydroPro Software) for two study areas on the navigation channel. A flowchart is shown that summarizes the operation of bathymetry measurements in Figure 1.5.a. CTD RBR 620 was used to determine speed of sound and the physical properties of seawater as shown Figures 1.5.b.

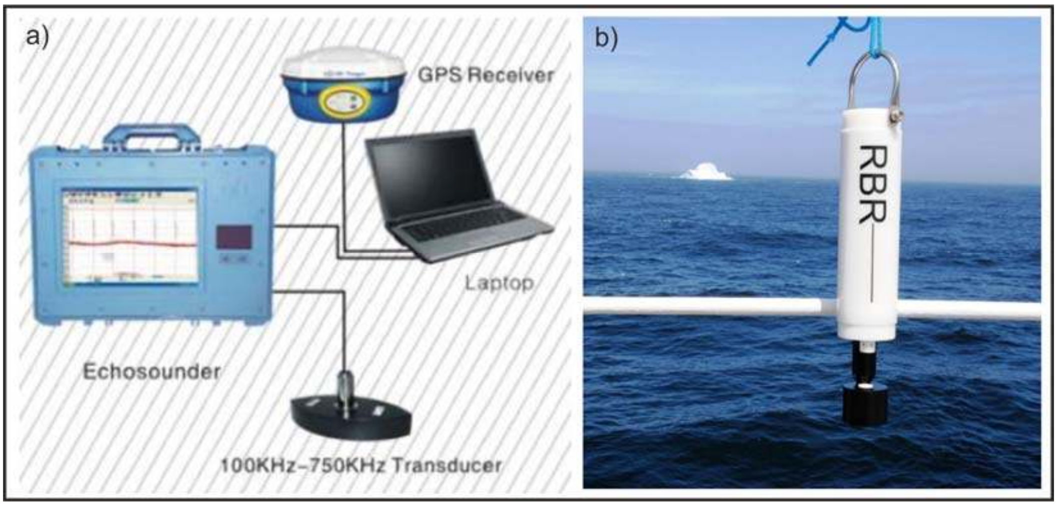

Figure 1.5 a) A flowchart that summarizes the operation of bathmetry, b) CTD RBR 620 instrument

1.4 Aim of Study

Aim of the present study is to determine an optimum and economic overall slope angle for new navigation channel under various loads such as wave, tide (hydrostatic) and seismic loads both in short and long terms. For this purpose the following has been carried out;

- An extensive literature survey for gathering information about geological, geotechnical, hydrographic and oceanographic properties of İzmir bay and Alsancak port-navigation channel.

- to investigate the geotechnical and geological properties of total 12 soil samples taken from two different study areas along the navigation channel, and to obtain the necessary parameters for slope stability analysis software with laboratory studies.

- to prepare 2D and 3D bathymetric, the inclination, and the vector maps of the study areas of the navigation channel. The sediment distribution map is aimed to generate with sediment samples taken.
- to determine optimum slope angle by means of available software packages for the cross-section obtained from the prepared bathymetric maps.

CHAPTER TWO

LITERATURE SURVEY

2.1 Past Projects Related To İzmir Bay

In the past, several Hydrographical, oceanographic, sedimentological, geological, geophysical, and geotechnical works had been carried out for İzmir Alsancak port and navigation channel by various institutions, organizations and individuals. The list of these works is presented in Table 2.1.

Table 2.1 Previous studies (Sonuvar, 2004)

Year	Author/Institution	Contents	Project/Descriptions
1957	MTNC	Geotechnical (Drilling)	Port Drilling from Site Plan in 1974 and 1996
1969	MTNC	Geotechnical (Drilling)	Port Drilling from Site Plan in 1974 and 1996
1972	MTNC	Geotechnical (Drilling)	Port Drilling from Site Plan in 1974 and 1996
1973	MTNC	Geotechnical (Drilling)	Port Drilling from Site Plan in 1974 and 1996
1974	Temel Araştırma Inc. Co. (for MTNC)	Geotechnic (Drilling)	Port Extension Construction Stability Investigation For 15, 16, 17, 18, 19, 20, 21, 22, 23, 24, 25, 26, 27, 28, 29, 30, 31, 32,33 Drilling and Laboratory Tests Report
1975	IMST-03	Geotechnical	Soil And Corrosion Reports of Izmir Alsancak Port Extension Construction
1975	Başoğlu	Sedimentology and Tectonic	Hydrogphy and Actual Sedimentology of Izmir's Inner Bay
1978	Başoğlu, Eftelioğlu, ve Köken.	Sedimentology	Sedimentology of Izmir's Inner Bay And Coastal Beaches of Çeşme
1980	Başoğlu	Sedimentology and Tectonic	Meles Delta And Izmir's Inner Bay-The Entry Regions of Bay, The Holocene Sedimentology
1980	IMST-07	Geotechnical	The Research Reports of Alsancak Port Extension Construction And Discharge Areas

Table 2.1 Cont.

1981	IMST-014	Oceanography and Geology	Oceanograpghy of Izmir Bay And The Bathmetric And Geological Survey Reports of Sea Discharge Areas
1985	Tekar Ltd. Co. (DLH için)	Geotechnical	The Assessment Reports of Geotechnical, Laboratory Tests, and Drilling of Izmir Port Yenikale Sand Quarry
1985	IMST-051	Geotechnical	Geomorphological Survey of Dredging Areas of Izmir Alsancak Port Extension Project
1991	Kayalar	Geotechnical	The Observed Settling Problems in Construction on These Sediments and The Settling Properties of Coastal Sediment of The Post Gediz Delta – Meles River
1992	Bayındır Inc.Co. (for General Directorate of Highways)	Geotechnical	Applied Project-Geotechnical Reports of Between Ikiztepe-Konak
1992	Uslu ve Akyarlı	Geotechnical	Geotechnical Aspects of Baseline Studies for Environmetal Impact Assesments of Dredging Operations – A Case Study in Izmir Harbour
1994	IMST-090	Geotechnical	Environmental Impact Assessment Report for Disposal of The Obtained Materials from Izmir Bay Dredging Project on The Land in Izmir-Çiğli
1996	Çalımcı	Geotechnical	Lime Stabilization Laboratory Research for The Base Soil of The Front of Izmir Port Within Geotechnical of Sea-Filling
1997	Bayındır Inc.Co. (for General Directorate of Highways	Geotechnical	Geotechnical Reports of Sea-Filling Between Konak-Alsancak
1997	Bayındır Inc.Co. (for General Directorate of Highways	Geotechnical	Geotchnical Reports of Applied Project of Alsancak Port Viaduct KM:2+900 - KM:3+700
1997	Efol Ltd. Co. (for MTNC)	Geotechnical	Geotechnical Reports of Alsancak Port

Table 2.1 Cont.

1998	Aksu, Yaşar ve Uslu	Geotechnical	Assessment of Marine Pollution in İzmir Bay: Heavy Metal and Organic Compound Concentration in Surficial Sediments
1999	Akyarlı ve Gürhan	Geotechnical	Assessment Possibility of Dredging Materials, and The New Suggestion for Izmir Port
1999	Koca ve Yılmaz	Geotechnical	Assessment As Statistical of Parameters of Foundation Base Soil of Coast Way on Between Gümrük and Üçkuyular (Izmir)
2000	Bayraktar	Geotechnical	Improvement of Dredging Materials of Alsancak Port-Navigation Channel
2001	Oksan	Geotechnical	Improvement of Dredging Materials of Alsancak Port-Navigation Channel

For dredging of the sediments in Izmir Bay, The Ministry of Transportation, Navigation and Communication [MTNC] (1992) proposed to use suction type dredgers, in spite of the possibility of the dissolution of the pollution within dredged materials is very high in the water during dredging activities. Bucket type dredger was used as an alternative to suction type dredger. However during using these types of dredger, the dissolution of a certain amount of pollution is caused in the dredging area. Therefore the operating system should be applied in a way that the dilution ratio will be the minimum.

A more recent study was made by Yıldız (2004) about dredging activities. Yıldız (2004) proposed an operating system to set the criteria for all of the future dredging works in Turkey. The proposed operating system was applied over navigation channel and turning basin of İzmir-Alsancak port. Yıldız (2004) found out that the most appropriate dredging operation should be performed in two stages with the type of suction dredger and the obtained materials can be evaluated with two different techniques from dredging works.

Sonuvar (2004) has carried out studies on stabilizing lime geotechnical properties of the dredging material from İzmir bay. Samples were taken from five different locations over the navigation channel of Alsancak port and the engineering properties of soil of navigation channel were determined. Also soil improvement methods and one of these methods, effect of “Lime Stabilization Method” was investigated in laboratory environment. Sonuvar (2004) identified that Lime Stabilization Method is not acceptable for soils with high silt content, and when this method is applied to suitable soils, the determination of the effective rate of lime is very difficult in the results of these investigation.

Coşkun (2009) investigated morphological properties of İzmir bay with the generated highly detailed three dimensional bathymetry maps produced by multi-beam Echo-Sounder bathymetry system. Artificial and natural structures was interpreted in İzmir bay with side scan sonar and chirp seismic methods and also the latest information related to the seismicity of the region was presented.

Göktürkler (2002) studies the behaviour of soil under seismic forces and the effects of the possible earthquakes together with determining of the active faults in İzmir bay and environment. Göktürkler (2002) carried out three dimesional (3D) seismic wave refraction simulations for İzmir bay and environment by staggered-grid finite difference method. This method bases on the velocity-stress expression of wave equation. A three dimesional (3D) velocity model was formed benefiting from the previous studies on geophysical and geotechnical properties of İzmir bay and environment. As a result of the application of the model, the velocity distributions of P-waves are observed to be very high magnitude for Karşıyaka, Bostanlı and Balçova areas, which means that the seismic forces will be more effective in case of an earthquake in Karşıyaka-Bostanlı and Balçova.

Ulu (2006) presented the importance of bathymetrical and seismic studies in dredging works. These surveys were investigated over the sample of Samsun port. The bathymetric properties of the port were observed after and before dredging works with multi-beam bathymetry system. The volume of dredging material was calculated using the seismic profiles obtained in the study. According to Ulu (2006), the seismic and bathymetric survey should be done periodically and supported with drillings where dredging have been made.

2.2 Dredging Works (In Izmir Bay)

Several dredging works were made at navigation channel of Alsancak port and İzmir bay between the years 1920 and 1990. In the past, the dredged materials were discharged in the outer-1 region and around the Hekim island. However a certain amount of dredged material was also used as fill to increase of the port capacity in sea in the back stage of the port. Detailed of the dredging works which has been undertaken between 1930-1990 years is shown in Table 2.2. Although the dredging works have not been intensive after 1990, the majority of works have been concentrated in the north of the İzmir bay.

Table 2.2 Applied dredging works for İzmir bay and port between 1930 and 1990 years (MTNC, 1992)

Dredging Company	Years	Dredged Area	Damping Area	Account (m^3)
Hollanda Royal Company	1930-1951	Front of I.K.Cargo Pier	Front of Elevator Station	210.000
Hollanda Royal Company	1955-1958	Front of I.K.Traveler Pier, and Regions of I.K. Turning Basin and I.K.Port	The Front of Göztepe Station	2.356.786
MTNC 6. Regional Office	1966-1967	I.K. Ferryboat Quay and Turning Basin	The Front of Göztepe Station	70.685
MTNC 6. Regional Office	1973-1974	Melez Creek Diversion Channel	The Front of Göztepe Station	180.000
MTNC 6. Regional Office	1975-1977	II.K.Pier Bottom	Environment of Uzun Island	1.080.000
MTNC 6. Regional Office	1978-1979	Melez Creek	Environment of Uzun Island	160.000
MTNC 6. Regional Office	1978-1979	II.K.Ore Pier, I. Regions	Environment of Uzun Island	64.000
MTNC 6. Regional Office	1978-1979	II.K.Ore Pier and II. Regions	Environment of Uzun Island	513.000
MTNC 6. Regional Office	1980-1982	Front of II.K. Pier	Environment of Uzun Island	720.000
MTNC 6. Regional Office	1980-1984	II. Mole Area	Environment of Uzun Island	1.350.000

Table 2.2 Cont.

MTNC 6. Regional Office	1985	III.S. Engine Pier	Environment of Uzun Island	315.000
MTNC 6. Regional Office	1986	Front of III.TMO	Environment of Uzun Island	420.000
MTNC 6. Regional Office	1987	Front of II.S. Container Pier	Environment of Uzun Island	450.000
MTNC 6. Regional Office	1987	Slope Dredging For II.S. Merchandise Pier	Environment of Uzun Island	280.000
MTNC 6. Regional Office	1980-1986	II.S. Area	Environment of Uzun Island	130.000
Italian Dragomar S.P.A	1986	II.S. Ore Pier	Environment of Uzun Island	129.000
Italian Dragomar S.P.A	1987-1988	III.S. Mole and Construction Area	Environment of Uzun Island	3.172.723

2.3 Studies Made About Stability of Submarine Slope

Feeley (2007) highlights sampling and mapping techniques, and in situ testing methods related to offshore landslide triggering mechanics within the research reports titled “Triggering Mechanics of Submarine Landslides”. Feeley (2007) focuses on faster research and lower cost of mapping techniques, and finding easier techniques to obtain undisturbed sampling from seafloor.

Hance (2003) gives a database of submarine slope failures documented in the literature. The collected information are presented in categories like soil properties, slope angle and type of failure with regard to these seafloor failures. Hance (2003) observed that the studies on submarine slope failures were mostly lack geotechnical information.

Raaijmakers (2005) investigated morphological development and macro-micro stability of submarine slopes and the behavior of soil in dredged channels. MSTAB by GeoDelft was used to calculate factor of safety under both drained (for sand, silt, and clay) and un-drained (for clay) conditions in macro stability. Non-cohesive soils was evaluated for micro stability. Also the calculations of liquefaction were executed with SLIQ2D software for loosely sand soil on the different slope angles. SUTRENCH (2DV) software developed by Delft Hydroulics was applied to understand the morphological development of navigation channel. Raaijmakers

(2005) considered only wave loads in the slope stability calculations and observed that hydrodynamic–wave loads and motions play much more important role than estimated for both stability and morphological development of channel.

Zreik (1991) studied the un-drained shear strength of very soft cohesive soils on the samples taken at Boston Harbor Mud by new fall cone apparatus. When the obtained un-drained strength values by the standard fall cone was compared with those obtained from a lab vane, the similar results were obtained. However the fall cone showed limitations when the strength values C_u of testing very soft soil is approximately 0.1 to 0.2 kPa.

CHAPTER THREE
PROPERTIES OF ALSANCAK NAVIGATION CHANNEL

3.1 Introduction

In this chapter, the hydrographical, oceanographic, and geological properties of Alsancak navigation channel and the Izmir bay is reviewed in the light of carried out the previous studies.

3.2 Geology

In the Izmir city center and its environment, Oligonece – Miocene aged conglomerate-sandstone-mudstone-marl-limestone, in flysh facies and volcanic rocks are found in the base and, Quaternary alluvial deposits are found at the top of these units. The similar results are given by Göktürkler (2002) based on marine seismic studies for İzmir bay at the Institute of Marine Science and Technology of Dokuz Eylül University. Göktürkler (2002) presents that there are four different geological units as Quaternary sediments, Neogene sediments, Neogene volcanic rocks and Cretaceous flysh in the bay area.

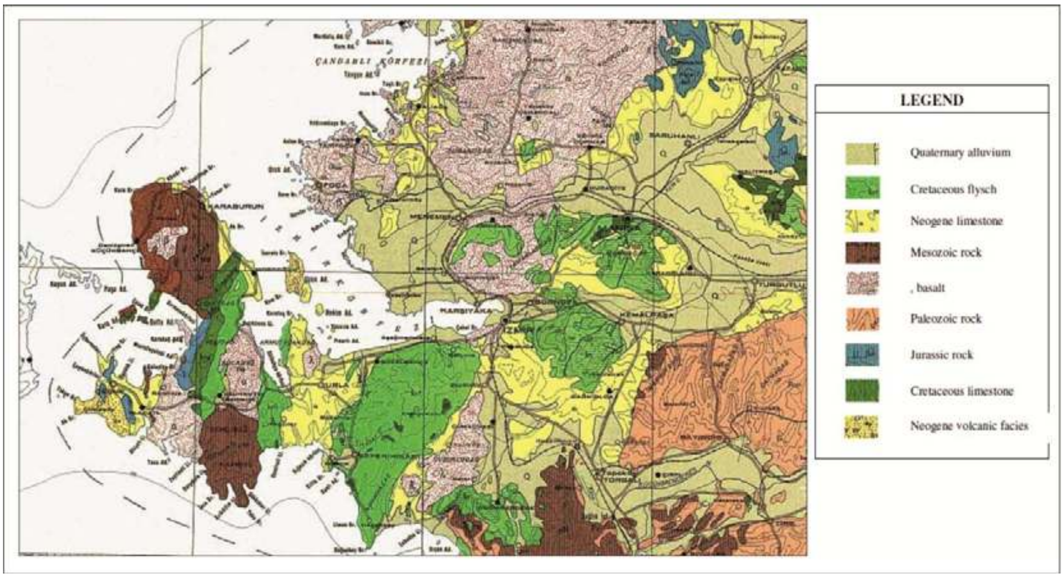

Figure 3.1 Geology map (1/500.000) of İzmir and environment (Yalçın, 2008)

Kaya (1999) denotes that Late Cretaceous formations have been comprised of extremely fractured mudstone and sandstone, and limestone blocks. According to Kaya (1999), one of the major important volcano cones of Neogene is at the foothill of Yamanlar mountain that extends to Menemen, Çiğli and Hatay area. Volcanic cones are generally consists of andesitic lava, lava breccia, tuff and lahar units. Lahar formations causes in-stability on the land slopes as in Yeşildere area (Kaya, 1999).

The investigated area is covered by quaternary alluvium deposits and it overlies on a neogene volcanic unit composed of the andesitic rocks. The thickness of this alluvium deposit varies according to regions. These alluvium units consist of sand, silt, clay and organic material. These sediments are mainly water saturated due to low elevation (Göktürkler, 2002). Koca & Yılmaz (1999) pointed out that the discordant andesite was cut at 35.0 and 40.0 m. levels in drillings in Konak port area.

About the surface sediments; Aksu et. al. (1998) classifies the surface sediments of the İzmir bay with respect to grain size. According to their work, the inner parts of Izmir bay consist of 60-70% clay, 20-30% silt, and 10% sand. Generally surface sediments of the inner bay are silty, silty clay, clay, organic clay and little sandy. In the works carried out to determine the properties of surface sediments in the environment and navigation channel, and in the front of harbor, surface sediments is observed to have heterogeneous distributions. The main reason of having a heterogeneous distribution for surface sediments in inner bay is that Gediz and Meles rivers have variable flow regime and the amount of material transported depends on seasonal rainfall.

Institute of Marine Sciences and Technology, Dokuz Eylül University [IMST] (1985) presented the properties of the profile of seafloor with the use of seismic works. According to IMST (1985), the top seafloor consists of high plastic clay (CH). A thin layer of silty sand (SM) soil is present generally under "CH" soil in the first region of navigation channel as shown Figure 3.3. In third region, the top seafloor is observed to have high plasticity clay (CH) and low plastic organic clay

(OH) is present in approximately 6-10 m thickness under the “CH” soil as shown Figure 3.4.

In order to define the geotechnical properties of soil under the soft surface sediments, the soil samples were taken using Vibracore and Drilling equipments for first and third region of navigation channel by IMST (1985) (Figure 3.2). The soil samples obtained with these works were investigated in the soil laboratory report prepared by Kayalar et. al. (1985) from Civil Engineering Department, Dokuz Eylül University within the scope of Izmir Alsancak Port Extension Project-Geomorphological Surveys of Dredging Areas.

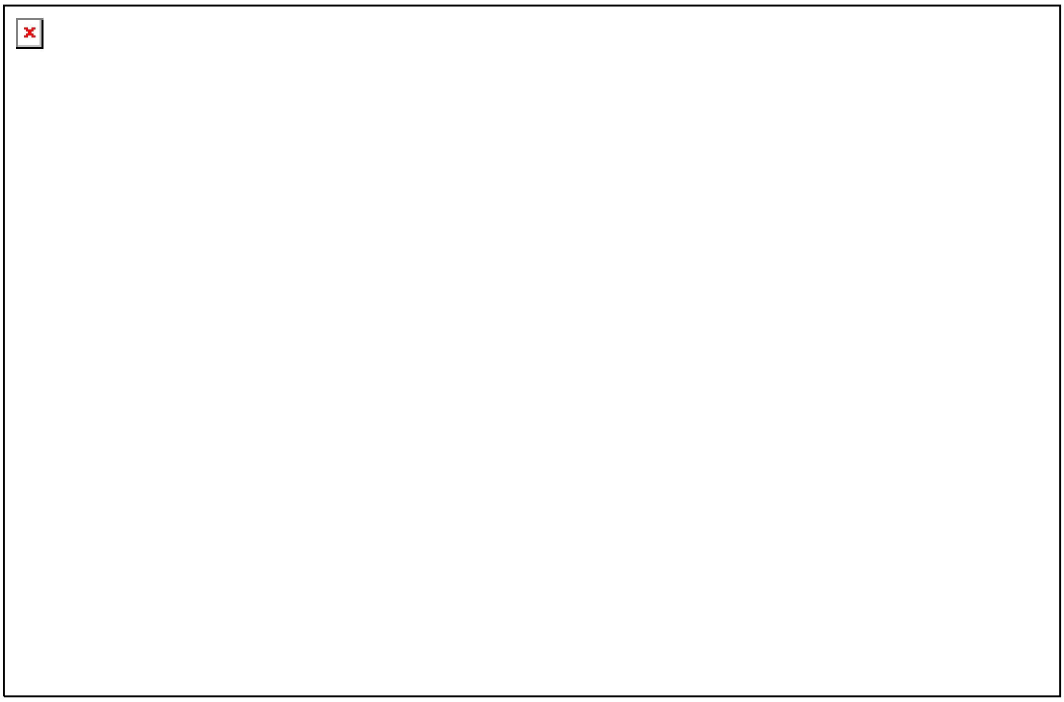

Figure 3.2 The location of soil samples taken by DBTE (1985) (Sonuvar, 2004)

The results of laboratory tests for gravity samples as G1, G2, G3 and Vibracore samples as V1, V2, V3, V4 are given as follows;

Table 3.1 G1 well in the first region (Kayalar et. al., 1985)

G1 (First Region) (Water Depth: 11.2 m)						
SampleDepth (m)	**Specific Gravity**	**Natural Water Content**	**Natural Unit Weight (kN/m^3)**	**Natural Void Ratio**	**Soil Classification**	**Shearing Strength (kg/cm^2)**
0.00-0.50	2.71	0.76	15.87	2.06	OH	0.045
0.50-1.02	2.70	0.89	17.93	2.40	SM	0.13

Table 3.2 G2 well in the first region (Kayalar et. al., 1985)

G2 (First Region) (Water Depth: 10.3 m)						
SampleDepth (m)	**Specific Gravity**	**Natural Water Content**	**Natural Unit Weight (kN/m^3)**	**Natural Void Ratio**	**Soil Classification**	**Shearing Strength (kg/cm^2)**
0.00-0.21	2.69	-	-	2.74		0.042
0.21-0.50	2.72	1.02	15.38	2.77		-
0.50-0.62	2.72	1.22	16.46	3.32	OH	0.06
0.62-1.66	2.71	1.22	16.36	3.31		0.064

Table 3.3 G3 well in the first region (Kayalar et. al., 1985)

G3 (First Region) (Water Depth: 17.1 m)						
SampleDepth (m)	**Specific Gravity**	**Natural Water Content**	**Natural Unit Weight (kN/m^3)**	**Natural Void Ratio**	**Soil Classification**	**Shearing Strength (kg/cm^2)**
0.00-0.15	2.71	-	-	-		-
0.15-0.50	2.72	0.91	15.77	2.47		-
0.50-0.88	2.73	0.79	-	2.16	OH	-
0.88-1.00	2.71	0.74	16.56	2.01		-
1.00-1.39	2.70	-	16.66	-		-

Table 3.4 V1 well in the first region (Kayalar et. al., 1985)

V1 well (Third Region) (Water Depth: 9.1 m)						
Layers	**Depth (m)**	**Specific Gravity**	**Natural Water Content**	**Natural Unit Weight (kN/m^3)**	**Soil Classification**	**Shearing Strength (kg/cm^2)**
1. Layer	**0.00**		-	13.72		-
	0.50		0.74	15.58		0.05
	1.00	2.61	0.71	15.38	CH	0.14

Table 3.4 Cont.

1.Layer	1.50		0.66	15.68		-
	2.00		0.65	15.48		-
	2.50		0.60	14.70		0.18
2.Layer	3.00		0.62	15.19		0.24
	3.50	2.61	0.69	15.97	CH	-
	4.00		0.56	16.36		0.16
	4.50		0.47	16.07		-
3.Layer	5.00		0.59	15.97		0.34
	5.50	2.62	0.53	15.77	CH	-
	-		-	-		-

Table 3.5 V2 well in the third region (Kayalar et. al., 1985)

V2 well (Third Region) (Water Depth: 9.9 m)						
Layers	**Depth (m)**	**Specific Gravity**	**Natural Water Content**	**Natural Unit Weight (kN/m^3)**	**Soil Classification**	**Shearing Strength (kg/cm^2)**
1.Layer	0.00		0.86	14.01		0.07
	0.50	2.64	0.77	14.70	CH	0.10
	1.00		0.77	14.99		0.05
	1.50		0.66	15.68		0.07
2.Layer	2.00	-	0.68	15.97		-
	2.50	2.65	0.67	16.36	CH	-
	3.00	-	0.64	16.07		0.23
	3.50	-	0.49	15.97		-
3.Layer	4.00		0.51	15.58		-
	4.50	2.63	0.67	15.09	CL	-
	5.00		0.68	15.87		0.12
	5.50		0.49	15.48		0.20

Table 3.6 V3 well in the first region (Kayalar et. al., 1985)

V3 well (First Region) (Water Deth: 12.0 m)						
Layers	**Depth (m)**	**Specific Gravity**	**Natural Water Content**	**Natural Unit Weight (kN/m^3)**	**Soil Classification**	**Shearing Strength (kg/cm^2)**
1.Layer	0.50		0.76	14.50		0.05
	1.00	2.60	0.48	15.38	CH	0.07
	-	-	-	-	-	-
2.Layer	1.25					-
	1.50	2.59	0.41	17.77	ML	0.05
	-	-	-	-	-	-
3.Layer	1.80					-
	2.00	2.61	0.68	16.17	OL	0.05
	2.50		0.70	15.97		0.06
4.Layer	-	-	-	-	-	-
	3.00	2.57	0.31	18.32	ML	0.10
	-	-	-	-	-	-
5.Layer	3.50		0.85	16.17		0.07
	4.00	2.62	0.54	15.97	OH	0.09
	4.50		0.77	15.97		0.09
	5.00		0.41	16.17		0.17
6.Layer	-	-	-	-	-	-
	5.50	2.58	0.37	17.05	ML	0.21
	6.00		0.35	20.58		0.21

Table 3.7 V4 well in the first region (Kayalar et. al., 1985)

V4 well (First Region) (Water Depth: 11.3 m)						
Layers	**Depth (m)**	**Specific Gravity**	**Natural Water Content**	**Natural Unit Weight (kN/m^3)**	**Soil Classification**	**Shearing Strength (kg/cm^2)**
1.Layer	0.50		0.87	12.64		0.06
	1.00	2.67	0.74	13.81	OH	0.06
	1.50		0.82	14.01		0.06
2.Layer	2.00		0.34	15.68		0.14
	2.50	2.61	0.34	18.32	SM	0.11
	-	-	-	-	-	-

Table 3.7 Cont.

3.Layer	-	-	-	-	-	-
	3.00	2.70	0.51	17.05	OL	0.08
	-	-	-	-	-	-
4.Layer	3.50	-	0.39	18.32	-	0.08
	4.00	2.64	0.38	19.89	SM	0.07
	-	-	-	-	-	-
5.Layer	4.50	2.66	0.61	15.77		0.08
	5.00		0.56	16.46	OH	0.15
	-	-	-	-	-	-
6.Layer	-	-	-	-	-	-
	5.50	2.56	0.34	17.15	OL	-
	-	-	-	-	-	-

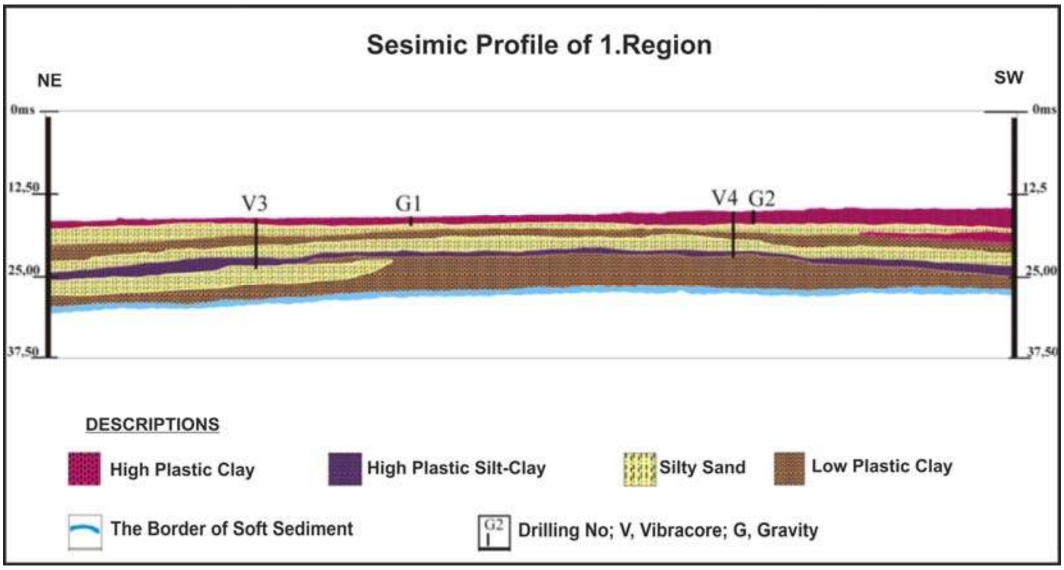

Figure 3.3 Seismic profile in the first region of navigation channel (Sonuvar, 2004)

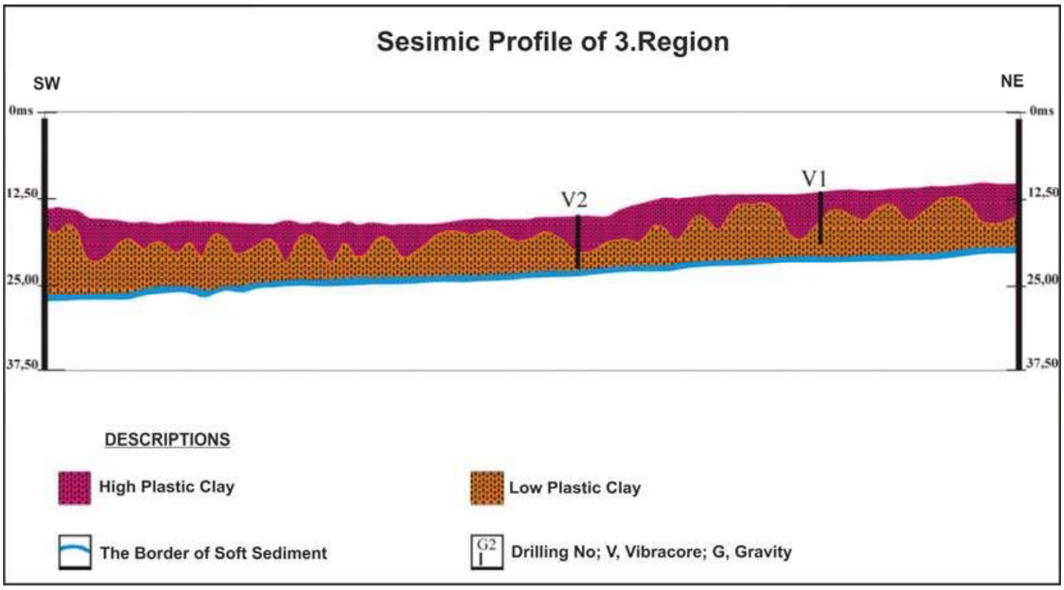

Figure 3.4 Seismic profile in the third region of navigation channel (Sonuvar, 2004)

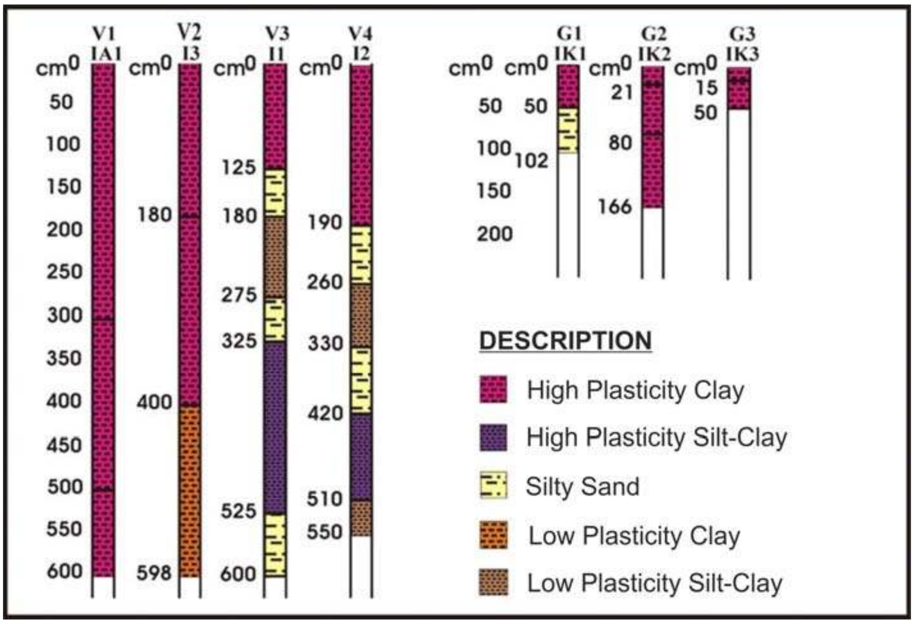

Figure 3.5 Gravity core and Vibracorel (Sonuvar, 2004)

According to Kayalar et. al. (1985), In the well of Gravity core and Vibracore, the different types of soil are observed due to the lenticular structure (Figure 3.5). Although there are different types of soil, the shear strength values of soil samples are close to each other. The minimum value of shear strength is 0.05 kg/cm^2 for CH in V2 well, and the maximum value of shear strength is 0.34 kg/cm^2 for CH in V1 well. The shear strength value is approximately 0.21 kg/cm^2 under the depth of 2.0

meter for the first region. The shear strength value is approximately 0.18 kg/cm^2 under the depth of 4.5 meter for the third region.

In this study, the shear strength values are used as **17.50 kPa** and **21.00 kPa** respectively for the soils under soft surface sediments of the first and second line for slope stability analysis according to Table 3.4, 3.5, 3.6 and 3.7.

In the turning basin and its close environment, Çalımcı (1996) determined that surface sediments is high plastic type organic clay (OH) nearby the turning basin, and additionally the samples taken deeper is high plastic type silt (MH); Bayraktar (2000) and Oksan (2001) defined “CH-MH” for the similar area. Generally, CH and MH type of soils are observed in the third region and at the turning basin. Sonuvar (2004) presented that soil is shelled and organic high plastic type silt at the turning basin area.

According to the environmental impact report of Dokay Engineering (2013), the soil samples taken from turning basin area were investigated and the surface sediments were found to be consists of 17.46-19.98% gravel; 11.36-16.82% sand; 42.64-54.08% silt and 17.10-22.10% clay. Moreover, the dominant soils are found to be silt and clay in the zone.

In this study, 12 pieces of soil samples were taken by Grab from two different regions in order to investigate submarine slope stability of Alsancak navigation channel (Figure 3.6). Additionally, three specimens were taken at the circulation channel, two of which are surface sediments and other specimen is from 4 meters below the seafloor. Engineering properties of surface sediment of navigation channel is found.

The surface sediments are mostly silty sand “SM” for the northwest area, and is shell containing medium plastic clayey silt “MIO” in the southwest side of the first line. Additionally, soil is defined shell containing highly plastic clayey silt “MHO” from the southwest to the northwest as shown in Figure 3.6. Generally, the amount of silt and clay in the soil can be said to increase proportionally with plasticity of the soil. In the second line (in third region), the type of soil is defined as shell containing highly plastic clayey silt “MHO” (Figure 3.6). In the previous studies, the soil is said to be generally organic highly plastic clay “OH-CH” and highly plastic silt “MH” in the turning basin. Generally, the third region consists of highly plastic clay and highly plastic silt type soils, increasing in plasticity from the southwest to the turning basin.

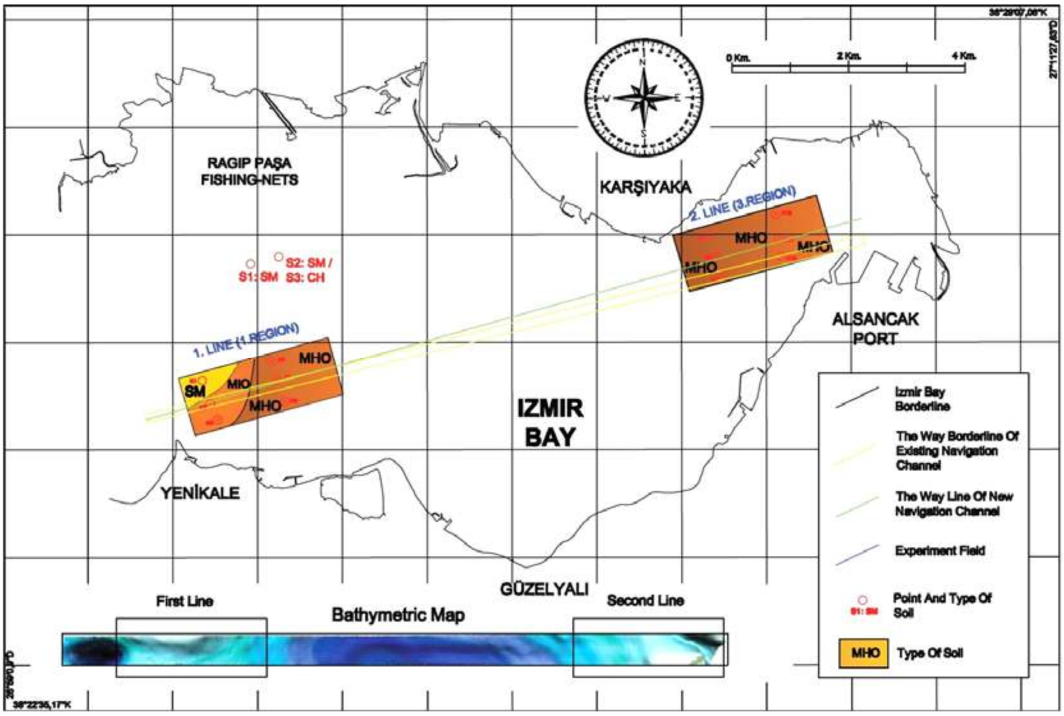

Figure 3.6 The distribution map of surface sediments

In this chapter, the general properties of surface sediments are presented and the distribution of sediment was denoted with the support of map in the experimental field (Figure 3.6). Others engineering properties and strength parameters of soil were presented in the chapter 6.

3.3 Hydrographic Properties of Izmir Bay and Navigation Channel

Bathymetric maps have been prepared for both the Izmir bay and the navigation channel by the various institutions and organizations. The most detailed study about navigation channel and turning basin was made by Institute of Marine Sciences And Technology, Dokuz Eylül University [IMST] (1985). The general situation of the planned dredging zones and the channel was determined by MTNC based on IMST (1985). During and after dredging works, bathymetry works has been made to observe topographic changes on small scale and specific zones. Additionally, hydrographic studies have been made at the inner harbor and at the harbor entrance based on dredging works and according to the present requirements. Office of Navigation, Hydrography and Oceanography (ONHO, 2004) prepared one of the newest bathymetry maps of Izmir bay for navigation purposes (Figure 3.7). Analysis and modeling of current system of Izmir gulf including the bathymetric and seismic properties of Izmir gulf was carried out by (IMST, 2012) within the scope of "Rehabilitation of Izmir bay and harbor" project conducted by GDSRRT.

Within the scope of this project, IMST (2012) carried out seismic studies and produced bathymetric maps of the Izmir bay and the related areas. Also current regime of Izmir bay was determined and modeled with the data obtained at four different current measurement stations. The detailed information was presented about the current system of the Izmir bay in the following section.

According to the above mentioned studies, the depth values generally increases from inner bay to outer bay. While the depths are seen to be between 10.0 and 20.0 meters in the inner bay, the depths values of outer bay can be observed to reach to 60 meters. The seawater depth is very shallow in the north side of Izmir bay and Ragıp Pasa Fishing-net area, and the seawater depths are between 0.5 and 4.0 meters.

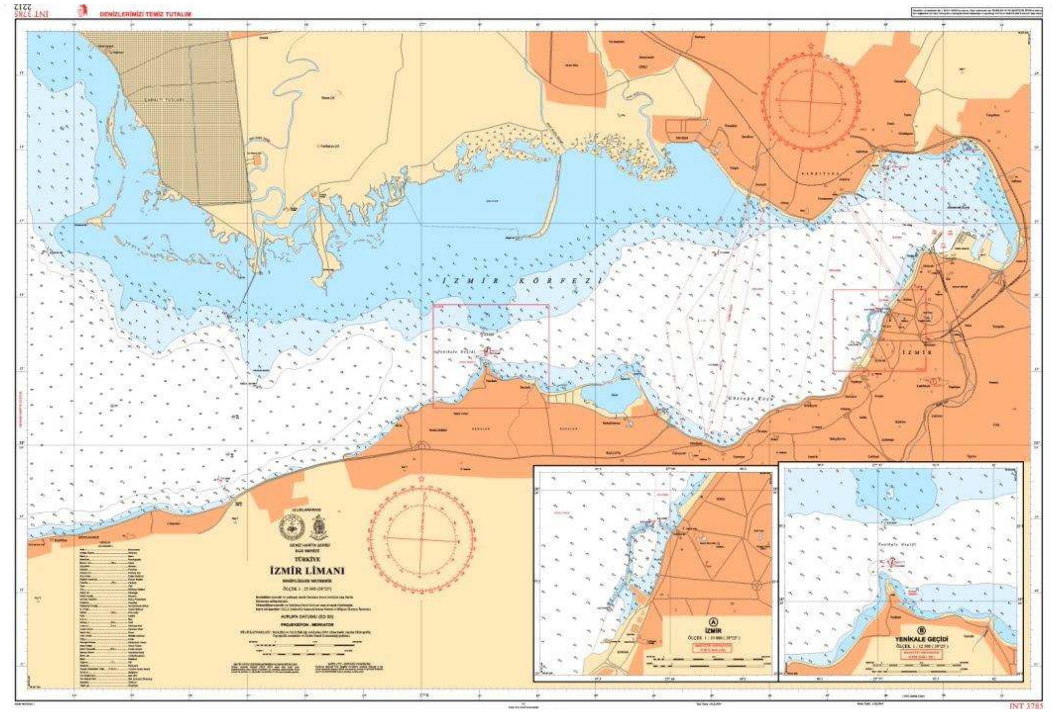

Figure 3.7 Bathymetric maps by ONHO (2004) (Dokay Engineering, 2013)

In the previous studies, Alsancak navigation channel has been divided into three regions in order to investigate in more detail for different studies. The bathymetric maps of the navigation channel and turning basin prepared by IMST (1985) is digitized as in the following figures within the scope of this study. According to these bathymetric maps, the properties (depths and length) of these regions are presented as follows:

- For the first region, the length is 4420 meter, the shallowest depth is 10.5 meter and the deepest area is approximately 10.0 meter (Figure 3.10).
- For the second region, the length is 5500 meter, the shallowest depth is 14.5 meter and the deepest area is approximately 18.0 meter (Figure 3.11).
- For the third region, the length is 2954 meter, the shallowest depth is 8.0 meter and the deepest area is approximately 14.5 meter (Figure 3.12).
- The diameter of the turning basin is 580 meter (Figure 3.13).

Within the scope of "Rehabilitation of the Izmir Bay and Harbor" project, the depth of channel is planned to increase gradually to 14.0 m, 16.0 m and 17.0 m by dredging works.

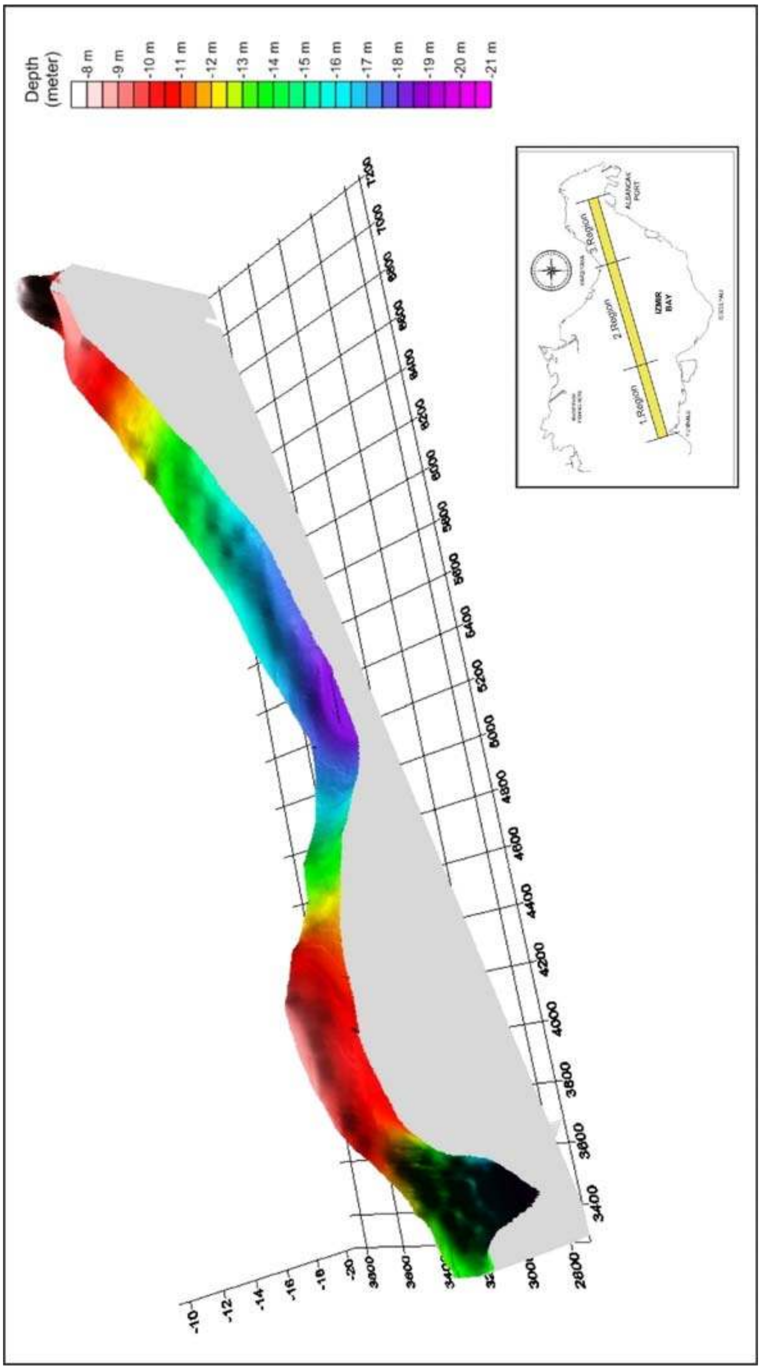

Figure 3.8 The three dimensional bathymetric map of navigation channel

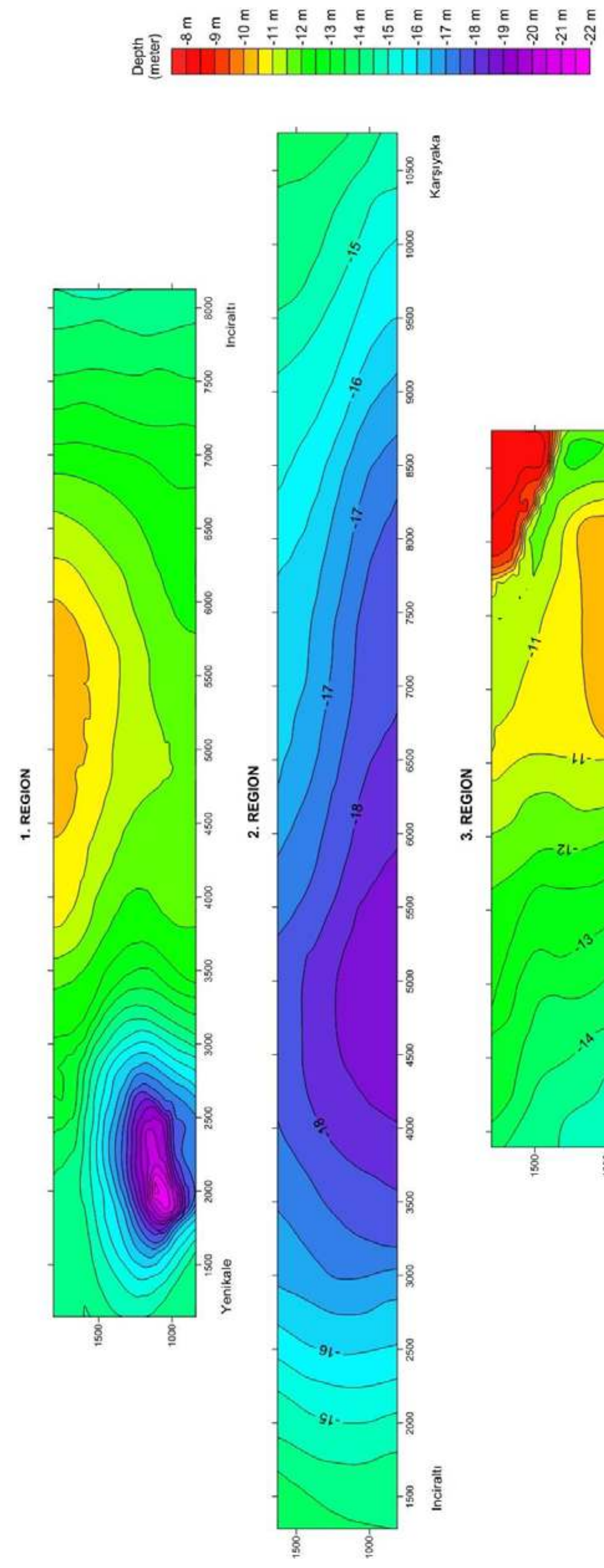

Figure 3.9 The 2D bathymetric maps of three regions

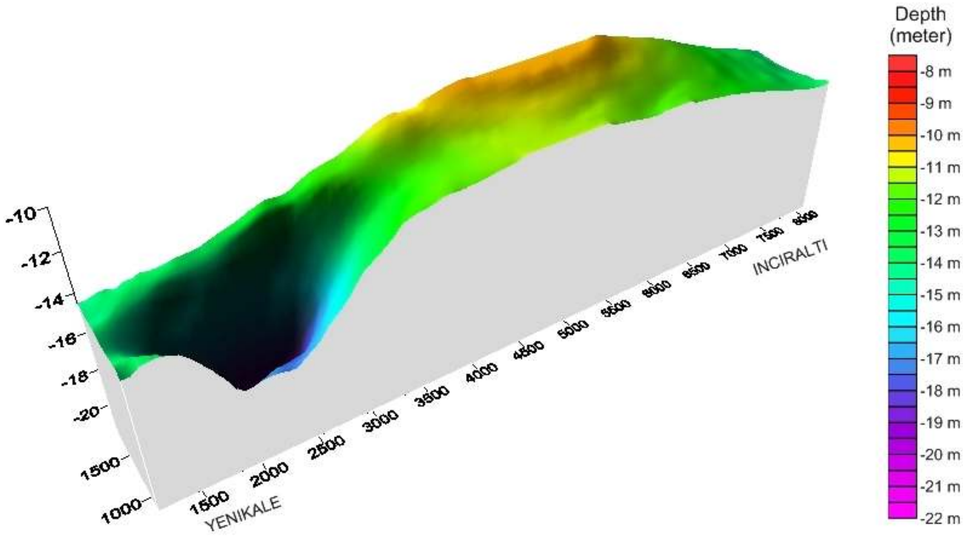

Figure 3.10 The 3D bathymetric map of the first region

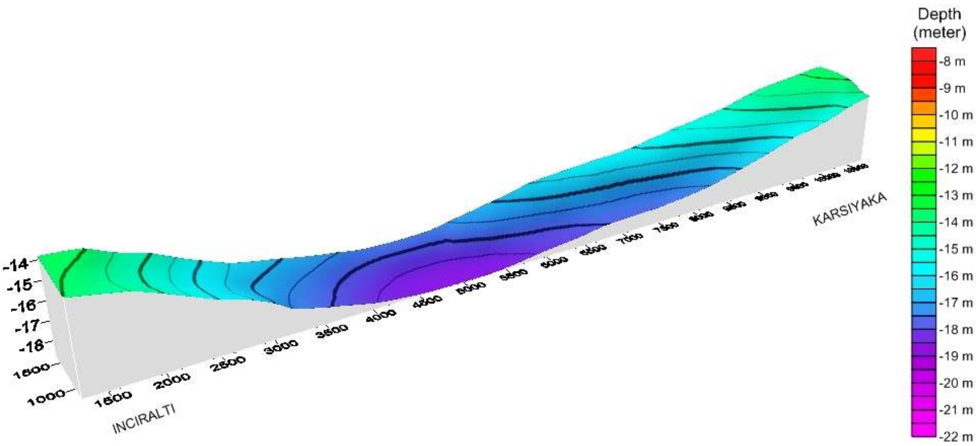

Figure 3.11 The 3D bathymetric map of the second region

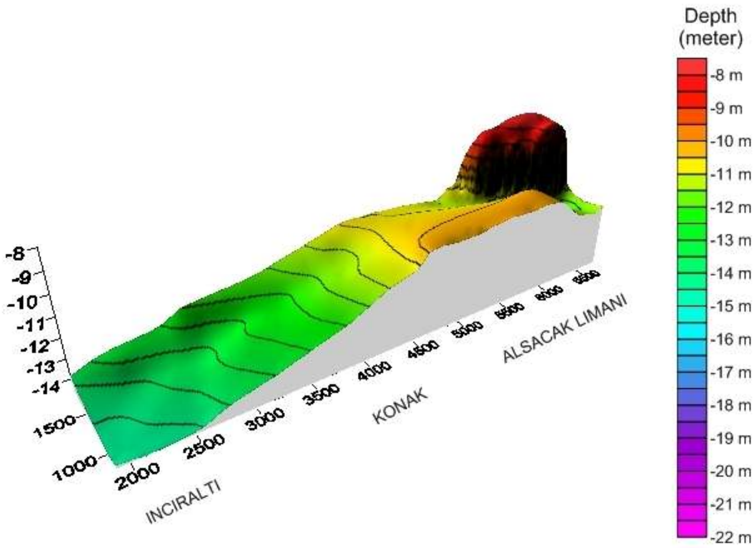

Figure 3.12 The 3D bathymetric map of the third region

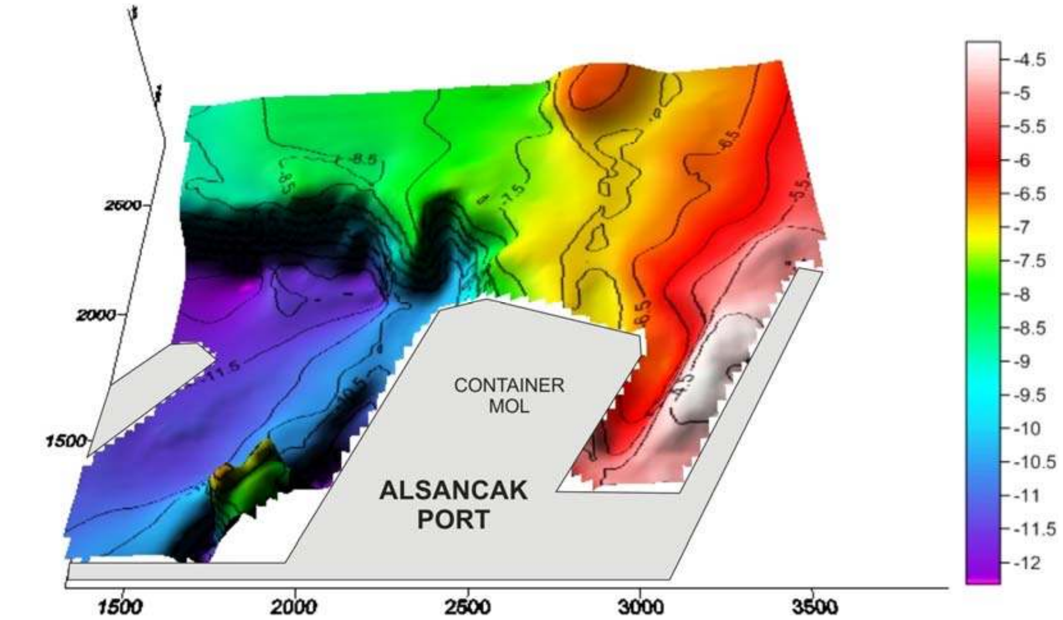

Figure 3.13 The 3D bathymetric map of the turning basin

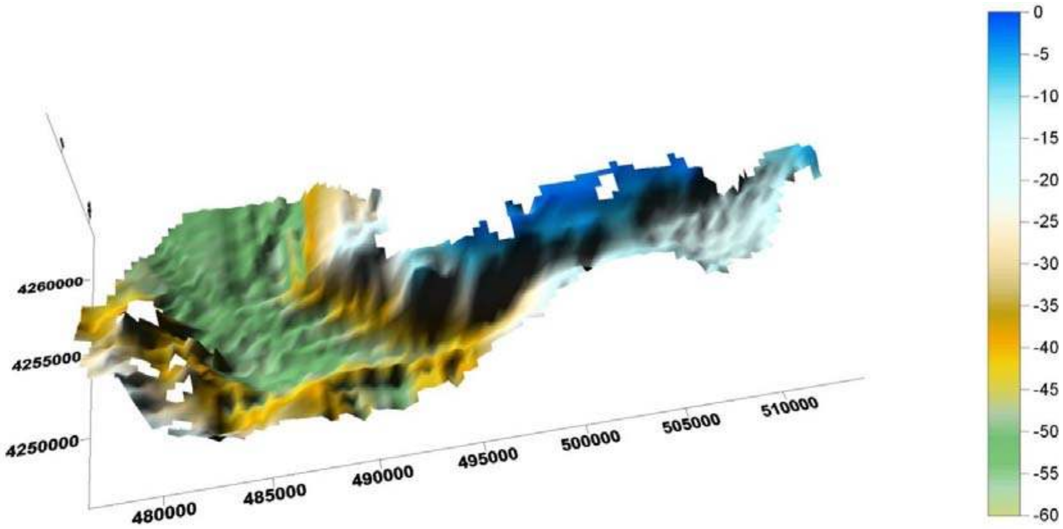

Figure 3.14 3D bathymetric map by Institute of Marine Sciences And Technology, Dokuz Eylül University (2012) (Dokay Engineering, 2013)

Within the scope of this study, critical areas for submarine slope stability were determined on the navigation channel. Bathymetric map of these critical areas were made. The slopes were modeled for the stability analysis using the bathymetric maps. The detailed information about the profiles and techniques of bathymetric maps was presented in Chapter 6.

3.4 Oceanographic Properties of Izmir Bay and Navigation Channel

3.4.1 Wave Climate Properties

Within the scope of “Rehabilitation of the Izmir Bay and Harbor” project, wave climate properties of Izmir bay was determined by Yüksel Project (2012). Yüksel Project (2012) firstly obtained wind climate, wind roses and wind histograms of the study area. Later, wave climate of area was obtained using wind data. Wind data of ECMWF (European Centre for Medium-Range Weather Forecasts) and Izmir Meteorological Station (IMS) was used to determine wind and wave climate properties of experimental area.

According to Yüksel Project (2012), the wind data of ECMWF covers between the years 1983 and 2010. The direction and velocity of winds were calculated from the available atmospheric pressure data by means of a mathematical model. The given wind data is in six hours intervals. The wind rose and histogram of the ECMWF wind data are given in Figure 3.15.

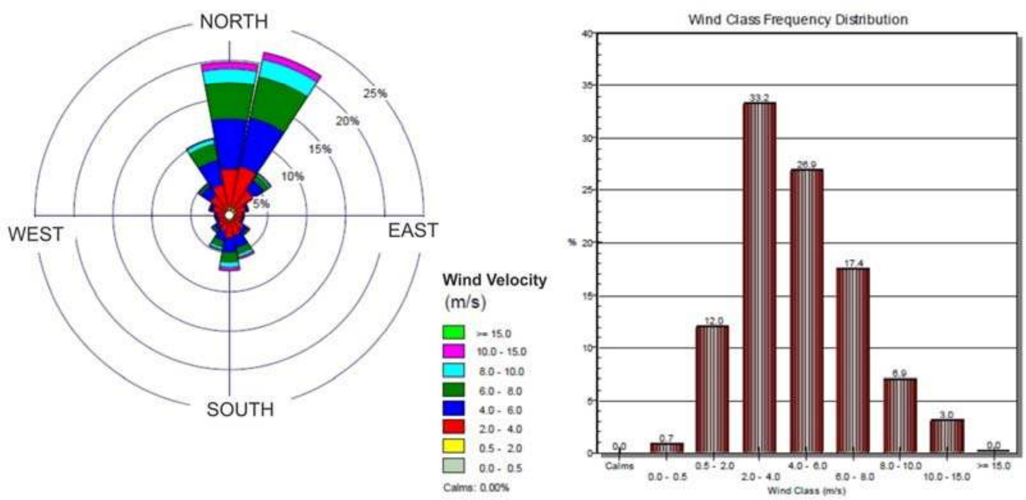

Figure 3.15 The obtained wind rose and histogram using the wind data of European Centre for medium-range weather forecasts (Yüksel Project, 2012)

As seen from Figure 3.15, 90% of the wind velocities is between 0.5 and 10.0 m/s, and 3% of the wind velocities is between 10.0 and 15.0 m/s. Also, the dominant of wind directions are north (N) and north-east (NE).

IMS wind data covers between years 1956 and 2010. The main difference between the wind data of IMS and ECMWF is that IMS is located on the ground and ECMWF is located on the sea. Additionally, the measured wind data of ECMWF was calculated 6 hourly, but the wind data of IMS measured one hourly. However both of them are located 10.0 meters above the mean sea level. The wind rose and histogram of the IMS wind data are given in Figure 3.16.

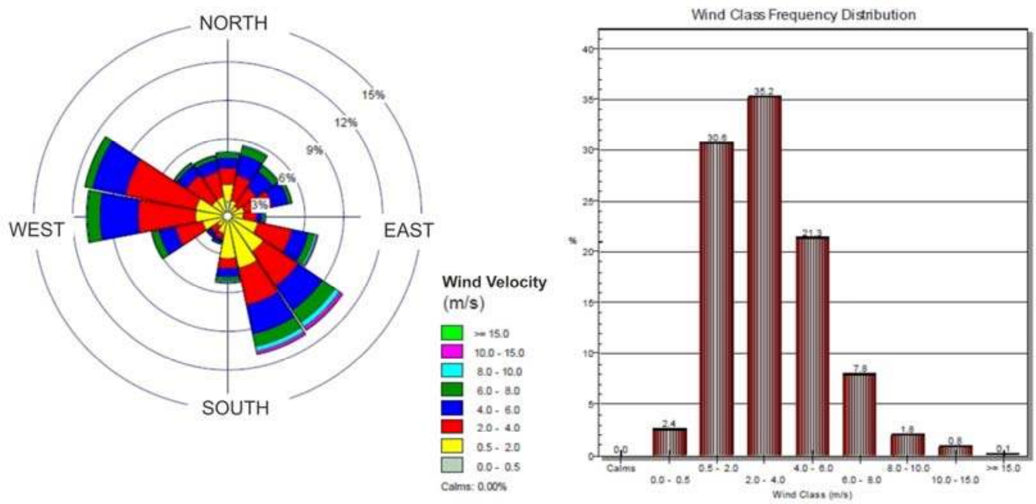

Figure 3.16 The obtained wind rose and histogram using the wind data of Izmir Meteorological Station (Yüksel Project, 2012)

As seen from Figure 3.16, the dominant of wind directions are south-east (SE), west (W) and north-west (NW). The 95% of wind velocities are observed between 0.5 and 10.0 m/s. The velocity of the strongest wind is presented between 10.0 and 15.0 m/s and the ratio is 0.8 percent. The velocity of the lowest wind is presented between 0 and 0.5 m/s and the ratio is 2.4 percent.

Wave hindcast was carried out using the effective fetch distances and the wind data for the selected points at the study area in the bay as shown in Figure 3.17. Wave statistics (long-term and short-term) was studied using the hindcast deep-sea wave properties. Both wave hindcast and statistics were carried out for these study points. The bathymetric maps of ONHO (2004) and IMST (2012) was used to calculate the effective fetch distances in the wave hindcast study.

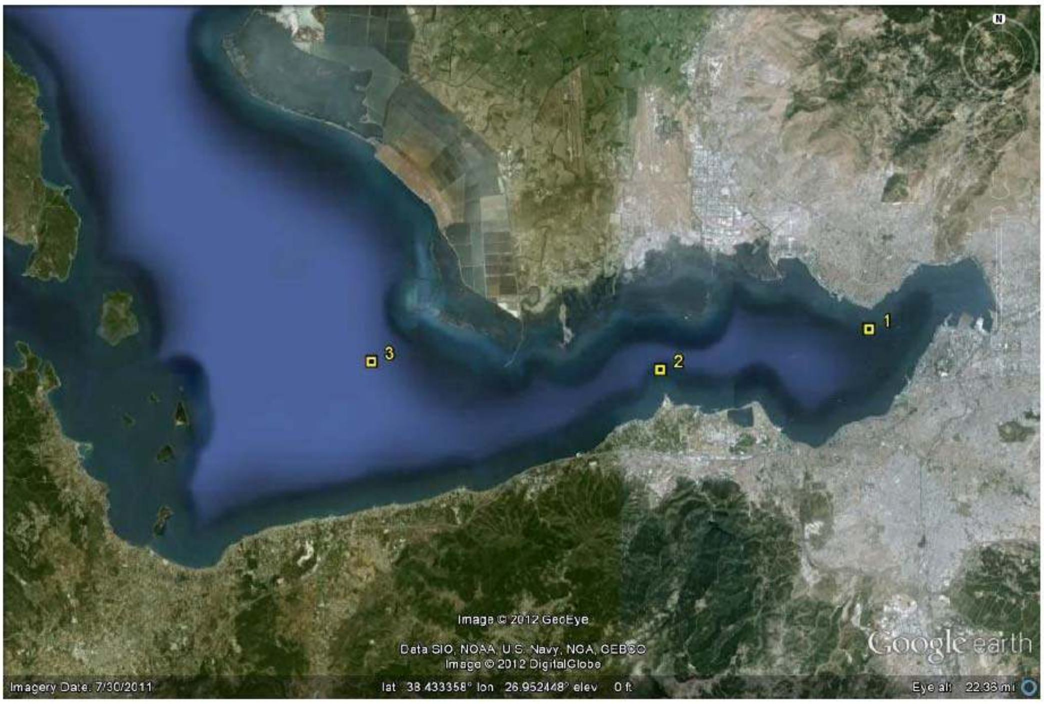

Figure 3.17 The study areas for wave climate works in Izmir bay (Yüksel Project, 2012)

The extreme wave statistics study was presented in two different ways both non-directionally and for each effective wave direction;

Non-directional; The results of the extreme wave statistics are presented without any wave directions in Table 3.8 and 3.9. According to the extreme wave statistics for the ECMWF's data, the deep water significant wave height (H_{s0}) with the return period of 100 years are ***0.63±0.11 m***, ***0.86±0.15 m***, and *1.55±0.24 m* for points 1,2 and 3 respectively. The periods of these wave heights are ***3.13 s***, ***3.74 s*** *and 4.63 s* respectively.

Table 3.8 The results of the extreme wave statistics by ECMWF's data (Yüksel Project, 2012)

	Return Period (years)				
Study Points	**5**	**10**	**20**	**50**	**100**
	Deep Water Significant Wave Height, H_{s0} (m) **Deep Water Significant Wave Period, T_{s0} (s)**				
1	0.41 ± 0.05 2.51	0.46 ± 0.06 2.68	0.51 ± 0.08 2.83	0.58 ± 0.10 3.01	**0.63 ± 0.11** **3.14**
2	0.56 ± 0.06 3.00	0.63 ± 0.08 3.19	0.70 ± 0.10 3.37	0.79 ± 0.13 3.59	**0.86 ± 0.15** **3.74**
3	1.05 ± 0.10 3.81	1.17 ± 0.13 4.02	1.29 ± 0.16 4.22	1.43 ± 0.21 4.46	1.55 ± 0.24 4.63

According to the extreme wave statistics using IMS's data, the deep water significant wave heights (H_{s0}) with the return period of 100 years are ***0.90±0.06 m***, ***1.11±0.07 m***, and *2.26±0.22 m* for points 1,2 and 3 respectively. The periods of these wave heights are ***3.84 s***, ***4.14 s*** *and 5.54 s* respectively.

Table 3.9 The results of the extreme wave statistics by IMS's data (Yüksel Project, 2012)

	Return Period (years)				
Study Points	**5**	**10**	**20**	**50**	**100**
	Deep Water Significant Wave Height, H_{s0} (m) **Deep Water Significant Wave Period, T_{s0} (s)**				
1	0.75 ± 0.02 3.49	0.78 ± 0.03 3.58	0.82 ± 0.04 3.66	0.87 ± 0.05 3.77	**0.90 ± 0.06** **3.84**
2	0.90 ± 0.03 3.73	0.95 ± 0.04 3.83	1.00 ± 0.05 3.93	1.06 ± 0.06 4.05	**1.11 ± 0.07** **4.14**
3	1.62 ± 0.09 4.69	1.77 ± 0.12 4.91	1.92 ± 0.15 5.11	2.11 ± 0.19 5.36	2.26 ± 0.22 5.54

According to table 3.8 and 3.9, the results of the extreme wave statistics of IMS are observed larger values than the results of the extreme wave statistics of ECMWF.

Directional; the ***directional*** extreme wave statistics is calculated using IMS's data (years 1956-2010) and the results are presented in Table 3.10, 3.11, and 3.12 for three study points.

For the first study point, the extreme wave statistics is presented in Table 3.10. According to these results, the extreme wave heights (H_{s0}) are observed in west-south-west (WSW) and west (W) directions for the return period of 100 years. The deep water significant wave heights for these two directions are 0.99±0.10 and 0.89±0.05 meters respectively. Also the corresponding significant wave periods are 4.02 and 3.81 s respectively.

Table 3.10 The results of the extreme wave statistics by IMS' datas for first study point (Yüksel Project, 2012)

	Return Period (years)				
Effective Direction	**5**	**10**	**20**	**50**	**100**
	Deep Water Significant Wave Height, H_{s0} (m) **Deep Water Significant Wave Period, T_{s0} (s)**				
ENE	0.14 ± 0.00 1.52	0.14 ± 0.00 1.53	0.15 ± 0.00 1.54	0.15 ± 0.00 1.55	0.15 ± 0.00 1.56
E	0.19 ± 0.01 1.76	0.20 ± 0.01 1.81	0.21 ± 0.01 1.85	0.22 ± 0.01 1.91	0.23 ± 0.01 1.95
ESE	0.14 ± 0.00 1.52	0.15 ± 0.00 1.54	0.15 ± 0.00 1.56	0.15 ± 0.01 1.59	0.16 ± 0.01 1.61
SE	0.15 ± 0.00 1.58	0.15 ± 0.00 1.59	0.16 ± 0.00 1.60	0.16 ± 0.00 1.62	0.16 ± 0.00 1.64
SSE	0.18 ± 0.00 1.72	0.18 ± 0.00 1.74	0.19 ± 0.00 1.75	0.19 ± 0.00 1.76	0.19 ± 0.00 1.77
S	0.22 ± 0.00 1.90	0.23 ± 0.01 1.93	0.23 ± 0.01 1.96	0.24 ± 0.01 2.00	0.25 ± 0.01 2.03
SSW	0.25 ± 0.01 2.03	0.26 ± 0.01 2.08	0.28 ± 0.01 2.13	0.30 ± 0.02 2.20	0.31 ± 0.02 2.24
SW	0.37 ± 0.02 2.47	0.41 ± 0.03 2.59	0.45 ± 0.04 2.70	0.49 ± 0.05 2.83	0.52 ± 0.05 2.93
WSW	0.71 ± 0.04 3.40	0.77 ± 0.05 3.56	0.84 ± 0.07 3.70	0.92 ± 0.08 3.89	**0.99 ± 0.10** **4.02**
W	0.74 ± 0.02 3.47	0.77 ± 0.03 3.55	0.81 ± 0.04 3.63	0.85 ± 0.05 3.73	**0.89 ± 0.05** **3.81**
WNW	0.38 ± 0.03 2.49	0.42 ± 0.03 2.63	0.46 ± 0.04 2.75	0.51 ± 0.05 2.90	0.55 ± 0.06 3.00

For the Second study point, the extreme wave statistics are presented in Table 3.11. According to these results, the extreme wave heights (H_{s0}) are observed in west (W), west-north-west (WNW) and west-south-west (WSW) directions for the return period of 100 years. The deep water significant wave heights for these three directions are 1.11±0.0077, 0.89±0.06 and 0.83±0.07 meters respectively. Also the corresponding significant wave periods are 4.14, 3.71 and 3.57 s respectively.

Table 3.11 The results of the extreme wave statistics by IMS' datas for second study point (Yüksel Project, 2012)

	Return Period (years)				
Effective Direction	**5**	**10**	**20**	**50**	**100**
	Deep Water Significant Wave Height, H_{s0} (m) **Deep Water Significant Wave Period, T_{s0} (s)**				
NNE	0.31 ± 0.01 2.18	0.33 ± 0.01 2.25	0.34 ± 0.02 2.30	0.37 ± 0.02 2.37	0.38 ± 0.03 2.43
NE	0.35 ± 0.01 2.33	0.37 ± 0.01 2.38	0.38 ± 0.02 2.44	0.41 ± 0.02 2.50	0.42 ± 0.03 2.55
ENE	0.45 ± 0.02 2.64	0.48 ± 0.02 2.72	0.51 ± 0.03 2.81	0.55 ± 0.04 2.91	0.58 ± 0.04 2.98
E	0.40 ± 0.02 2.48	0.44 ± 0.03 2.59	0.47 ± 0.04 2.70	0.52 ± 0.05 2.84	0.56 ± 0.06 2.93
ESE	0.21 ± 0.00 1.81	0.22 ± 0.01 1.84	0.23 ± 0.01 1.87	0.24 ± 0.01 1.91	0.24 ± 0.01 1.94
SW	0.32 ± 0.02 2.21	0.35 ± 0.03 2.34	0.39 ± 0.04 2.45	0.43 ± 0.05 2.59	0.47 ± 0.05 2.69
WSW	0.63 ± 0.03 3.12	0.68 ± 0.04 3.23	0.72 ± 0.05 3.34	0.78 ± 0.06 3.48	**0.83 ± 0.07** **3.57**
W	0.90 ± 0.03 3.73	0.95 ± 0.04 3.83	1.00 ± 0.05 3.93	1.06 ± 0.06 4.05	**1.11 ± 0.07** **4.14**
WNW	0.71 ± 0.03 3.31	0.75 ± 0.03 3.41	0.80 ± 0.04 3.51	0.85 ± 0.05 3.63	**0.89 ± 0.06** **3.71**
NW	0.40 ± 0.02 2.49	0.43 ± 0.02 2.58	0.46 ± 0.03 2.67	0.50 ± 0.04 2.78	0.53 ± 0.05 2.86
NNW	0.28 ± 0.02 2.06	0.30 ± 0.02 2.16	0.33 ± 0.03 2.25	0.36 ± 0.03 2.37	0.39 ± 0.04 2.45

Table 3.11 Cont.

N	0.26 ± 0.01 2.00	0.27 ± 0.01 2.04	0.28 ± 0.01 2.09	0.30 ± 0.01 2.14	0.31 ± 0.02 2.18

For the third study point, the extreme wave statistics are presented in Table 3.12. According to these results, the extreme wave heights (H_{s0}) are observed in west-north-west (WNW) and north-west (NW) directions for the return period of 100 years. The deep water significant wave heights for these two directions are 1.90±0.16 and 2.44±0.29 meters respectively. Also the corresponding significant wave periods are 5.08 and 5.75 s respectively.

Table 3.12 The results of the extreme wave statistics by IMS' datas for third study point (Yüksel Project, 2012)

	Return Period (years)				
Effective Direction	**5**	**10**	**20**	**50**	**100**
	Deep Water Significant Wave Height, H_{s0} (m) **Deep Water Significant Wave Period, T_{s0} (s)**				
WSW	0.64 ± 0.03 2.95	0.69 ± 0.04 3.06	0.73 ± 0.05 3.16	0.79 ± 0.06 3.28	0.84 ± 0.07 3.37
W	0.62 ± 0.03 2.91	0.66 ± 0.04 2.98	0.69 ± 0.05 3.05	0.72 ± 0.06 3.14	0.75 ± 0.07 3.20
WNW	1.45 ± 0.06 4.44	1.56 ± 0.08 4.60	1.66 ± 0.11 4.75	1.80 ± 0.13 4.94	**1.90 ± 0.16** **5.08**
NW	1.60 ± 0.12 4.67	1.81 ± 0.16 4.95	2.00 ± 0.20 5.21	2.25 ± 0.25 5.53	**2.44 ± 0.29** **5.75**
NNW	1.21 ± 0.08 4.05	1.34 ± 0.10 4.27	1.46 ± 0.13 4.46	1.63 ± 0.16 4.70	1.75 ± 0.19 4.87

In summary, wind and wave statistics were carried out by Yüksel Project (2012) using wind data of ECMWF and IMS for selected study points within the scope of "Rehabilitation of the Izmir Bay and Harbor" project (Table 3.13).

Table 3.13 The studies about wave properties

Studies	ECMWF	IMS
Wind Statistics	x	x
Long-Term Wave Statistics	x	x
Non-Directional, The Extreme Wave Statistics	x	x
Directional, The Extreme Wave Statistics		x

The results of extreme wave statistics are summarized for both directional and non-directional analyses, for three study points in Table 3.14. As it is given in Table 3.14, the extreme deep water significant wave height and its corresponding significant period at the inner bay are found to be approximately 1.00 m and 4.00 s respectively for the return period of 100 years.

Table 3.14 The extreme wave values (Yüksel Project, 2012)

			Return Period (years)				
Study Points	**Data Source**	**Effective Direction**	**5**	**10**	**20**	**50**	**100**
			Deep Water Significant Wave Height, H_{s0} (m) Deep Water Significant Wave Period, T_{s0} (s)				
1	IMS	Non-Directional	0.75 ± 0.02 3.49	0.78 ± 0.03 3.58	0.82 ± 0.04 3.66	0.87 ± 0.05 3.77	**0.90 ± 0.06 3.84**
1	IMS	WSW	0.71 ± 0.04 3.40	0.77 ± 0.05 3.56	0.84 ± 0.07 3.70	0.92 ± 0.08 3.89	**0.99 ± 0.10 4.02**
1	IMS	W	0.74 ± 0.02 3.47	0.77 ± 0.03 3.55	0.81 ± 0.04 3.63	0.85 ± 0.05 3.73	**0.89 ± 0.05 3.81**
2	IMS	Non-Directional	0.90 ± 0.03 3.73	0.95 ± 0.04 3.83	1.00 ± 0.05 3.93	1.06 ± 0.06 4.05	**1.11 ± 0.07 4.14**
2	IMS	W	0.90 ± 0.03 3.73	0.95 ± 0.04 3.83	1.00 ± 0.05 3.93	1.06 ± 0.06 4.05	**1.11 ± 0.07 4.14**
2	IMS	WNW	0.71 ± 0.03 3.31	0.75 ± 0.03 3.41	0.80 ± 0.04 3.51	0.85 ± 0.05 3.63	**0.89 ± 0.06 3.71**

Table3.14 Cont.

2	IMS	WNW	0.63 ± 0.03 3.12	0.68 ± 0.04 3.23	0.72 ± 0.05 3.34	0.78 ± 0.06 3.48	**0.83 ± 0.07 3.57**
3	IMS	Non-Directional	1.62 ± 0.09 4.69	1.77 ± 0.12 4.91	1.92 ± 0.15 5.11	2.11 ± 0.19 5.36	2.26 ± 0.22 5.54
3	IMS	NW	1.60 ± 0.12 4.67	1.81 ± 0.16 4.95	2.00 ± 0.20 5.21	2.25 ± 0.25 5.53	2.44 ± 0.29 5.75
3	IMS	WNW	1.45 ± 0.06 4.44	1.56 ± 0.08 4.60	1.66 ± 0.11 4.75	1.80 ± 0.13 4.94	1.90 ± 0.16 5.08

3.4.2 Sea Level Changes

There are a lot of sea level monitoring stations in the most of the coasts of the world in order to follow the sea level changes. The sea level monitoring studies have been carried out since 1927 in Turkey. These studies have been handled in three groups that I period (1927-1983), II period (1984-1998) and III period (1998-cont.). The sea level changes in and around İzmir bay have been followed at the Menteş station by Yıldız et. al. (2003) from General Command of Mapping (GCM) since 1984 (Figure 3.18).

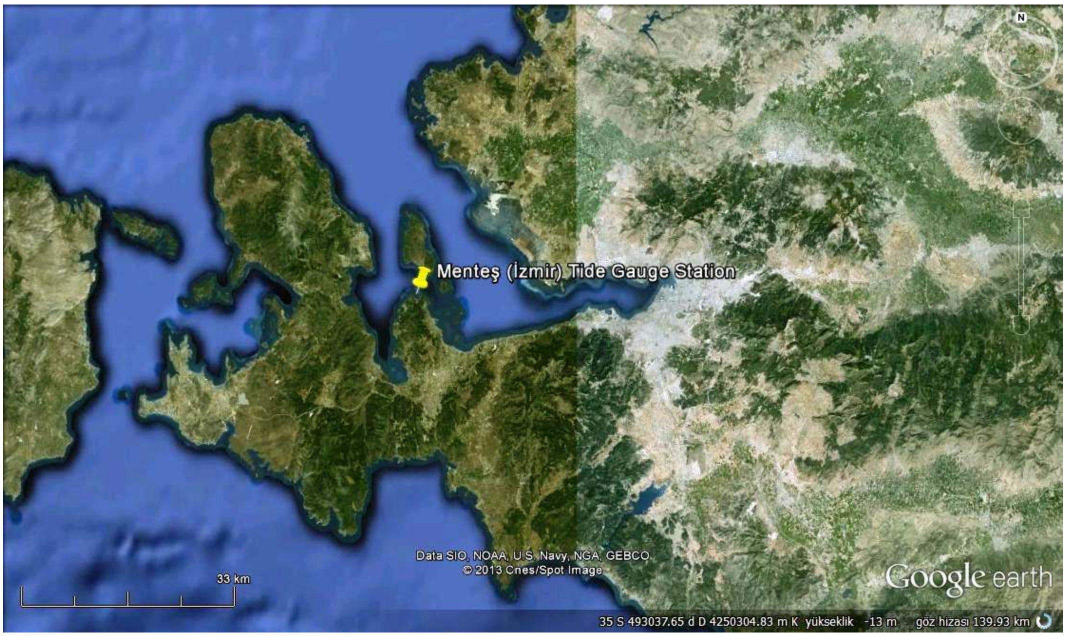

Figure 3.18 Menteş (İzmir) tide gauge station (1984-2010) (Google Earth, 2013)

Table 3.15 Geographical location and positioning of Menteş tide gauge station (ΔH is height difference between machine zero and Roper tide gauge) (Yıldız et. al., 2003)

Station	N	E	ΔH (m)	Station Datum (m)
Menteş (İzmir)	38°25'60.00"	26°42'60.00"	0.6851 (MAR 85-1)	3.442

By Yıldız et. al. (2003), the hourly values of the sea level had been obtained by manual digitization of diagrams until 1995. Later, these values have been obtained with using quality control software from analog tide gauge stations since 1995. After originated time and datum errors in raw sea level measuring has been resolved from hardware and operators, daily and monthly average values of sea level has been obtained. The hourly average values of the change in mean sea level measured by Menteş station are given in Figure 3.19.

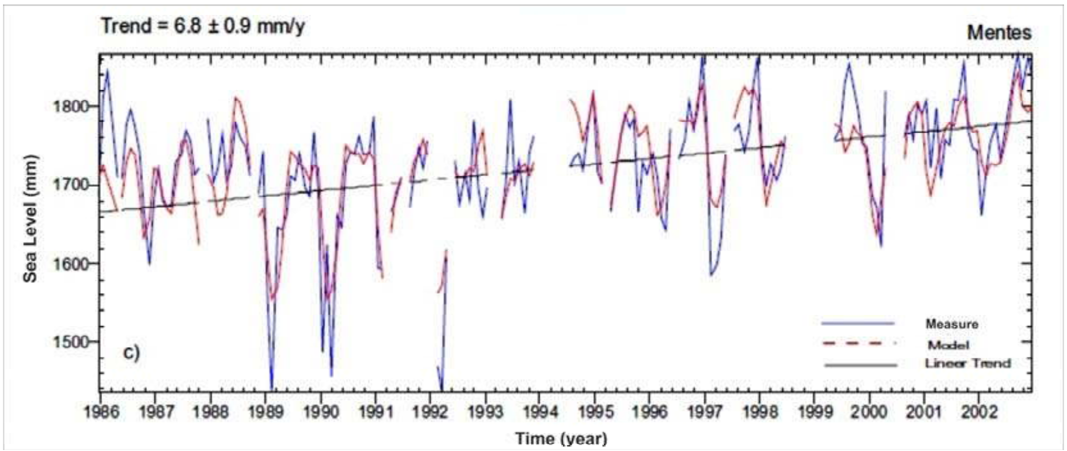

Figure 3.19 The changes of the average sea level in Menteş tide gauge station (blue line, the monthly changes of the sea level; red line, the modelled values of the sea level; black line, the trend of the sea level) (Yıldız et. al., 2003)

As seen from Figure 3.19, the mean sea level is determined to be rising 6.8±0.9 mm/year (Figure 3.19). When the maximum, minimum, and average changes in the sea level are investigated, the found results are seen to be parallel to the trend of the sea level in harmonic analysis (Figure 3.19). In addition, the average daily variation of the mean sea level is approximately 20 cm with a maximum of 60 cm within years 1985-2002 as given by Yıldız et. al. (2003) in Figure 3.21 and 3.22.

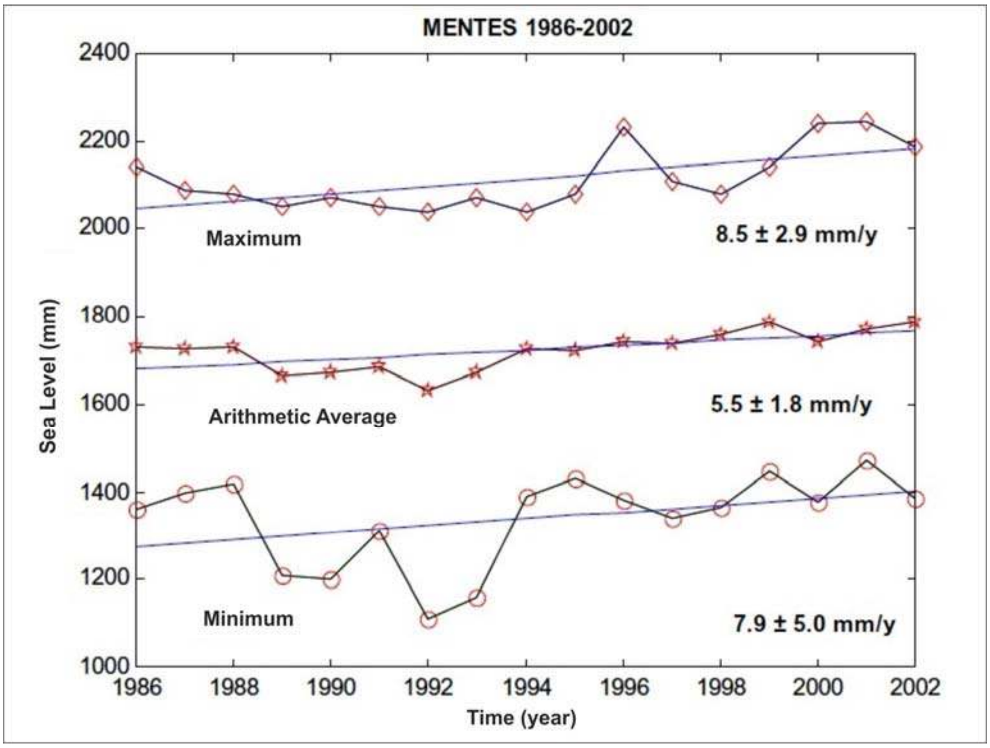

Figure 3.20 The max, min, and average changes of the sea level during the period of 1985-2002 in Menteş tide gauge station (Yıldız et. al., 2003)

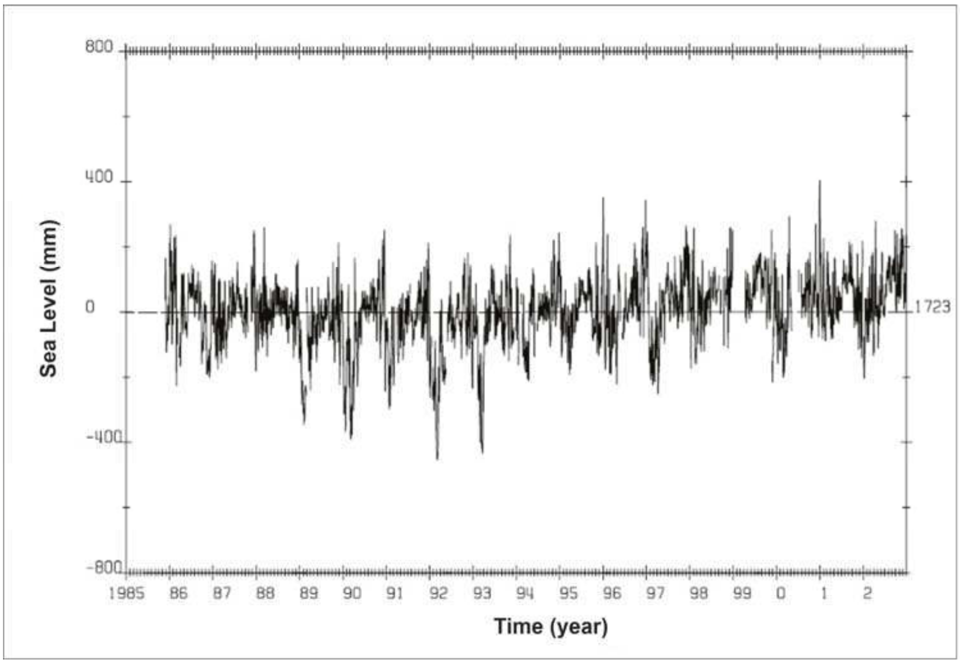

Figure 3.21 The daily average values of the changes of the sea level during the period of 1985-2002 in the tide gauge station of Menteş (Yıldız et. al., 2003)

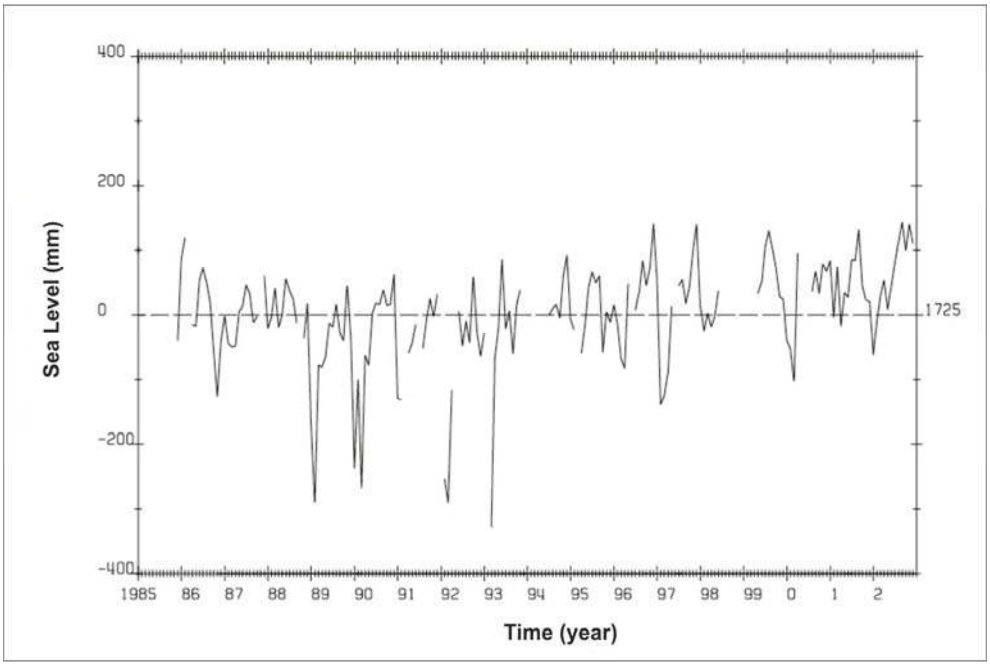

Figure 3.22 The monthly average values of the changes of the sea level during the period of 1985-2002 in the tide gauge station of Menteş (Yıldız et. al., 2003)

In this thesis study, the maximum change in the mean sea level has been taken as approximately 80 cm considering the worst conditions in the slope stability analysis of the navigation channel.

3.4.3 Current Regime

Numerous studies have been done about the current measurements and the mathematical modeling of current regime for Izmir bay from past to present. Institute of Marine Sciences and Technology, Dokuz Eylül University (IMST, 1977-1978) measured current velocities for the Izmir bay within the scope of "The Construction and The Expansion of Alsancak Port and Casting Areas Research". The first mathematical modeling of the circulation for the inner and middle regions of Izmir bay was studied by Uslu & Saner (1987). Karahan (1988) modeled current regime for the whole bay using current measurements of IMST (1977-1978). Also the effects of tide and wind on current measurements were investigated. According to this study, Karahan (1988) presented that the current velocities reaching 3-5 cm/s from middle bay to inner bay.

The actual information about current regime of Izmir bay was benefited from the prepared the environmental impact assessment report. According this report, IMST (2012) measured the current regime of bay in long-term. The measurement station was located at four different points of bay as north and south of Yenikale, Göztepe and Bostanlı (Figure 3.23).

Figure 3.23 The located current measurement stations in İzmir bay

Bostanlı station was located at a depth of 10.8 m. The current velocities were measured between 0.09 and 14.40 cm/s. Average current velocity was calculated as 4.13 cm/s. The dominant current direction is determined to be between south (S) and west (W).

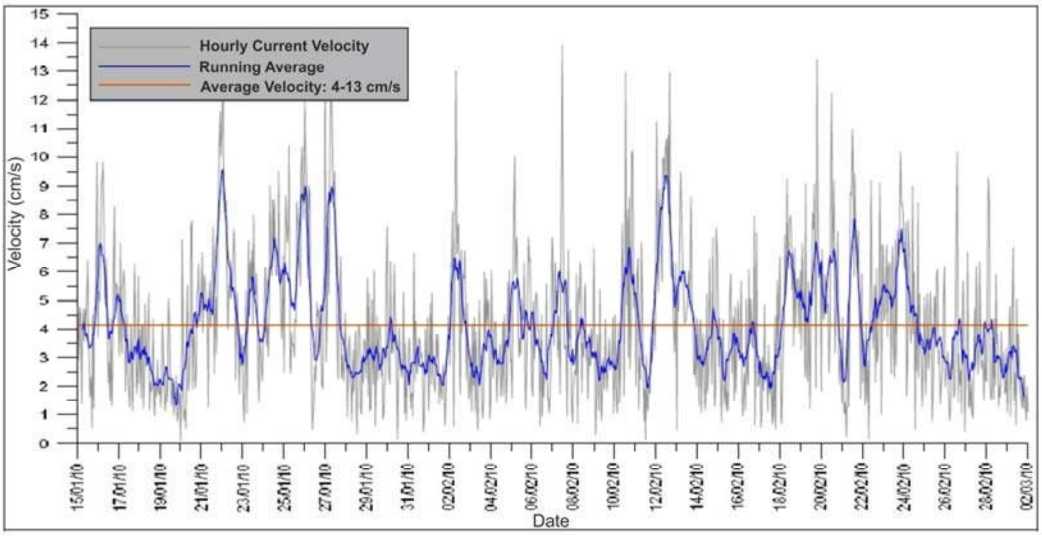

Figure 3.24 The hourly variation of measured current velocity for Bostanlı station in between 15.01.2010 and 02.03.2010 (Dokay Engineering, 2013)

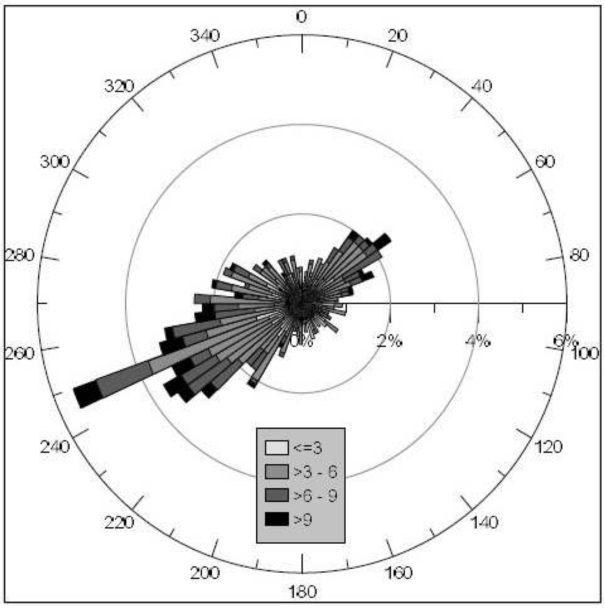

Figure 3.25 The measured current velocities and directions for Bostanlı station in between 15.01.2010 and 02.03.2010 (Dokay Engineering, 2013)

Göztepe station was located at a depth of 10.6 m. The current velocities were measured between 0.10 and 17.28 cm/s. Average current velocity was calculated as 3.08 cm/s. There is not any dominant current direction in the zone. However the currents are mostly orientated from South-East to North-West.

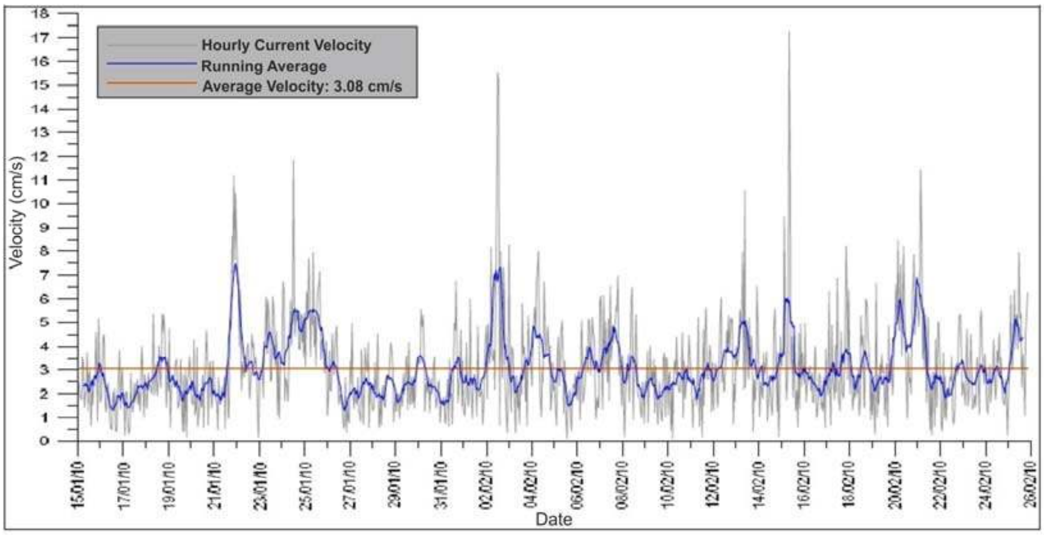

Figure 3.26 The hourly variation of measured current velocity for Göztepe station in between 15.01.2010 and 02.03.2010 (Dokay Engineering, 2013)

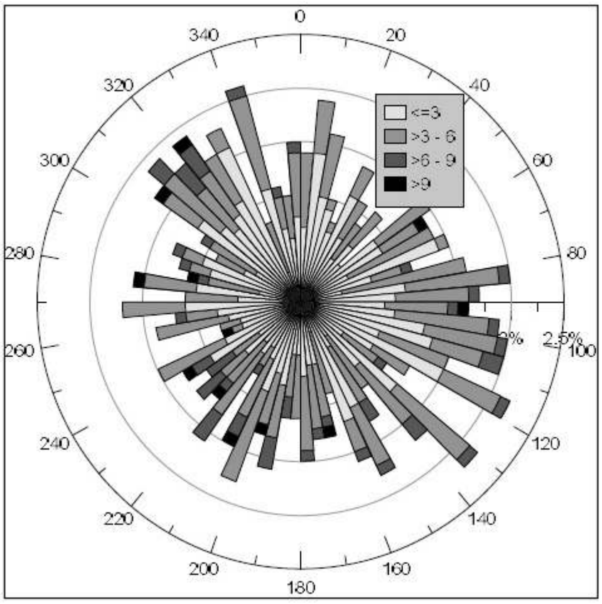

Figure 3.27 The measured current velocities and directions for Göztepe station in between 15.01.2010 and 02.03.2010 (Dokay Engineering, 2013)

The south Yenikale station was located at a depth of 11.8 m. The current velocities were measured between 0.32 and 17.58 cm/s. Average current velocity was calculated as 6.20 cm/s. The currents are orientated from South to North.

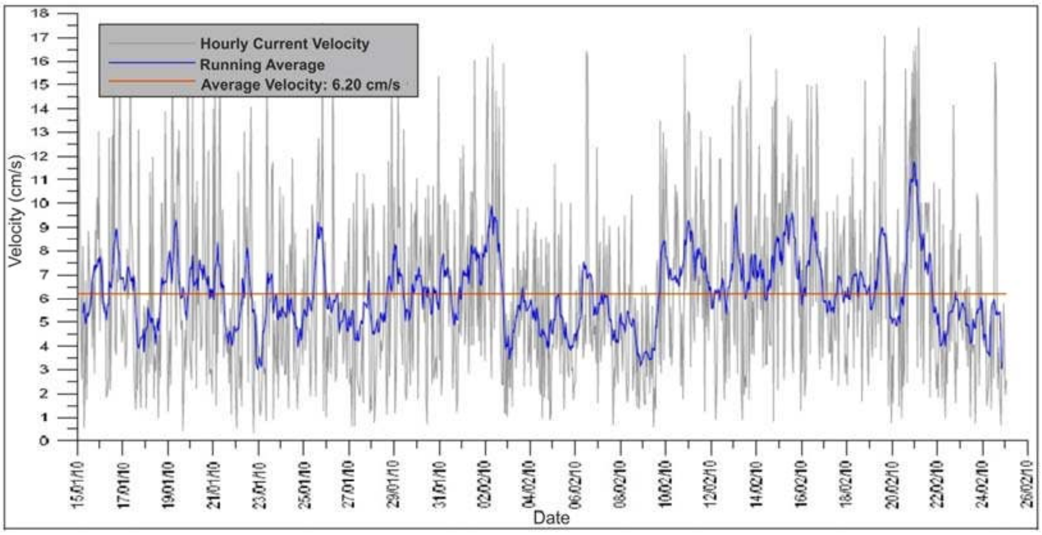

Figure 3.28 The hourly variation of measured current velocity for the south of Yenikale station in between 15.01.2010 and 02.03.2010 (Dokay Engineering, 2013)

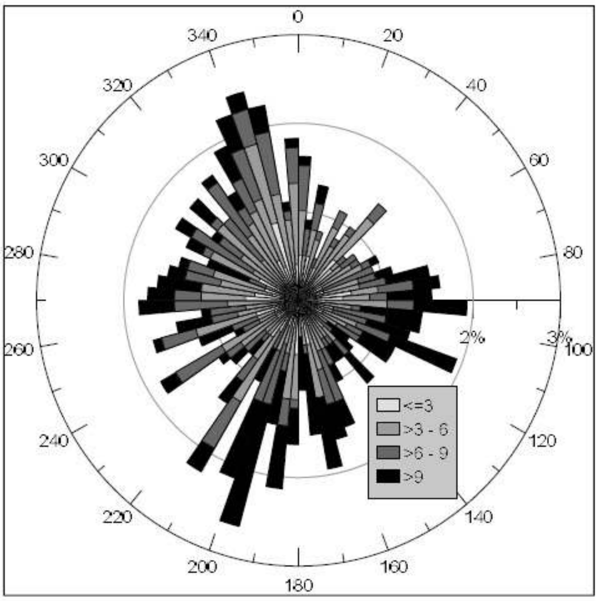

Figure 3.29 The measured current velocities and directions for the south of Yenikale station in between 15.01.2010 and 02.03.2010 (Dokay Engineering, 2013)

The north Yenikale station was located at a depth of 11.2 m. The current velocities were measured between 0.14 and 17.33 cm/s. Average current velocity was calculated as 5.9 cm/s. The dominant current directions are West and East.

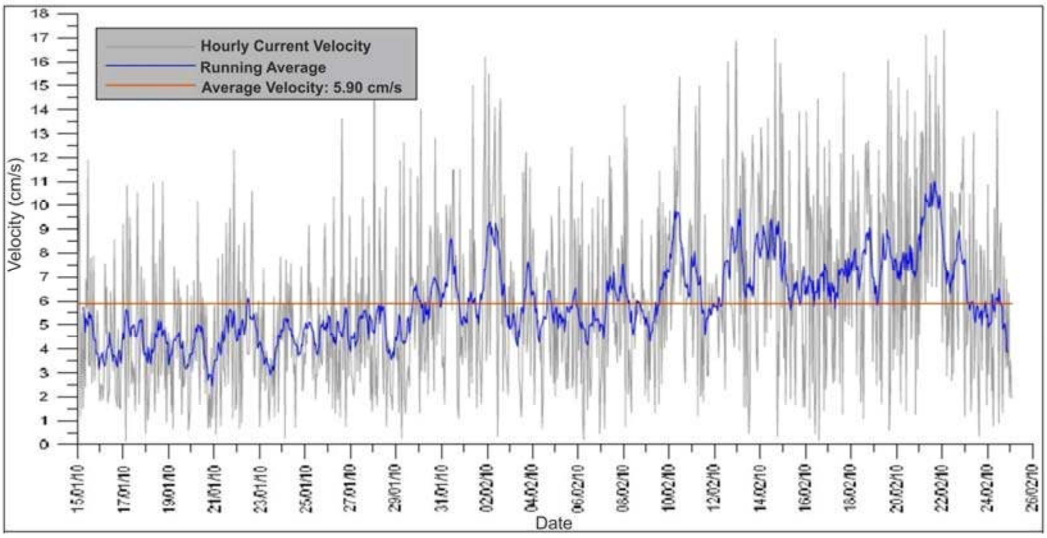

Figure 3.30 The hourly variation of measured current velocity for the north of Yenikale station in between 15.01.2010 and 02.03.2010 (Dokay Engineering, 2013)

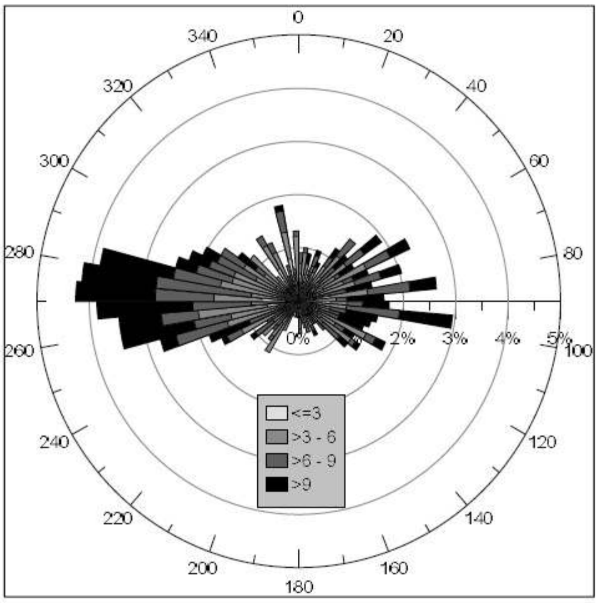

Figure 3.31 The measured current velocities and directions for the north of Yenikale station in between 15.01.2010 and 02.03.2010 (Dokay Engineering, 2013)

The current regime of İzmir bay was determined at two different depths: water surface and 10.0 m water depth. The measured values are observed to be 5-7 cm/s for both surface currents and currents at 10.0 m water depth. However the surface currents may increase up to 15 cm/s with effect of the wind.

Moreover, disparities in current directions are observed depending on water depth.

- At water surface, Surface currents entry from the front of Yenikale to inner bay. The currents are observed to have orientation from South to North of inner bay (Figure 3.32). The currents go out of the inner bay increasing in velocity.

- At a depth of 10.0 meter, the currents are observed to have orientation from Yenikale to Alsancak port (Figure 3.33).

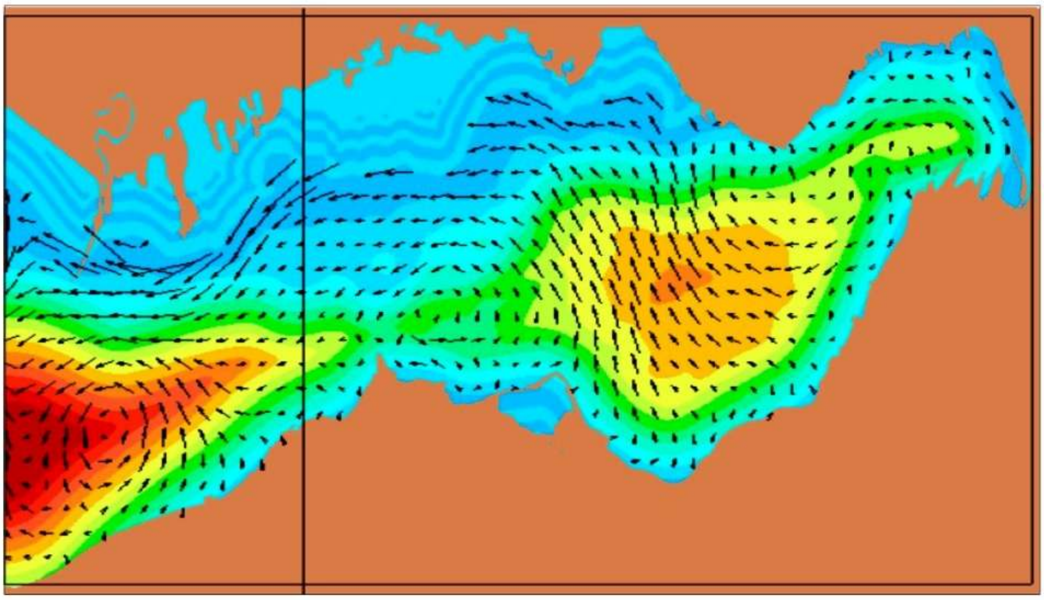

Figure 3.32 The modeled current regime for surface current on the bathymatric map (Dokay Engineering, 2013)

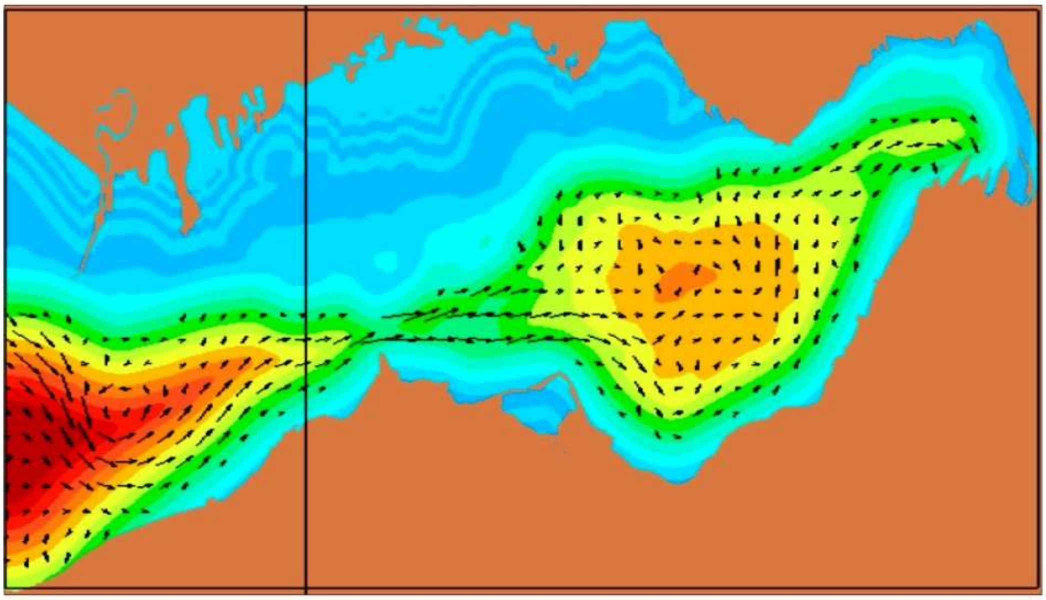

Figure 3.33 The modeled current regime for the depth of average 10.0 meter (Dokay Engineering, 2013)

CHAPTER FOUR
TRIGGERING MECHANISMS

4.1 Introduction

Many geohazards can affect seriously or slightly marine and continental formation and seafloor slope stability. The stability of seafloor and submarine slopes depend on different factors. The cause instability factors are also referred to as triggering mechanisms. These triggering mechanisms can be follows;

- Earthquakes (and Faulting etc.)
- Sediment Accumulation and Erosion Processes
- Tectonic Reasons (Magma, Volcanic Activity etc.)
- Wind waves
- Sea Level Changes (Tide etc.)
- Change of Certain Physical-Chemical Properties
- Gas Hydrate Dissociation
- Long Period Waves (Tsunamis, tidal wave, storm surge, and surf beat)
- Flood Events
- Creep
- Human Activity

The triggering mechanisms are classified with respect to their impact on seafloor slope stability in Figure 4.1. The accumulation of sediment, earthquakes, tectonic reasons, and current and waves (as tsunamis) have significant effects as shown in Figure 4.1.

Submarine slope slides might be caused by either only one triggering mechanism or multiple mechanisms occurring at the same time. Because the many different mechanisms and factors can triggers each other as shown in Figure 4.2. Figure 4.2 shows a flowchart of the known triggering mechanisms of submarine landslides.

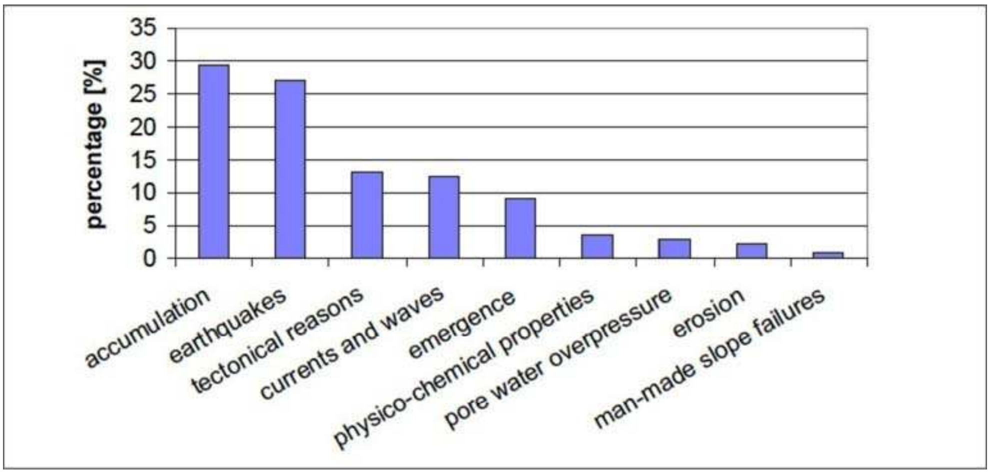

Figure 4.1 Percentage of reported slope failures; classification in triggering mechanisms (Raaijmakers, 2005)

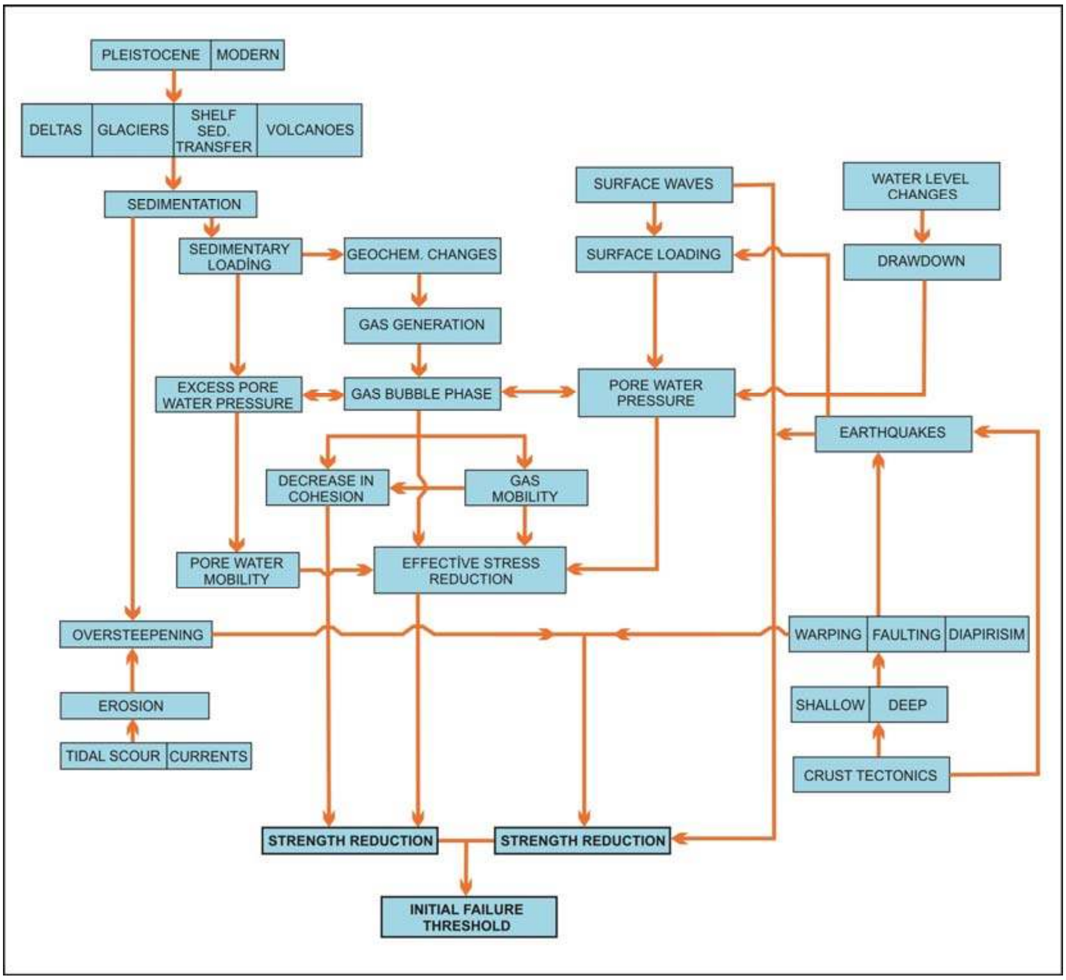

Figure 4.2 A flow chart of serve of the triggering mechanisms of submarine landslides (Feeley, 2007)

In this chapter, the identified triggering mechanisms are described and explained briefly how each mechanism affects submarine slope stability. Also the possible triggering mechanisms, which may disrupt the stability of navigation channel in İzmir bay and surrounding are referred briefly.

4.2 Triggering Mechanisms

4.2.1 Tectonic Movements

One of the triggering mechanisms is the tectonic movements that include volcanic activities and faults. Therefore tectonic movements and earthquakes are very closely related.

More than 80 percent of the surface above and below the sea is of volcanic origin. The vast majority of the volcanic activity that continually remakes the surface of Earth takes place at the bottom of the ocean, where most of the world's volcanoes are located. Most of the seafloor landslides in the ocean environment are the end result of volcanic activities.

As a result of volcanic activities, the volcanic and erupting lava directly accumulates over the top surface of the seafloor slopes. After that, rapid soil accumulation can produce an increase in total stresses and shear strength of soil decreases because of rapid deposition. Therefore the top of the seafloor slope becomes unconsolidated, and the soil moves. As a result, the submarine slopes lose stability, and slips occur. This situation generally applies to the oceans as shown in Figure 4.3.

There is not any volcanic activity around İzmir bay, so volcanic activities is not a factor affecting seafloor slope's stability in İzmir bay and environment. However tectonic reasons play a very active role in and around İzmir.

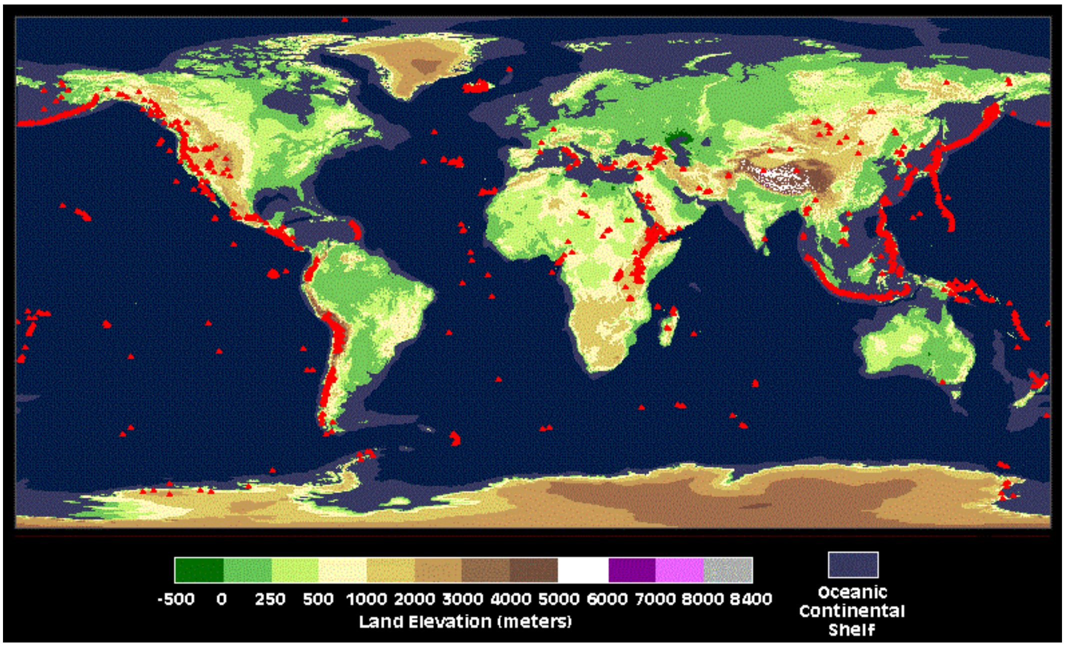

Figure 4.3 This map shows the location of active, inactive, and extinct volcanoes throughout the world (Prentiss, n.d.)

The faults are neotectonic structures in and around İzmir bay. These neotectonic structures extend in three main directions as E-W, NE-SW and NW-SE. However E-W trending structures which are more dominant than other structures in terms of the morphologic. These structures show normal fault character to the western end of İzmir bay and graben system. Especially, NE-SW and NW-SE directional faults are dominant around area. Although all of these structures shows different kinematic properties, the region has a very complex structure. The most important and active faults are İzmir, Bornova, Gülbahçe and Tuzla in İzmir bay and environment. In addition to these faults, Küçük Menderes, Foça-Bergama, Karaburun, Çandarlı, Dumanlı Dağ, Cumaovası and Gümüldür faults play important roles in shaping the region’s (Coşkun, 2009). Therefore large and small faults cause medium and small intensity earthquakes observed in and around İzmir bay (Figure 4.4).

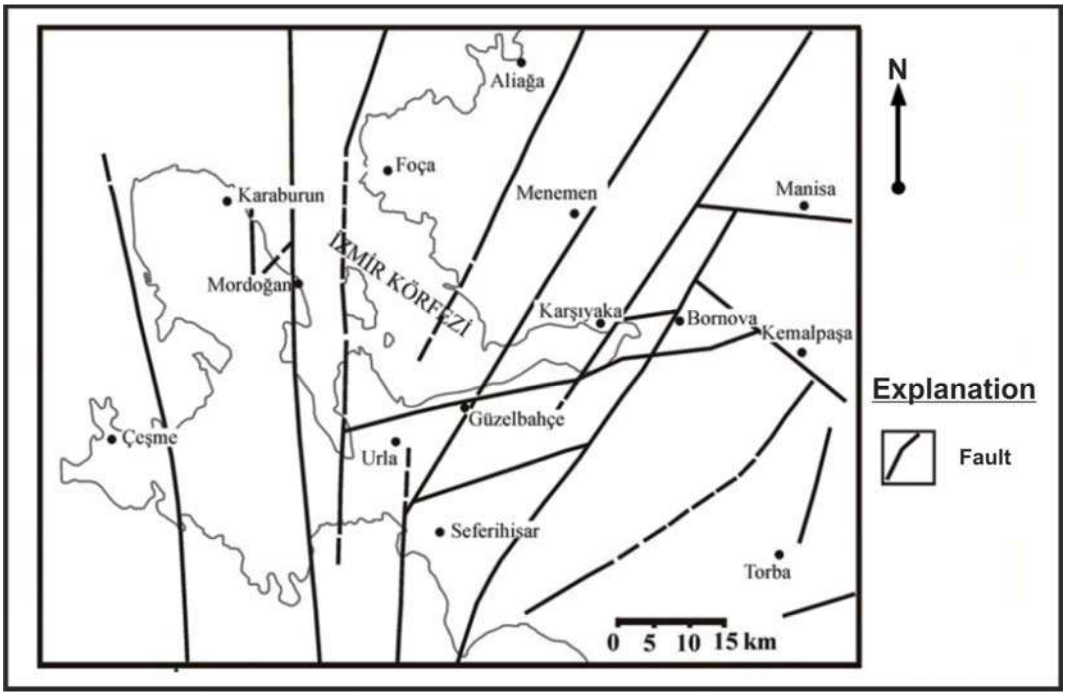

Figure 4.4 Faults around İzmir (Sonuvar, 2004)

In the previous studies, Ekiz (2005) explained the seismic activities and seismological properties of the Izmir bay shown on seismotectonic map. He found that the earthquake activities are mainly due to dip-slip and strike-slip faults in the region. Ekiz (2005) & Ocakoğlu et. al. (2004) denoted that the jamming-component of N-S and NE-SW directional active fault systems are observed according to the principal stresses and pressure axis maps.

4.2.2 Earthquakes

Earthquakes and faults are important triggering mechanisms that result from plate tectonic activity. The most effective sudden trigger mechanism of all triggering mechanisms is earthquakes. Earthquakes can increase the driving stresses in the slope via seismic accelerations and also reduce the shear strength in the soil via liquefaction (Hance, 2003).

Hance (2003) gives "A global seismic hazard map provided by Giardini et. al. (1999) in Figure 4.5. This map only includes the seismic hazard for regions of the continental crust and not the oceanic crust, i.e. seafloor".

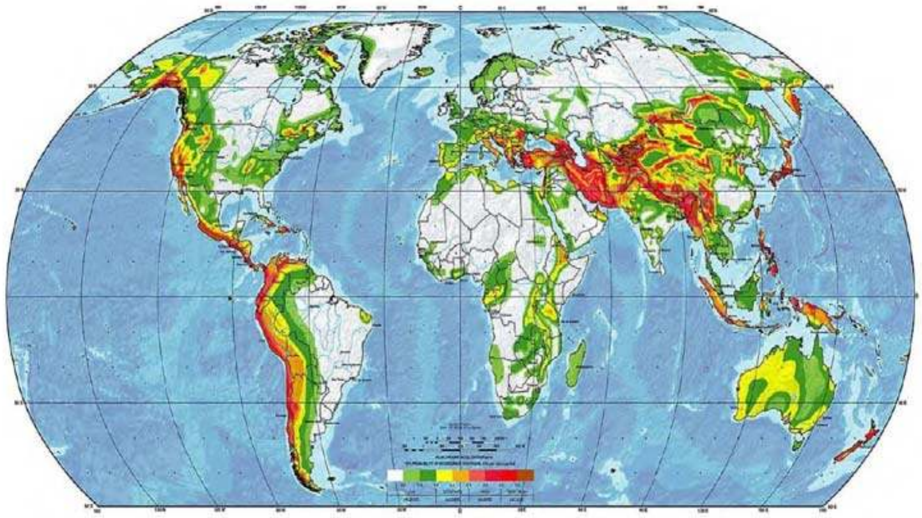

Figure 4.5 Global seismic hazard map by Giardini et. al., (1999) (Hance, 2003)

When the past earthquakes are investigated around İzmir bay, there is an increase in the number of earthquake occurrence after specially 1985 (Figure 4.6). Coşkun (2009) notes that the numbers of the earthquakes had been measured more than 100 between 1992 and 1994. This number had passed about to 450 in 2005. Generally, the magnitude of the most of the earthquakes had been 3-3.9 (Figure 4.6).

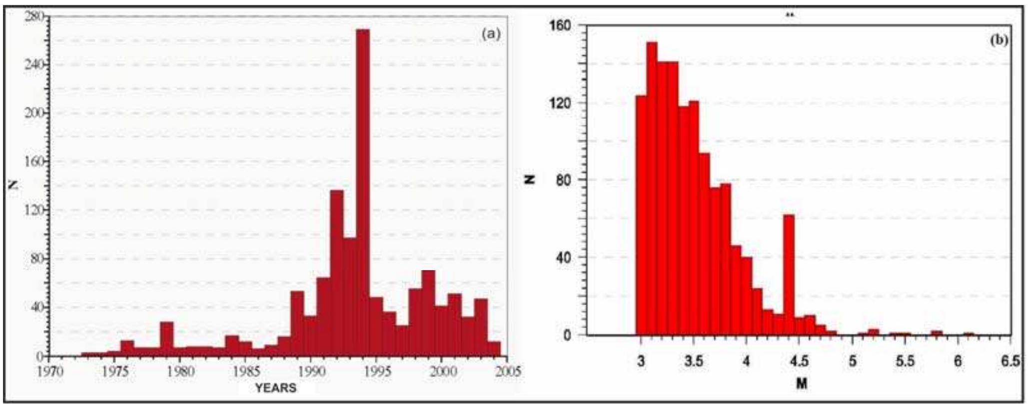

Figure 4.6 a)The number of earthquake occurrence according to years in and around İzmir – N is earthquake number, b) Earthquake magnitude relationship between the number of occurrences (Ekiz, 2005)

Looking at the distribution of the epicenters of the earthquakes (see Figure 4.7), they are mostly focused in the Aegean Sea, along Foça-Bergama and Seferihisar-Cumaovası line, Karaburun peninsula and along Tuzla fault, and these earthquakes are observed to be closely located to each other.

Coşkun (2009) denoted that “The earthquakes focus along main grabens in these places and are observed in form of conjugate pairs. Since there exist many horst and grabens that are linked to each other.

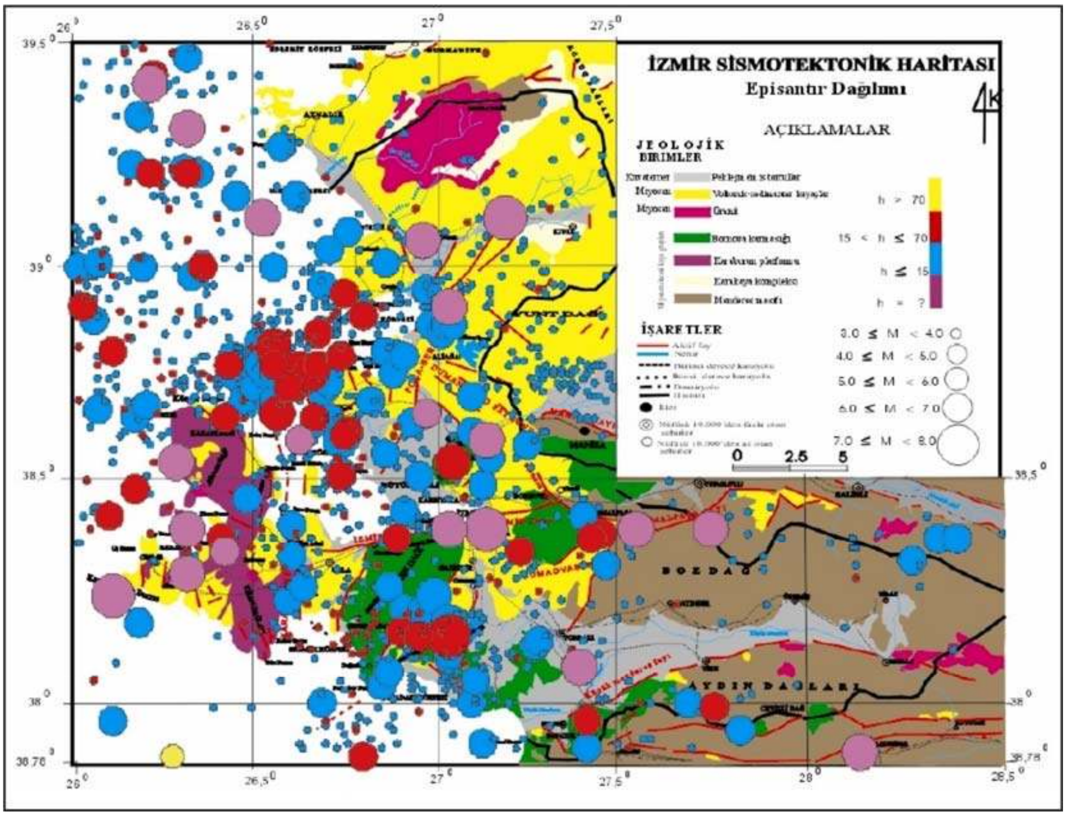

Figure 4.7 The prepared distribution of epicenters for seismotectonic map of İzmir using datas of U.S.G.S (Ekiz, 2005)

Ekiz (2005) gives detailed information on the properties of earthquakes observed in Aegean region and then fault plane solutions. The information of the some important earthquakes is given in Table 4.1 such as date, location, time, latitude, longitude, depth, magnitude, and energy. The distribution of these earthquakes in between 1949 and 2003 is shown as Figure 4.8.

Table 4.1 The some important earthquakes occurred in Aegean region between 1949 and 2003 (Ekiz, 2005)

No	Date (dd/mm/yy)	Location	Time	Latitude	Longitude	Depth (km)	Magnitude (M_w)	Energy ($x10^{20}$) ERG
1	23/07/1949	Karaburun	-	38.60	26.20	10.0	6.7	75.8578
2	28/03/1969	Alaşehir	01:48:30	38.50	28.40	6.4	4.0	14.4544
3	06/04/1969	Karaburun	03:49:33	38.40	26.40	16	5.5	0.1
4	26/04/1972	Western Anatolia	06:30:23	39.40	26.30	18	5.0	0.0063095
5	01/02/1974	İzmir	00:01:02	38.50	27.20	24	5.2	0.0019
6	16/06/1979	Aegean Sea	18:42:03	38.46	26.77	15	5.4	0.0575
7	23/04/1984	Kuşadası	12:11:35	37.83	26.87	27	4.8	0.00208
8	18/12/1985	Midilli	05:46:00	39.20	26.17	17	5.0	0.00630
9	15/08/1989	Midilli	17:03:29	39.18	26.29	10	4.6	0.00069
10	06/11/1992	İzmir	19:08:13	37.84	26.98	24.5	6.1	1.58489
11	28/01/1994	Manisa	15:45:32	38.97	27.01	15	5.2	0.01905
12	24/05/1994	Karaburun	02:45:32	38.66	26.23	21.4	4.9	0.00363
13	10/04/2003	Seferihisar	00:40:11	38.05	26.86	15	5.7	0.30199
14	10/04/2003	Seferihisar	00:40:15	38.22	26.95	13	5.8	0.52440
15	17/04/2003	Kuşadası	22:34:29	37.92	26.75	15	5.2	0.01905

Table 4.2 The accelerations calculated for some important earthquakes occurred in Aegean region between 1949 and 2003

No	Location	Magnitude (M_w)	Distance (km)	a (g)	No	Location	Magnitude (M_w)	Distance (km)	a (g)
1	Karaburun	6.7	79	0.03	**9**	Midilli	4.6	106	0.003
2	Alaşehir	4.0	116	0.001	**10**	İzmir	6.1	66	0.02
3	Karaburun	5.5	60	0.018	**11**	Manisa	5.2	60	0.01

Table 4.2 Cont.

4	Western Anatolia	5.0	127	0.003	**12**	Karaburun	4.9	78	0.007
5	İzmir	5.2	12	0.12	**13**	Seferihisar	5.7	46	0.03
6	Aegean Sea	5.4	27	0.05	**14**	Seferihisar	5.8	25	0.08
7	Kuşadası	4.8	69	0.008	**15**	Kuşadası	5.2	63	0.01
8	Midilli	5.0	117	0.003	**-**	-	-	-	-

Figure 4.8 The distribution of the some important earthquakes in between 1949 and 2003

For engineering analysis, numerous methods have been provided by researchers for analyzing the effect of earthquake on engineering. One of these methods is Newmark-Rosenbluenth (1971) which is based on attenuation relations. The equation of Newmark-Rosenbluenth Method (1971) is as follow;

$$a = 1230e^{0.8M}(R+13)^{-2} \qquad \text{Eq 4.1}$$

Where; a is earthquake acceleration (g), R is perpendicular distance to earthquake generating fault (km), and R is taken 12 km, M is earthquake magnitude.

Newmark-Rosenbluenth method (1971) is used to obtain earthquake accelerations based on Table 1 for the earthquakes occurred in the Aegean region. The calculated earthquake accelerations values are given in Table 4.2.

According to Table 4.2, the minimum earthquake acceleration is found 0.001 (g) and the maximum earthquake acceleration is found 0.12 (g) depending on distance (R) and magnitude (M). In general, the distances are very high between the earthquake focal points and study area for the earthquakes presented in Table 4.1. Therefore the earthquake accelerations calculated are found to be very low.

Additionally, the earthquake acceleration is calculated for gradually increasing magnitude in the fixed distance range for the chosen İzmir-Bornova (No.5 in Figure 4.8). The earthquake acceleration calculated is given in Table 4.3. Two different earthquake accelerations are selected as **0.12 g** and **0.23 g** for submarine slope stability analysis.

Table 4.3 The earthquake accelerations calculated for No.5 (*used)

Description	**Calculation Values**			
M	5.2	5.5	6.0	6.5
R (km)	12	12	12	12
a (g)	**0.12***	0.16	**0.23***	0.35

4.2.3 Sediment Accumulation and Erosion Processes

Sedimentation and erosion processes are complex triggering mechanisms. Because they vary significantly with respect to time and location (Hance, 2003). Sediment accumulation may be both long-term and short-term (suddenly) in terms of time.

Accumulation of the short-termed heavy sedimentation is because of large river floods and the long-termed high sedimentation is observed at river mouths forming deltas. Sedimentation processes are influential in the most marine environments including fjords, river deltas, submarine canyon-fan system, open continental slopes and oceanic volcanic islands and ridges (Hance, 2003). Specially the most affected ones by sedimentation processes are man-made circulation and navigation channels.

According to Hence (2003), sedimentation and erosion processes can cause submarine slope failure via direct and indirect ways. For example, Terzaghi (1956) notes that rapid sediment deposition can produce an increase in total stresses at a rate faster than the rate of dissipation of excess pore water pressures, which leads to under consolidation of soils and correspondingly low shear strength (Hence, 2003).

4.2.4 Wave Loads (and Wave Properties)

The mathematical description of the periodic water wave is very difficult. The best way is to be assumed linear wave theory in order to describe and understand the water wave behavior (Figure 4.9).

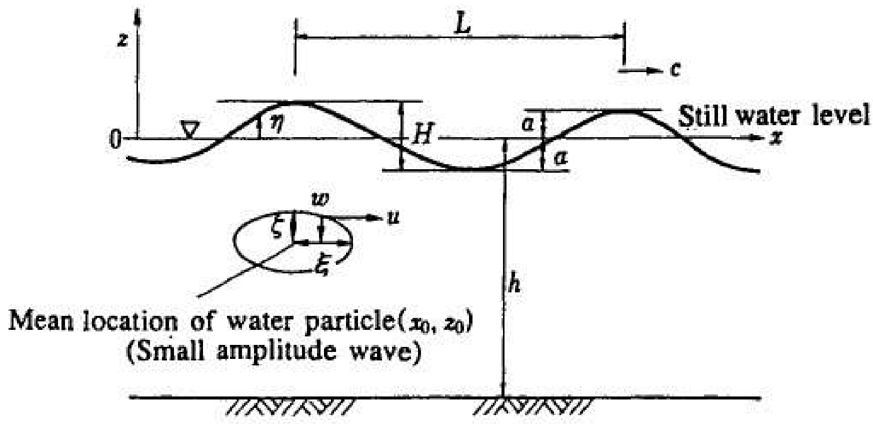

Figure 4.9 Wave profile (Sawaragi, 1995)

The linear wave theory defines the vertical displacement (η) of the sea surface from the still water level (SWL) as a function of time and space.

$$\eta = a\cos\left(\frac{2\pi}{L}x - \frac{2\pi}{T}t\right) \qquad \text{Eq 4.2}$$

The used Bernoulli equation is as follow for linear wave theory;

$$\frac{p}{\rho} = \frac{\partial\phi}{\partial t} - gz \qquad \text{Eq 4.3}$$

When the wave celerity is used for water wave in x-direction, Bernoulli equation is as follow;

$$\frac{p}{\rho} = -gz + \frac{g\cosh k(d+z)}{\cosh kd} a\sin(kx - \omega t) \qquad \text{Eq 4.4}$$

The acting forces are two such as static and dynamic on the seafloor due to wave (see Figure 4.7). The total, static and dynamic pressure may be denoted as follow Eq 4.5 benefit from Bernoulli Equation. T*he total wave load is composed of two components: static and dynamic pressures.*

- Static pressure is given as;

$$P_h = \rho gz \qquad \text{Eq 4.5}$$

- Dynamic pressure is given as;

$$P_d = \frac{\rho g\cosh k(z+d)}{\cosh kd}\eta \qquad \text{Eq 4.6}$$

- Total pressure is given as ;

$$P_t = \frac{\rho g\cosh k(z+d)}{\cosh kd}\eta - \rho gz \qquad \text{Eq 4.7}$$

Where; ρ is the density of water (typically around 1025 kg/m^3 for sea water), g is the gravitational acceleration, k is the wave number (k=2pi/L in which L is the wave length), z (-d) is the distance from still water level (SWL) to bottom, η is instantaneous vertical displacement of water surface above SWL, a is wave amplitude

Vertical Variations of wave pressure

Vertical variations of pressure is given for both under the crest and under the trough, on the sea bed (z=-d).

For under the crest;

$$\eta = a\cos(kx - \sigma t) = a \qquad \text{Eq 4.8}$$

For under the trough;

$$\eta = a\cos(kx - \sigma t) = -a \qquad \text{Eq 4.9}$$

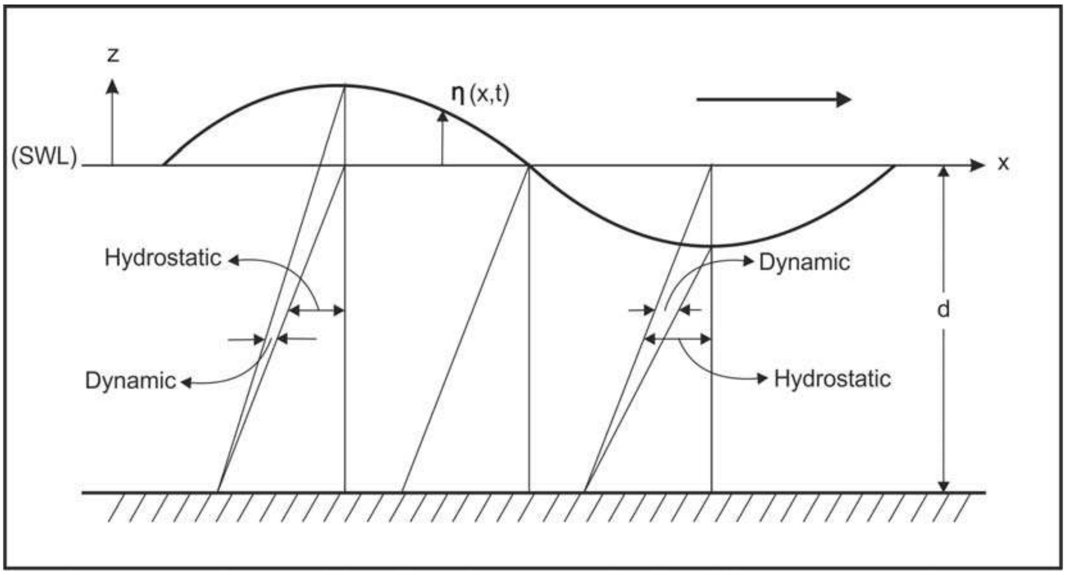

Figure 4.10 Hydrostatic and dynamic pressure components at various phase positions in a progressive water wave

Table 4.4 Total wave pressure values at sea bed (z=-d) (Ergin, 2009)

Wave Position	**Sea Bed (z=-d)**		
	Hydrostatic Pressure (P_h)	**Dynamic Pressure (P_d)**	**Total Pressure (P_t)**
Under Crest	ρ g d	a ρ g / cosh kd	$P_t = P_h + P_d$
Under Trough	ρ g d	-a ρ g / cosh kd	$P_t = P_h - P_d$

Dean & Dalrymple (1984) denotes that if the dynamic pressure p_d is isolated by subtracting out the mean hydrostatic pressure, then η is as follows, and $K_p(-h)$ is a function of the angular frequency of the waves (see Eq 4.11).

$$\eta = \frac{\rho_D}{\rho g K_p(-h)} \qquad \text{Eq 4.10}$$

$$K_p(-h) = \frac{1}{\cosh kh} \qquad \text{Eq 4.11}$$

According to Dean & Dalrymple (1984), because of the dependency of the pressure response factor on the wave frequency, if the wave has short period, the value of K_p is very small, but if the wave has long period, the value of K_p is very larger. Therefore, Dean & Dalrymple (1984) state that "the very short period waves may not even be recorded by the pressure gage".

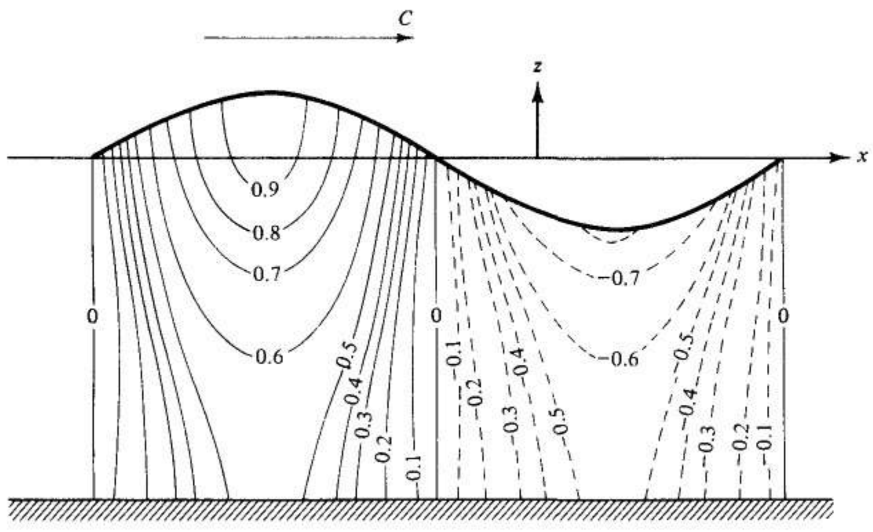

Figure 4.11 Isolines of pD/[y(H/2)f]o r progressive wave of h/L = 0.20 (Dean & Dalrymple, 1984)

According to the researchers, the slope failure or landslides occurs under both hydro-static and dynamic conditions. However, undrained behavior and liquefaction of the subsoil, as seen in the dynamic analysis, are not observed in the hydro-static analysis.

The maximum wave heights and periods for İzmir bay was determined in the study "*İzmir bay and İzmir Port Rehabilitation Studies, Design*" made for TCDD (The State Railways of The Republic of Turkey) by Yüksel Project. The detailed information about this study was given in Chapter 3.

In this study, submarine slope stability analysis of navigation channel is carried out for both static and dynamic conditions. The maximum wave height value used was presented in Chapter 3.

4.2.5 Sea Level Changes

Sea level change depends on many factors such as meteorological, oceanographic, astronomical tide, global warming, and vertical movements of the earth's crust.

Meteorological factors for sea level changes are atmospheric pressure and temperature changes and wind. While the rise of atmospheric pressure causes descend of sea level, the reduction of atmospheric pressure causes rise of sea level. In terms of the change of air temperature, although the air temperature depends on latitudes, sea level inclines directly from the poles to equator.

Global warming influences the change of the global air and the water temperature. Also because of melting of glaciers, the sea level increases by the effect of global warming. According to the results of the researches of Nave (2012), the air temperature has risen approximately 1°C until from 1880 to 2010 years (Figure 4.11 and 4.12). Additionally, the sea level has risen about 20 cm at the same time (Figure 4.13).

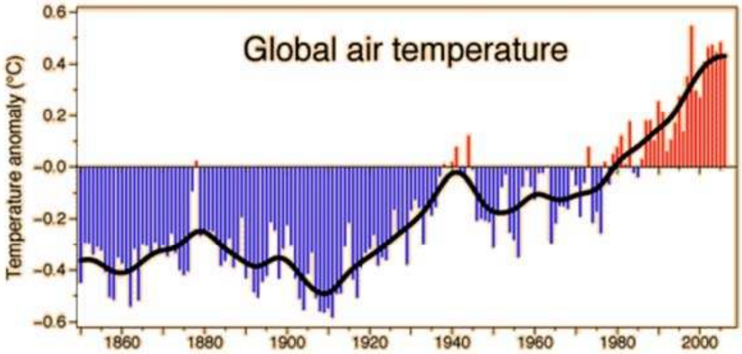

Figure 4.12 The global air temperature graph from Phil Jones on behalf of the Climatic Research Unit, UK. (Nave, 2012)

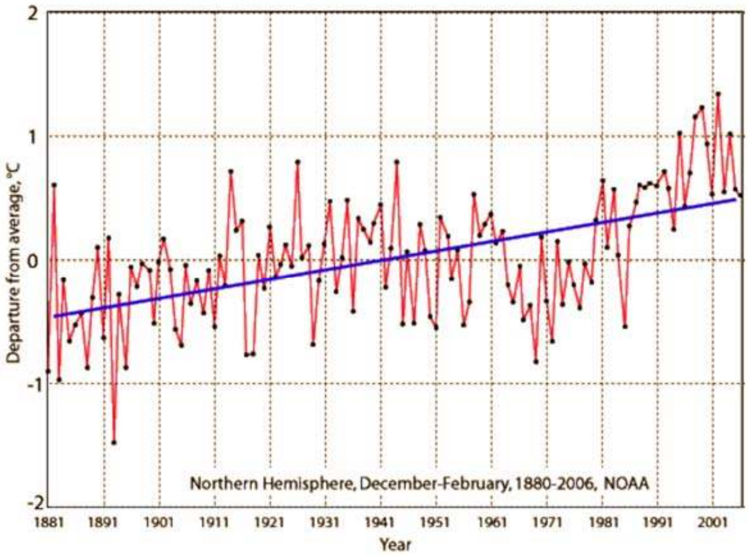

Figure 4.13 The mean temperatures in the northern hemisphere from NOAA (Nave, 2012)

Furthermore, the sea level is swelled by the impact of the wind. The swelling of sea level always changes according to speed and direction of wind. The wind waves cause changes in sea level from cm to meter. The density and temperature of sea water changes with the effect of the air temperature. These changes cause rise or fall of sea level.

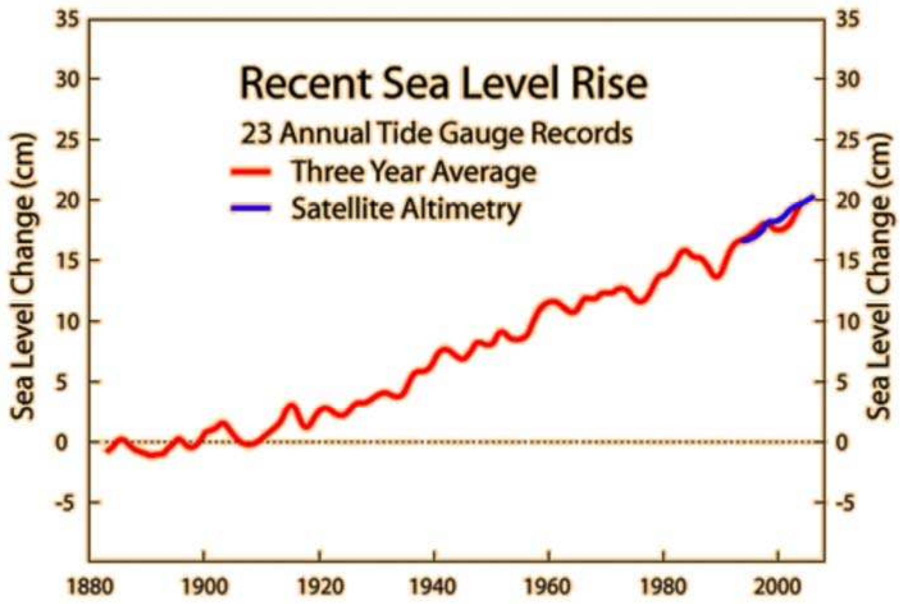

Figure 4.14 Depiction of recent sea level rise is from Bruce C. Douglas (Nave, 2012)

The effect of astronomical tide causes change of sea level, because of the gravitational force of the planets. The effect of astronomical tide is both long-term and short-term.

The movements of the earth's crust cause the change of the sea level in long-term or short-term. The most important and common movements of the earth's crust is due to tectonic activities, and others as sedimentation processes, slumps etc. The sudden tectonic movements can create important changes in the sea levels as the effect of the tsunami.

The sea level changes related with other triggering mechanisms could be given as gas hydrate disassociation, sedimentation and erosion, and volcanic activity. When the sea level decreases, the overall pressure on the seafloor slopes decreases and so gas hydrates are might generated. Also when the sea level decreases, sedimentation rate might increases because of decrease in discharge regime. Apart from a fall in the sea level, when sea level increases, erosion rate might increases in the environment.

The detailed information about the sea level changes of İzmir bay was presented in Chapter 3 – *Alsancak Navigation Channel*.

4.2.6 Gas Hydrate Dissociation

Hance (2003) gives that "Gas hydrates (clathrates) are ice-like substances consisting of natural gas and water that are stable under certain pressure and temperature conditions (Locat and Lee, 2002). If the pressure or temperature conditions change, gas hydrates may disassociate into natural gas, which can trigger slope failures. Kayen and Lee (1991) noted that the seafloor temperature and pressure in water depths exceeding about 300 to 500 m are adequate for the formation of hydrates. Gas hydrates are typically found within a range of depths below the seafloor known as a "hydrate stability field" where suitable pressure and temperature conditions exist. An ample supply of natural gas such as methane is also required for the formation of hydrates".

Hance (2003) denoted that "Gas hydrates occur in only a small portion (less than 10 percent) of the area covered by oceans for two reasons: First, according to Kvenvolden et al. (1993), gas hydrates are restricted to water depths that exceed about 300 m which limits them to the relatively small area of the continental slope and rise along the margins of continents. Secondly, in these areas there are also substantial organic-rich sediments that provide an adequate source of methane".

Whelan et al. (1976) indicated values of as much as 15% volume of methane in sediments. When total gas and water pressure increase in the soil voids, the cohesion and strength of sediments might decreases. Hance (2003) denoted that gas hydrates may be the direct trigger of a slope failure, or they may be associated with other triggering mechanisms.

Hance (2003) gives that "Locat and Lee (2002) noted that a drop in sea level, which reduces the pressure acting on the seafloor, can cause gas hydrates to disassociate. When gas hydrates disassociate, the natural gas that is released as bubble induces total stresses (σ), and excess pore air pressures ($\bar{u}_a$), and excess pore water pressures ($\bar{u}_w$), within the soil deposit, due to the low permeability of most marine soils. Thus, effective stresses (σ') in the sediment are reduced, i.e. $\sigma' = \sigma - u = \sigma\ (\bar{u}_a + u_a + \bar{u}_w + u_w)$ The shear strength is also reduced, and slope failure occurs".

When İzmir bay is evaluated in terms of gas accumulation, the gas accumulated may have become because of high sedimentation. Because there are two important sediments source as Gediz and Meles rivers (Figure 4.13).

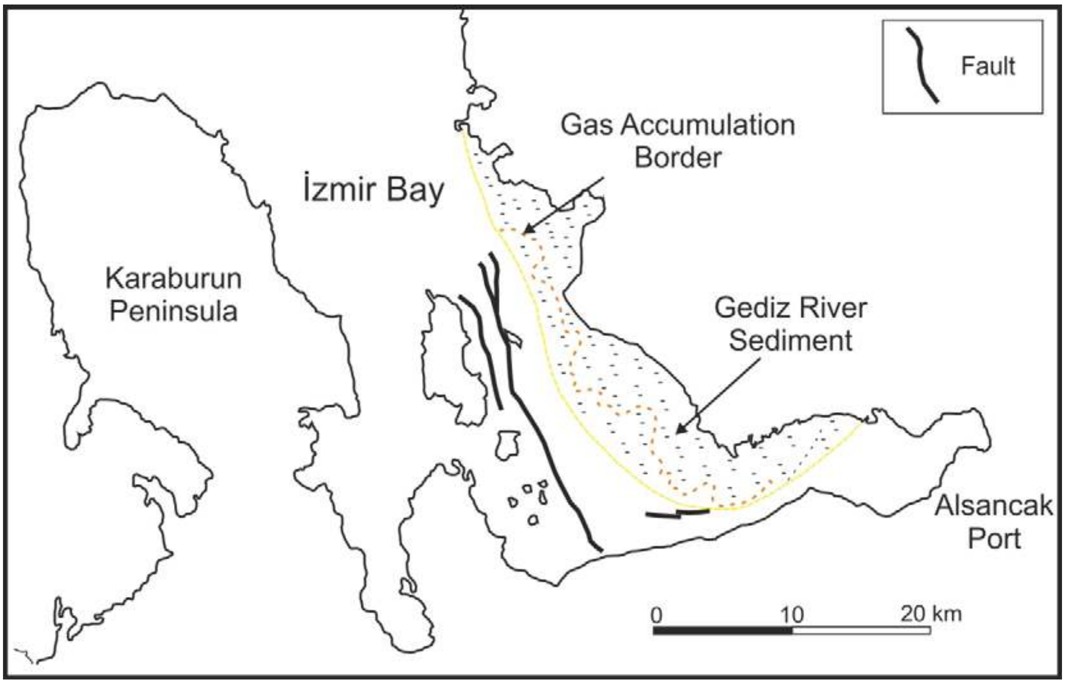

Figure 4.15 Gas and Sediment accumulation border of İzmir bay (Coşkun, 2009)

Coşkun (2009) investigated the gas accumulation in İzmir bay by using Chirp Side-Scan sonar. According to Coşkun (2009), when the seismic data are investigated, the transparent zones so-called "acoustic cover" are under 7-15 meters of sea floor (Figure 4.15 & 4.16). Also according to the description of Dondurur (2005), this zones masks other reflections over seismic profiles and this zones is defined as more or less continuous "acoustic space zone". The reason of existence of these transparent zones shaped of gas accumulations on seismic crossings is that the sediments containing gas sucks acoustic energy.

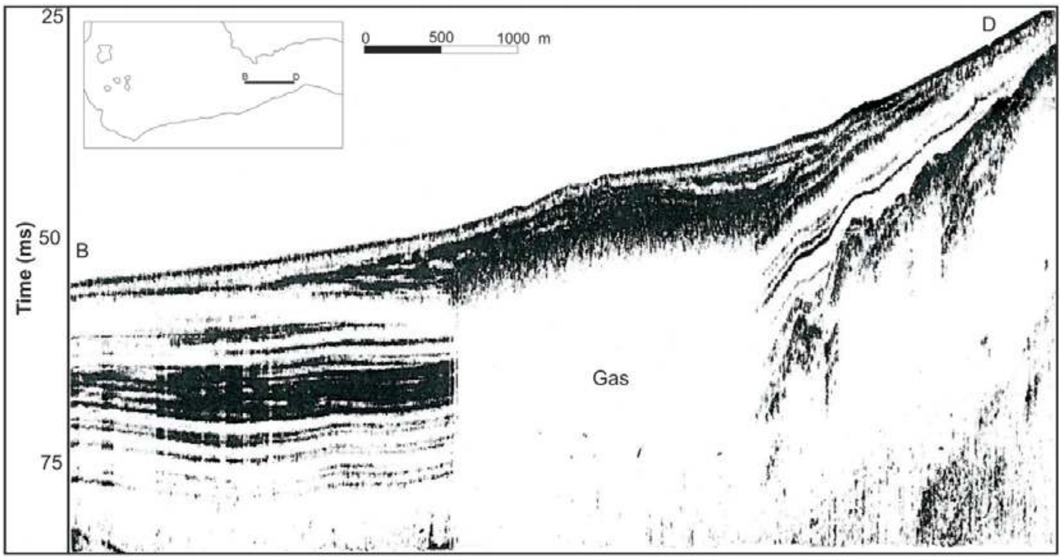

Figure 4.16 Seismic profile in the middle bay of İzmir (Coşkun, 2009)

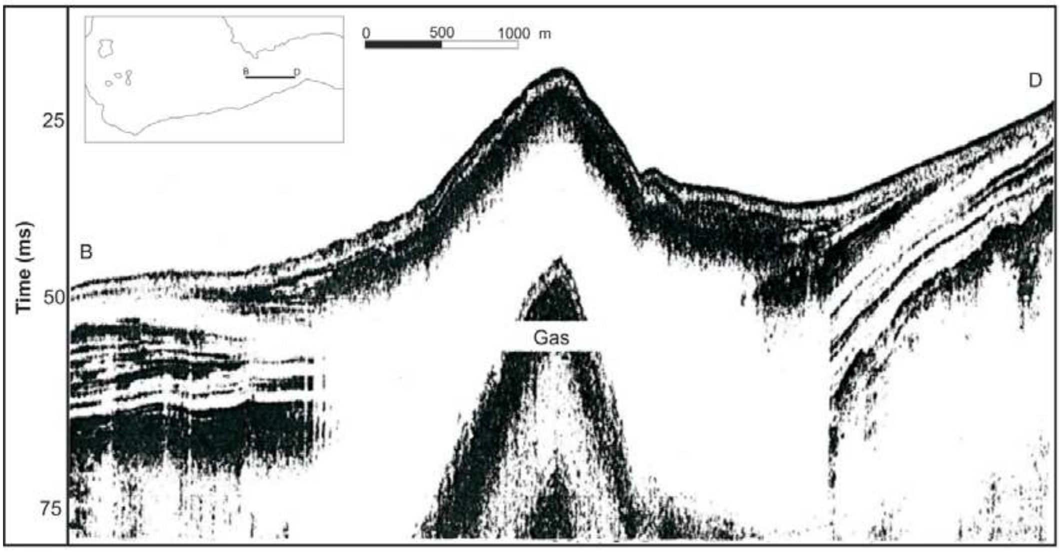

Figure 4.17 Seismic profile in the middle bay of İzmir (Coşkun, 2009)

Coşkun (2009) states that this gas accumulations are observed around the Gediz river and a part of the north-west (NW) of outer bay in generally (Figure 4.14). The prospect of being biological gas accumulation is high at the mouth of the Gediz river and the formation of the gas was thought because of the bacterial activation into the continental delta sediments (Coşkun, 2009). There are not any area where gas accumulation denoted the around navigation channel in İzmir bay, so the gas accumulation is far from being a triggering factor for the instability of navigation channel.

4.2.7 Change of Certain Physical-Chemical Properties

The change of chemical and physical properties of seawater affects directly or indirectly the seafloor. Specially, the changes of the physical properties of seawater affects directly the current regime of seawater, accumulation or disassociation of gas hydrate, erosion, deposition~~s~~ and velocity of deposition~~s~~ of sediments, pore-water pressure, changes in sea level, and the motion of seawater.

The physical properties of seawater depend on primarily pressure, temperature, salinity, density and conductivity. However, Bowditch (2002) denoted that factor like motion of the water and the amount of suspended matter affect such properties as color and transparency, conduction of heat absorption of radiation, etc. The physical properties of seawater may also be changed by rainfall and flood events.

Bowditch (2002) referred the physical properties of seawater such as salinity, temperature, pressure, density, sound speed in “The American Practical Navigator”. This properties of seawater was presented briefly benefit from the study of Bowditch (2002) as follows.

Salinity, Bowditch (2002) gives that “Salinity is a measure of the amount of dissolved solid material in water. It has been defined as the total amount of solid material in grams contained in one kilogram of seawater when carbonate has been converted to oxide, bromine and iodine replaced by chlorine, and all organic material completely oxidized. It is usually expressed as parts per thousand (by weight), for example the average salinity of seawater is 35 grams per kilogram which would be written “35 ppt” or “35%”. Historically the determination of salinity was a slow and difficult process, while the amount of chlorine ions (plus the chlorine equivalent of the bromine and iodine), called **chlorinity**, could be determined easily and accurately by titration with silver nitrate. From chlorinity, the salinity was determined by a relation based upon the measured ratio of chlorinity to total dissolved substances.”

$$\text{Salinity} = 1.80655 \times \text{Chlorinity} \qquad \text{Eq. 4.12}$$

Bowditch (2002) gives that “This is now called the absolute salinity, (S_A). With titration techniques, salinity could be determined to about 0.02 parts per thousand…. This definition of salinity has now been replaced by the **Practical Salinity Scale**, (S). Using this scale, the salinity of a seawater sample is defined as the ratio between the conductivity of the sample and the conductivity of a standard potassium chloride (KCI) sample….Since practical salinity is a ratio, it has no physical units but is designated **practical salinity units**, or **psu**…”

Bowditch (2002) gives that “Salinity generally varies between about 33 and 37 psu. However, when the water has been diluted, as near the mouth of a river or after a heavy rainfall, the salinity is somewhat less; and in areas of excessive evaporation, the salinity may be as high as 40 psu…”

Temperature, Bowditch (2002) gives that “Temperature in the ocean varies widely, both horizontally and with depth. Maximum values of about 32°C are encountered at the surface in the Persian Gulf in summer, and the lowest possible values of about -2°C (the usual minimum freezing point of seawater) occur in polar regions…” The vertical distribution of temperature of seawater shows a decrease of temperature with increasing of depth.

Bowditch (2002) denoted that the temperature of seawater is measured with using a platinum or copper resistance thermometer or a thermistor.

Bowditch (2002) gives that “The Conductivity-Temperature-Depths [CTD] is an instrument that generates continuous signals as it is lowered into the ocean; temperature is determined by means of a platinum resistance thermometer, salinity by conductivity, and depth by pressure. These signals are transmitted to the surface though a cable and recorded. Accuracy of temperature measurement is 0.005°C and resolution an order of magnitude better…”

Density, Bowditch (2002) gives that “Density is mass per unit of volume. The appropriate SI unit is kilograms per cubic meter. The density of seawater depends upon salinity, temperature, and pressure. At constant temperature and pressure, density varies with salinity….The density of surface water is increased by evaporation, formation of sea ice, and by cooling. If the surface water becomes denser than that below, convection currents cause vertical mixing. The more dense surface water sinks and mixes with less dense water below. This process continues until the density of the mixed layer becomes less tahn that of the water below…"

Sound Speed, Bowditch (2002) gives that "Sound speed in sea water is a function of its density, compressibility and, to a minor extent, the ratio of specific heat at constant pressure to that at constant volume. These properties depend on the temperature, salinity and pressure (depth) of seawater…"

Bowditch (2002) adopted a simple formula for the computation of the sound speed in sea water as follows;

$$U = 1449 + 4.6T - 0.055T^2 + 0.0003T^3 + 1.39\,(S - 35) + 0.017D \qquad \text{Eq 4.13}$$

Where; U is the sound speed (m/s^2), T is the temperature of seawater (°C), S is the salinity (psu), D is depth (m).

Pressure is commonly expressed in bar unit-wise, which is nearly equal to 1 Atmosphere (atm.). The measurements of all of the physical properties of seawater are affected by pressure. However this effect isn't the same with the effect of salinity and temperature, and even the effect of pressure is little lower than others.

Thermal Conductivity; in water, as in other substances one method of heat transfer is by conduction. Freshwater is a poor conductor of heat, having a coefficient of thermal conductivity of 582 Joules per second per degree, but increases with greater temperature or pressure (Bowditch, 2002).

Electrical Conductivity; the electrical current is transported by the ions in the water. Pure water is not ~~a~~ enough conductor of electricity. However the conductivity of the seawater increases with increase of salt ions in the water, and with an increase in temperature of the water.

The unit of the conductivity is generally Siemens per meter (S/m) in SI. When the conductivity of seawater is about 5 S/m, the conductivity of drinking water is between 0,005 and 0,05 S/m.

In this study, the physical properties of seawater were determined with the CTD (Conductivity-Temperature-Depths) instrument at various locations and depths of İzmir bay. However these studies were carried out in short time. Therefore the seasonal variations of physical properties of seawater could not be observed in the results of these studies. These works should be done long-term in order to reflect fully the physical properties of seawater in İzmir bay. The results of these studies were presented in Chapter 6.

4.2.8 Long Period Waves

Long period waves are classified according to wave period (time scale) and generating cause. Ergin (2009) gives This classification as in Table 4.5.

Table 4.5 Long period waves, their causes and periods are classified by Shore Protection manual (1984) (Ergin, 2009)

Long Period Waves	Generating Cause (Force)	Period
Tsunami	At the sea bed: Earthquake, landslide, volcanic eruption, meteor impact.	5 to 60 min
Tidal wave	Gravitational action of the moon and the sun	About 12-24h
Storm Surge	Wind stress and atmospheric pressure reduction	1 to 30 days
Harbor Resonance	Tsunami, surf beat	2 to 40 min.
Seiche	Wind variation	2 to 40 min.
Surf Beat	Wave group	1 to 5 min.

4.2.8.1 Tsunami

Tsunamis are great ocean waves generated by tectonic motions of the sea bottom as seismic events or submarine landslides (Figure 4.17). These waves are destructive. Ergin (2009) denoted that Tsunamis occur in average at every 10 years where being a lot of tectonic motions as the coasts of Japan, Hawaii, and Indonesia. They do not occur very often especially in Mediterranean Sea and Black Sea.

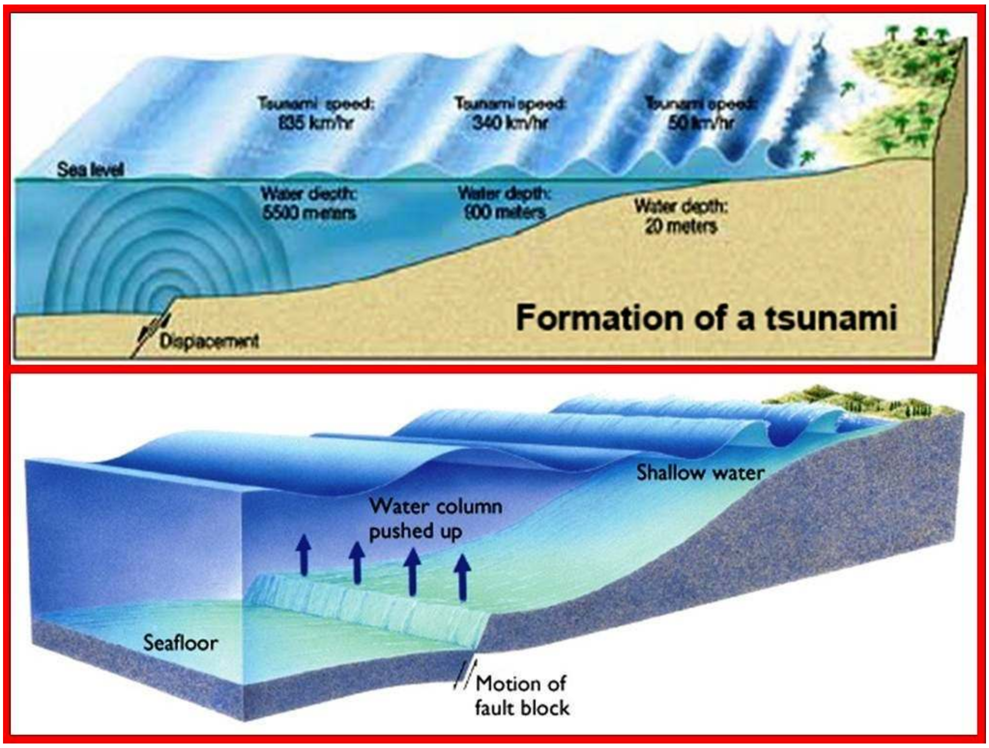

Figure 4.18 The formation of tsunami (Öncel, 2007)

According to Hance (2003), there are two ways that tsunamis can affect sea bottom slope stability.

Hance (2003) gives that "First, tsunamis can induce large hydrodynamic stresses on the seafloor. Secondly, tsunamis can also lower water levels as they approach shorelines, causing rapid drawdown…. The rapid lowering of the water level without time for drainage of the soil reduces the resisting force of the body of water with no change in soil shear strength, thus reducing the factor of safety…"

4.2.8.2 Tidal Waves

Ergin (2009) defined that "the sea surface rises and falls regularly ones or twice a day, and this periodic motion is called tidal motion". After that it can be that the tidal waves occur due to the gravitational forces of the planets.

Types of tide;

There are different types of the tide because of the effects of geometric relation of moon and sun's locations on the Earth's surface.

a) ***In Diurnal tide***; there are one high and one low water level in about 24 hours as seen in Figure 4.18 Diurnal tide is observed at the coasts of Mexico Gulf, at the west coasts of Australia, and at northern coasts of Japan etc.

b) ***In Semidiurnal tides***; there are two high water levels and two low levels in about 24 hours as shown in Figure 4.18. this type of tide occurs in many parts of the world (Figure 4.19)

c) ***In Mixed tides***; these tides have a higher high water and lower high water as well as higher low water and lower low water levels (Figure 4.18). These tides are especially observed in the coasts of Turkey.

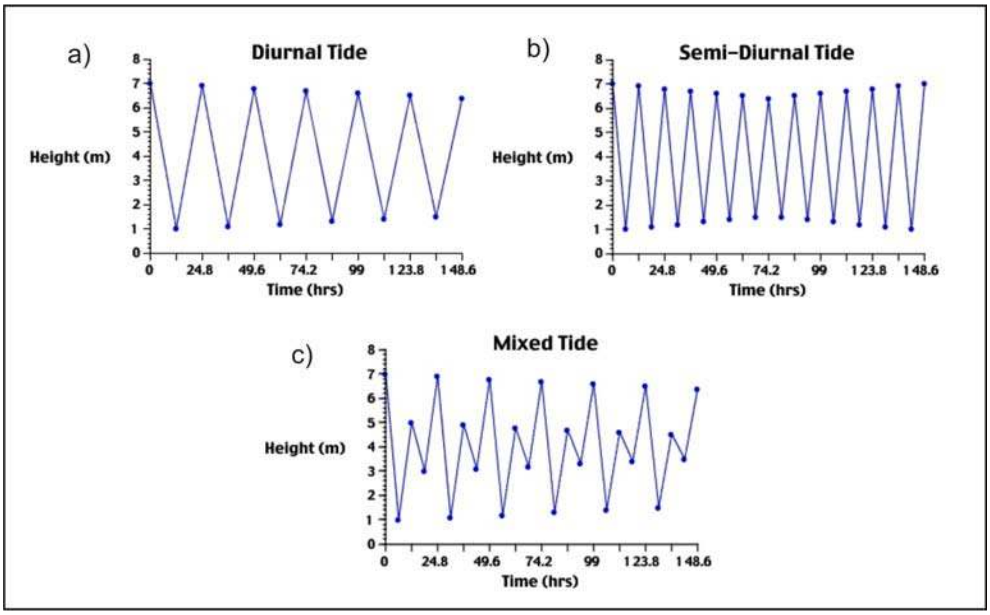

Figure 4.19 (a) Cyclical tidal cycles associated with a diurnal tide, (b) Cyclical tidal cycles associated with a semidiurnal tide, (c) Cyclical tidal cycles associated with a mixed tide (Natarajan, Mohan & Balasubramanian, n.d.)

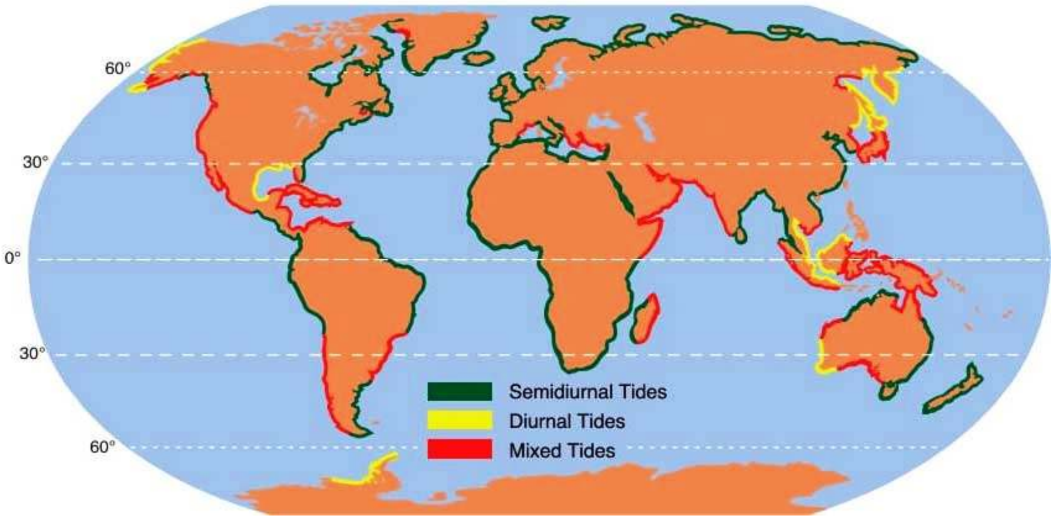

Figure 4.20 Global distribution of the three tidal types (Natarajan, Mohan & Balasubramanian, n.d.)

Ergin (2009) gives that "The strength of the tidal motion depends on the relative positions of the earth, moon, and the sun. It also depends on the size of the water body in question. Due to the amplification effect of coastal formation and undersea topography, the tidal range may be over 10 meters. In small, close seas as in the Black Sea and even in the Mediterranean Sea the tides are small. Because almost no tidal motion is penetrating from the great oceans, and the locally generated tides are of no significance either. The seas bordering Turkey are much smaller in size, compared to the size of ocean, therefore for Turkish seas the recorded maximum tidal range is 1.4 m.”

4.2.8.3 Storm Surge

The descriptions of Storm Tide and Storm Surge are denoted as follows by National Oceanic and Atmospheric Administration [NOAA].

Storm tide is water level rise during a storm due to the combination of storm surge and the astronomical tide.

Storm Surge is an unusual rise of water generated by a storm, over and predicted astronomical tide. Therefore storm surge should not be confused with storm tide. Because there are the combination of storm surge and the astronomical tide in storm tide.

Figure 4.21 Wind and pressure components of hurricane storm surge (Storm Surge Overview, n.d.)

The water level rises by the increasing water pressure in upward direction where air pressure is lower. As a result, storm surge is caused by the strong winds (Figure 4.20). Also the storm surge depends on various other factors, the most important of which is the depth of water. In deep water, there is very little indication of storm surge, because there nothing disrupts the formation of the storm surge (Figure 4.21).

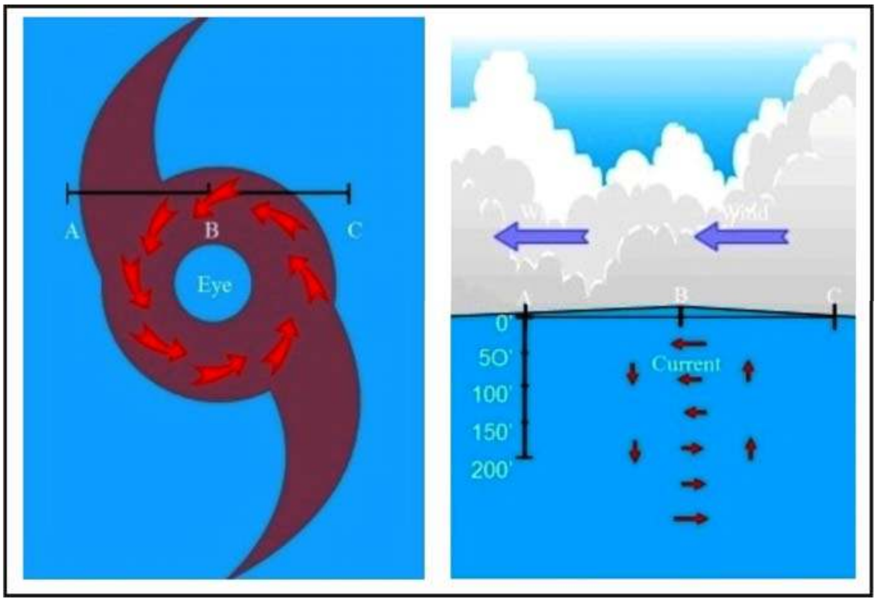

Figure 4.22 The formation of storm surge in the deep water (Introduction to Storm Surge, n.d.)

The created storm surge has a tendency to be large in shallow water regions. Where the water depth is very low or there is any disrupter, the swelling of the water is much more compared to the deep sea (Figure 4.22). So the effect of the storm surge is larger in ~~sizes~~ in coastal regions (Figure 4.23).

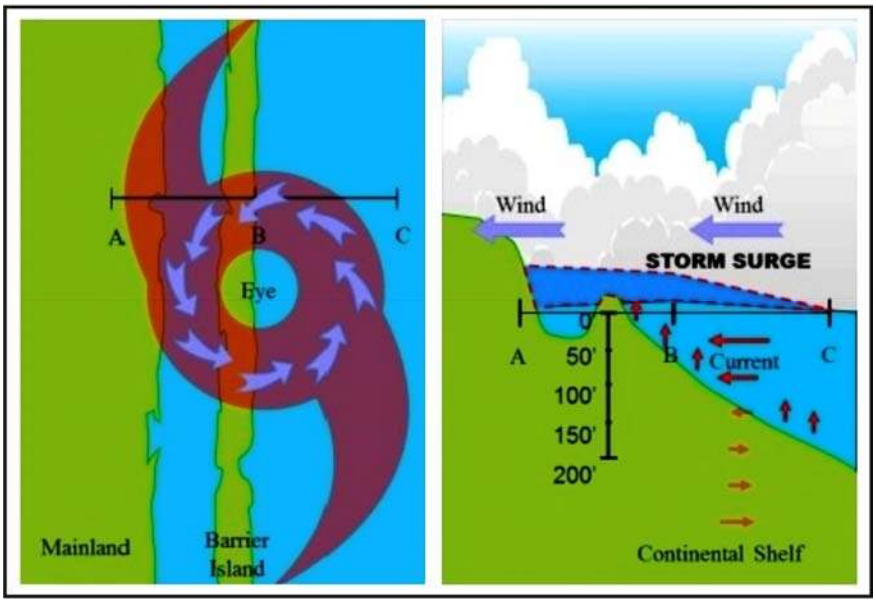

Figure 4.23 The formation of storm surge in the shallow water (Introduction to Storm Surge, n.d.)

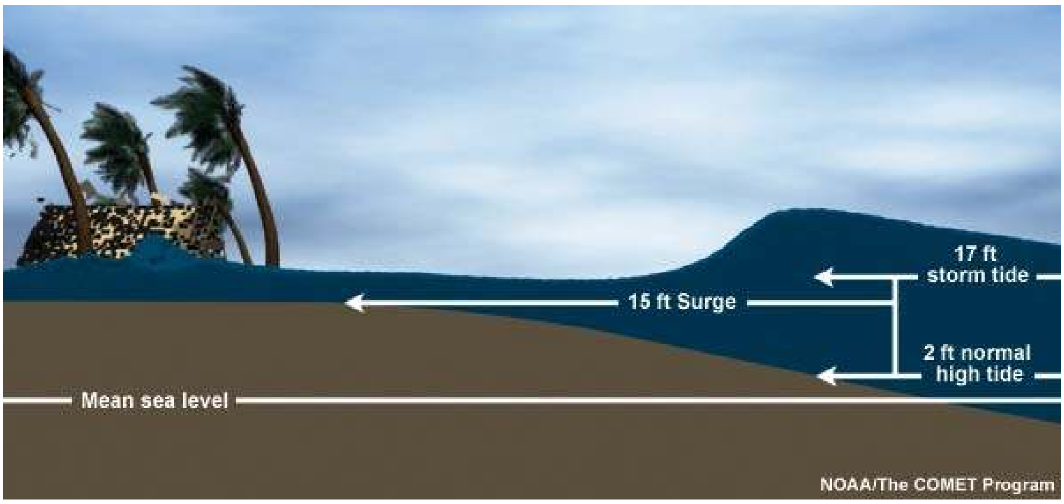

Figure 4.24 Storm tide and storm surge (Introduction to Storm Surge, n.d.)

4.2.8.4 Surf Beat

Ergin (2009) defined surf beat as “a long period oscillation which is radiating from slow oscillations in the mean water level in a surf zone due to more or less periodic variations in the breaker heights of the breaking waves”.

According to Hendersen (2002), although these waves have much low frequency as 0.005-0.05 Hz and the sea level changes slowly, these waves are not eye-catching.

4.2.9 Flood Events

Flood events can be observed depending on the topography due to heavy rainfall all over the world. Flood events that have been occurred since 1950 all the world is given in Figure 4.24.

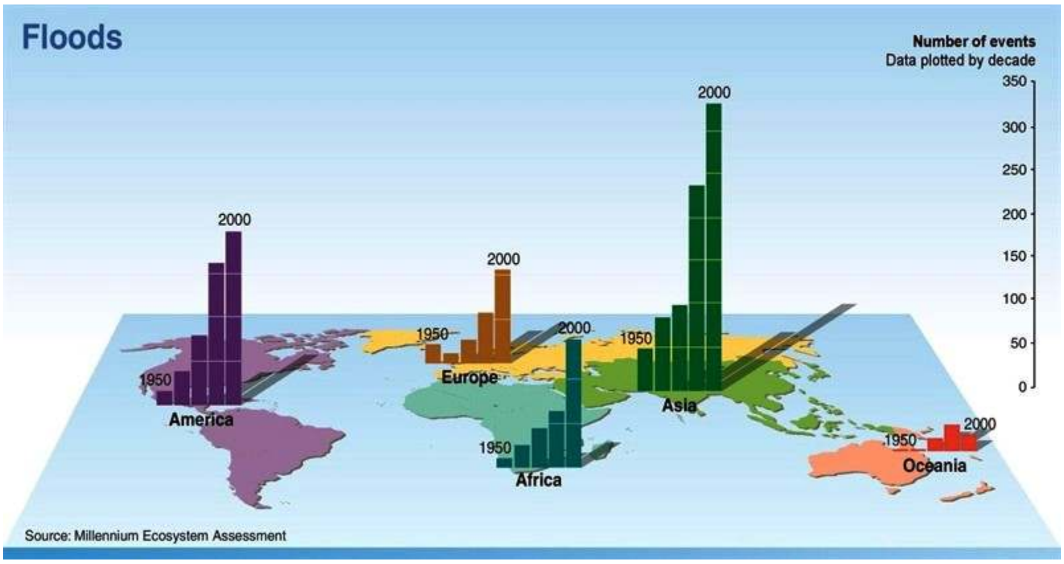

Figure 4.25 Number of flood events by continent and decade since 1950 (The Millennium Ecosystem Assessment, n.d.)

Flood events transport the sediments collected from land in coastal regions to the sea. As a result of flood events, rapid sedimentation is observed in the sea and the coasts. Rapid sedimentation ~~is~~ applies an extra load on the seafloor. The situated driving stresses on the seafloor sediments may be increased with this extra load.

Furthermore, these rapidly transported sediments may cause gas accumulation on the seafloor. So there might be observed gas leakage and liquefaction processes, which may lead to the seafloor failures or landslides.

Moreover, Hance (2003) denoted that “flood events may also erode river deltas, leading to turbidity currents, or low density landslides”. Gediz and Meles rivers are two important rivers that transport sediments in flood events in İzmir and environment.

4.2.10 Creep

Creep develops for large masses of soil under different loads in very wide areas in long-term. Hance (2003) gives additional information about creep in table 4.5.

Table 4.6 Information relevant to creep as a triggering mechanism

Type of Information	Database Field Containing Information	Comments
Geomorphologic Description	Slide Description; Triggering Mechanism	Lack of a distinct failure scar has been linked to creep-induced sliding.
Geophysical Description	Triggering Mechanism	Geophysical surveys have revealed internal deformation within seafloor sub-soils, which have been linked to creep.

4.2.11 Human Activity

The most of the seafloor slope failures are caused by natural events or human activities as construction works, fill placement, and dredging. For example, if fill material is placed or the navigation channel or trench is dredged where the soils are soft or loose, the soils are prone to failure. In order to prevent or decrease the possibility of the failure, the fundamental analysis must be done before the construction works.

CHAPTER FIVE
LABORATORY STUDIES AND FIELD EXPERIMENTS

5.1 Laboratory Studies

Soil index and engineering tests were carried out on the soil samples taken from Alsancak Navigation Channel, after their general description. These tests included particle size distribution, water content, Atterberg (liquid/plastic) limits, specific gravity, undrained shear strength. In these tests, American Society for Testing and Materials [ASTM] standards, British Standards and Turkish Standards were followed.

5.1.1 Particle Size Distribution

Particle size distribution analysis (including hydrometer test) was performed for each soil sample. In wet condition, sieve analyses were made using No. 4, 10, 40, 200 sieves according to ASTM D422-63 (2002) standard. According to the results of sieve analysis, the portions retained on the No. 40 sieve also called as shell are given in Table 5.1. *Hydrometer tests* were performed for the soil particles passing No. 200 sieve according to ASTM D422-63 (2002) standard. In this tests, ASTM E 100 151 H type hydrometer was used. Particle size distribution graph for all samples is given in Figure 5.1.

Table 5.1 The percentage of the retained shell, and the passing No.40, 200 sieve and 2μ

Samples No.	Shell (%)	Passing No. 40 Sieve (%)	Passing No.200 Sieve (%)	Passing through 2μ (%)
K1	2.45	97.55	5.24	-
K2	8.78	91.22	43.04	8.88
K3	16.13	83.87	63.67	12.35
K4	8.93	91.07	76.33	15.80
K5	16.76	83.24	65.31	10.08
K6	1	99	92.72	37.43
K7	10.33	89.67	87.35	35.03

Table 5.1 Cont.

K8	3.34	96.66	93.97	33.05
K9	18.95	81.05	76.52	22.66
K10	13.49	86.51	84.27	22.74
K11	3.89	96.11	94.14	19.30
K12	7.64	92.36	90.24	32.19

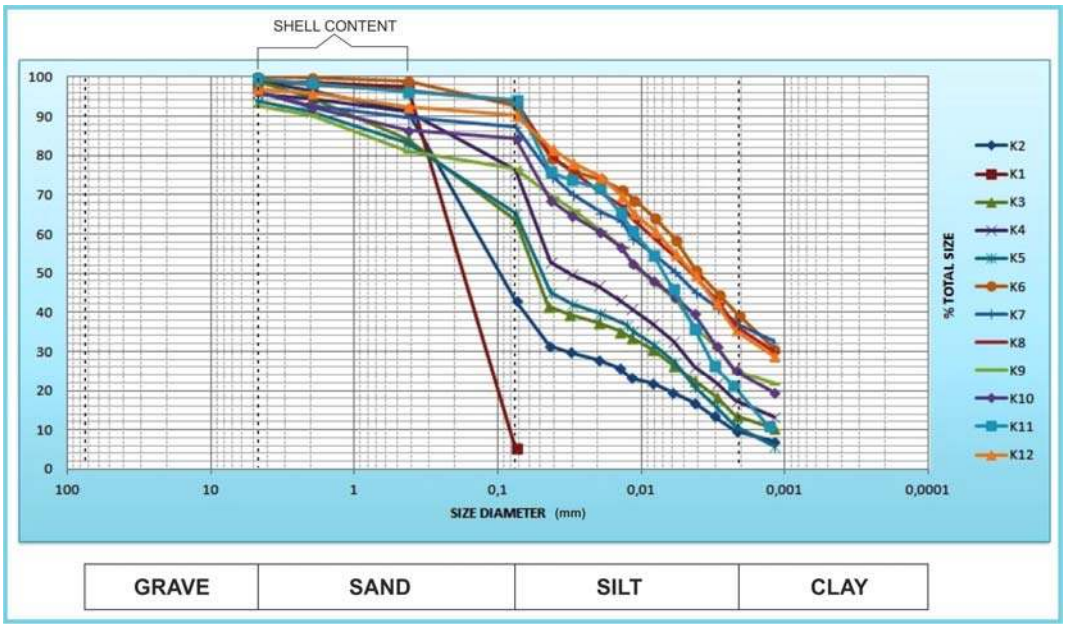

Figure 5.1 Grain size distribution graph

As seen in Table 5.1 and Figure 5.1, the average shell content of all soil samples is found as 9.30%. Additionally, the average material passing through No.200 sieve for K2-12 soil samples is 78.86%. The soil samples analyzed are generally observed to be shell clayey silt according to the results of particle size distribution except K1 soil sample. Because the material passing through No.200 sieve is 5.24% and the material passing through No.40 sieve is 97.55% for K1 soil sample. Also the amount of shell is 2.45%. Therefore K1 soil sample may be classified as shell silty sand.

5.1.2 Classification of Soil

The soils samples are classified according to ASTM D2487-00 and TS 1500/2000. In general, both the ASTM and Turkish Standards [TS] classify soils in a similar manner as shown in Table 5.2. Accordingly three different soil types are observed for

K1-12 soil samples that K1 sample is shell silty sand “SM”, K2-3 are shell medium plasticity organic clayey silt “MIO” and K4-12 samples are shell high plastic organic clayey silt “MHO” as given in Table 5.3.

In this study, the organic material content of soil is not defined. However soil is recognized to consist of organic material to some extent as stated in previous studies. In the classification of soil, this fact is considered.

Table 5.2 Grain size distribution of soils according to ASTM and TS standard (Sonuvar, 2004)

Material		ASTM D2487-90 (mm)	TS1500/2000 (mm)
Block		300	>200
Rock		75	200-60
Grave	Large	19	<60
	Medium	-	
	Fine	4.75	
Sand	Large	2.00	
	Medium	0.425	≤2
	Fine	0.075	
Silt	Large	<0.075	0.076
	Medium	-	
	Fine	-	
Clay		0.002	0.002

Table 5.3 The classification of soil samples (K1-12)

Sample No	Water Depth (-m)	Soil Type	Sample No	Water Depth (-m)	Soil Type
K1	4.00	SM	**K7**	11.00	MHO
K2	12.00	MIO	**K8**	12.00	MHO
K3	13.00	MIO	**K9**	13.00	MHO
K4	8.20	MHO	**K10**	11.00	MHO
K5	10.00	MHO	**K11**	11.00	MHO
K6	12.00	MHO	**K12**	10.00	MHO

5.1.3 Water Content (w)

The water content of the samples (K1-12) taken by Grab from İzmir Bay were determined according to ASTM D-2216-98 (2005). In order to reduce decomposition rate in the soil samples which include highly organic material, the test samples were dried at 60^0 C temperatures. The measured water content for the samples is given in Table 5.4.

Table 5.4 Water content of marine samples (K1-12)

Sample No	**Water Depth (-m)**	**Water Content (%,w)**	**Sample No**	**Water Depth (-m)**	**Water Content (%,w)**
K1	4.00	41.65	**K7**	11.00	219
K2	12.00	59.42	**K8**	12.00	229
K3	13.00	73.58	**K9**	13.00	165.38
K4	8.20	107.92	**K10**	11.00	106.29
K5	10.00	88.8	**K11**	11.00	224
K6	12.00	85	**K12**	10.00	163.7
Average Water Content, w (%)					**130.31**

As seen from Table 5.4, the average water content (w %) of the soil samples collected from depths between 4-13 m. is found as 130.31%. The maximum water content is found as 229%, and the minimum water content is found as 41.65%. The average water content of the soil samples taken from along the first line is 76.06%, and the average water content of the soil samples taken from the second line is 184.56%. The water content of samples of the second line is larger than the water content of samples at the first line due to the increase in the clay content.

5.1.4 Atterberg Limits, Liquidity Index and Plasticity Chart

5.1.4.1 Atterberg Limits

Liquid Limit values of soil samples were defined by Cone Penetration Testing according to British Standards [BS] 1377: Part 2: 1990: 4.3. Also the undrained cohesion values (Cu) of soils samples were described by means of Cone Penetration Testing.

The plastic limit of soils samples were determined according to ASTM D-4318 (2005) and BS 1377: Part 2: 1990: 5.3. And the plasticity index (PI) values of soils using both Plastic Limit (PL) and Liquid Limit (LL) were calculated based on ASTM D-4318-00 (2005).

Table 5.5 Liquid limit, plastic limit, plasticity index, natural water content of marine samples (K1-12)

Sample No	Water Depth (-m)	LL (%)	PL (%)	PI (Ip) (%)
K1	4.00	NP	NP	NP
K2	12.00	38.5	27.76	10.74
K3	13.00	48	35.37	12.63
K4	8.20	63.1	42.01	21.09
K5	10.00	58.6	41.6	17
K6	12.00	64.3	42.73	21.57
K7	11.00	114.7	77.5	37.2
K8	12.00	116.3	83.38	32.92
K9	13.00	99.7	54.36	45.34
K10	11.00	80.5	55.6	24.90
K11	11.00	118.2	87.2	31
K12	10.00	91.5	70.7	20.8

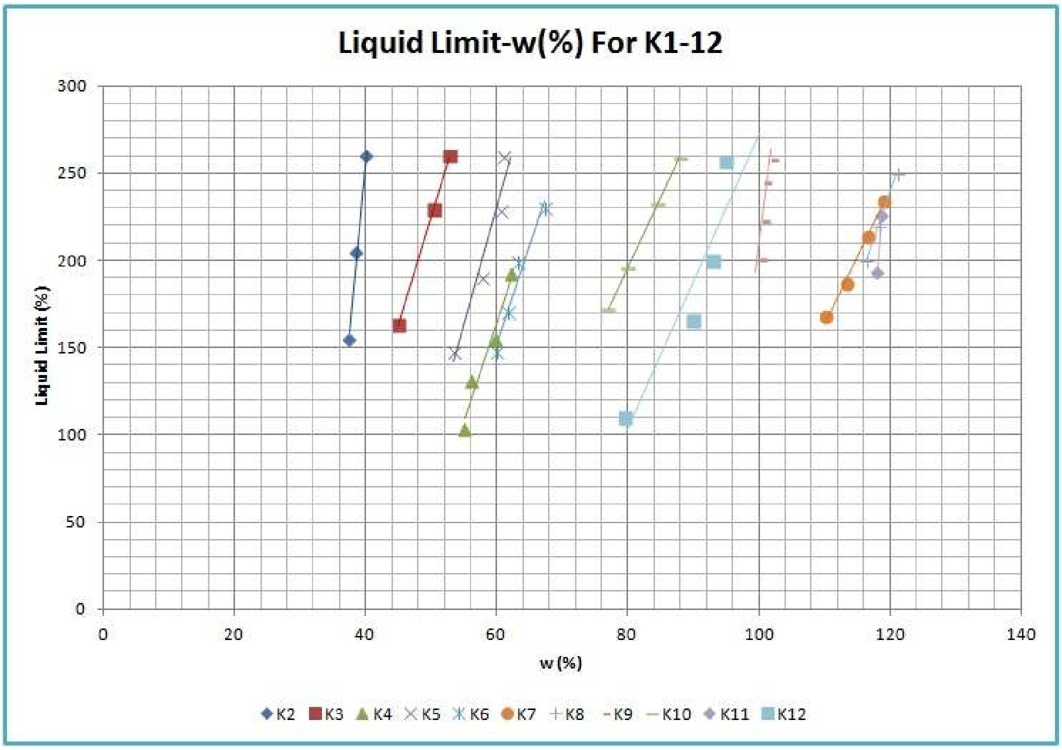

Figure 5.2 Liquid limits of soil samples (K1-K12)

As seen from Table 5.5 and Figure 5.2, K1 soil sample is found to be on non-plastic (NP) as it is a shell silty sand type of soil. The liquid limit values of K2-12 soil samples are found between 38.5% and 118.2%. The liquid limit of K2-6 soil samples taken from the first line are found between 38.5% and 64.3%, whereas liquid limit values of K7-12 soil samples taken from the second line are found to be between 80.5% and 118.2%. Although the clay content of soil samples of the second line is higher than the clay content of soil samples of the first line, the liquid limit values of the second line are higher than liquid limit values of the first line.

Sonuvar (2004) determined the soil properties such as liquid limit, plastic limit and plasticity index of soil samples taken from the navigation channel using the Casagrande Method. Sonuvar (2004) found the liquid limit values between 59.37% and 140.32%, the plastic limit values between 40.48% and 64.29%, and the plasticity index values between 18.89% and 76.03%. The liquid limit values found for the samples taken in this study are in agreement with the liquid limit values given by Sonuvar (2004).

5.1.4.2 Liquidity Index (I_L)

The liquidity index of soil samples was determined according to ASTM D-3282 (2004) and ASTM D-4318 (2004). Liquidity index (I_L) is defined for each penetration using Eq 5.1.

$$I_L = \frac{w - w_p}{w_L - w_p} \qquad \text{Eq 5.1}$$

Where, I_L is liquidity index, w is natural water content (%), w_P is plastic limit (%), and w_L is liquid limit (%).

The values of the liquidity index (I_L) of soil samples (K1-12) are given in Table 5.6;

Table 5.6 Liquidity index of marine samples (K1-12)

Sample No	Water Depth (-m)	Liquidity Index (I_L)	Sample No	Water Depth (-m)	Liquidity Index (I_L)
K1	4.00	-	**K7**	11.00	3.80
K2	12.00	2.94	**K8**	12.00	4.42
K3	13.00	3.02	**K9**	13.00	2.44
K4	8.20	3.12	**K10**	11.00	2.11
K5	10.00	2.77	**K11**	11.00	4.41
K6	12.00	1.95	**K12**	10.00	4.47
Average Liquidity Index, I_L					**3.22**

As seen from Table 5.6, liquidity index values of K2-12 soil samples are between 1.95 and 4.47. The average liquidity index is found as 3.22.

5.1.4.3 Plasticity Chart

According to ASTM D2487, if liquid limit (LL) value of a soil sample is equal or smaller than 50%, the sample is classified as “CL-OL” or “ML-OL”, and if liquid limit value of a sample is equal or smaller than 30%, the sample is classified as non-plastic (NP). This situation has been recognized as inconsistent and medium plasticity is defined on plasticity chart for both clay and silt by TS 1500/2000. Medium plasticity for clay and silt on plasticity chart is defined for liquid limit values between 35% and 50%.

The plasticity chart is prepared according to TS1500/2000 standard. Plasticity index (PI) vs. liquid limit distribution of soil samples on the plasticity chart are shown in Figure 5.3., In ASTM D2487 and TS1500/2000, the “U” line has been empirically determined to be approximate “Upper limit” for natural soils, and the “A” line is separated clay and silt on the plasticity chart.

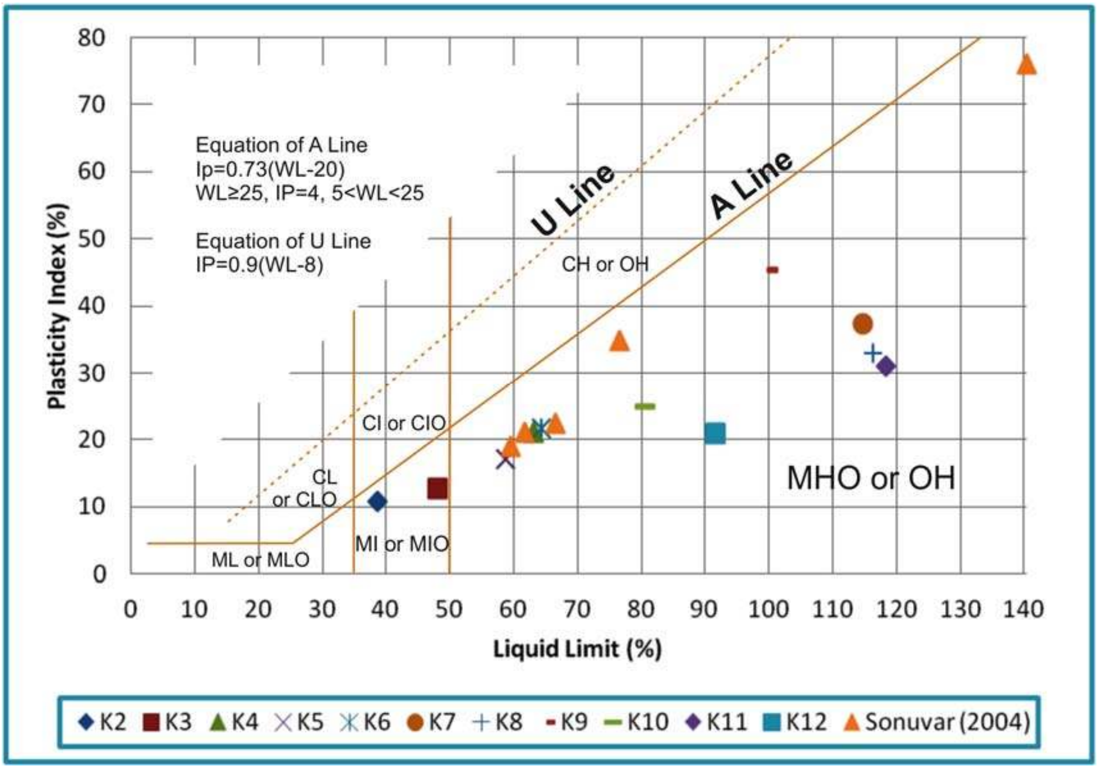

Figure 5.3 The results of tests showing on TS1500/2000 plasticity chart

As seen in Figure 5.3, K2 and K3 samples are classified “MI or MIO” and K4-12 samples are classified “MHO or OH” due to the increase in their liquid limit values. According to the prepared plasticity chart, all samples (K2-12) are found under A line. This indicates that the silt content of the samples are higher than the clay content.

5.1.5 Specific Gravity (G_s)

Specific gravity of marine samples (K1-12) were determined according to ASTM D-854 (2005). This test covers the determination of the specific gravity of soil that pass the 4.75 mm. (No.4) sieve, by means of a water pycnometer. This test was carried out following the Method A of ASTM D-854 (2005). The method A of ASTM D-854 is applied for organic, highly plastic, fine grained soils, tropical soils, and soils containing halloysite. In this test, 500 ml. pycnometer, and approximately 50 g. soil samples were used. The results of these tests are given in Table 5.7.

Table 5.7 Specific gravity of marine samples (K1-12)

Sample No	Water Depth (-m)	Specific Gravity (Gs)	Sample No	Water Depth (-m)	Specific Gravity (Gs)
K1	4.00	2.68	**K7**	11.00	2.57
K2	12.00	2.58	**K8**	12.00	2.58
K3	13.00	2.58	**K9**	13.00	2.60
K4	8.20	2.60	**K10**	11.00	2.53
K5	10.00	2.63	**K11**	11.00	2.55
K6	12.00	2.56	**K12**	10.00	2.54
Average Specific Gravity, Gs					**2.58**

As seen from Table 5.7, the average specific gravity of the soil samples collected from depths between 4-13 m. is found to be 2.58. The maximum and minimum specific gravities are found as 2.68 and 2.54 respectively. Soils were classified according to specific gravity by Önalp (2002). This classification is given in Table 5.8.

Table 5.8 Relationship between specific gravity and type of soil (Önalp, 2002)

Type of Soil	Specific Gravity (G_s)
Gravel and Sand	2.65-2.68
Silt	2.62-2.68
Inorganic Clay	2.68-2.76
Organic Clay	2.58-2.65

According to Table 5.8, the soil samples might be classified as organic clay, sand and silt based on the specific gravity values. Moreover, the organic material content of the soil may significantly affect its specific gravity.

5.1.6 Undrained Shear Strength

The shear strength of soils is measured by various instruments and tests such as traxial shear test, vane test, direct simple shear and fall cone test. The Lab. vane test is still commonly used to determine shear strength of very soft marine sediments in USA. The fall cone test is used to estimate both liquid limits and shear strength of marine sediments in North Europe , as it's a more reliable and simple method.

A lot of studies have been made to estimates strength of soil at the liquid limits. Some of the previous studies about the fall cone and lab vane test, and determining strength of cohesive soils by fall cone or lab vane tests were summarized as follows;

Houlsby (1982) gives a theoretical analysis of the fall cone test and direct calculation of the undrained shear strength (Cu) at the liquid limit (W_L). Houlsby and Koumoto (2001) give a static analysis of the fall cone test in which the theoretical values of cone factor (K) are defined. Chaney and Demars (1985) provide in-situ testing techniques and previous works about determination of the strength index of marine soils by the fall cone penetrometer, the torsional vane shear device (torvane) and the pocket penetrometer. Zreik (1991) measured the undrained shear strength of extremly weak and soft cohesive soils of Boston Harbour by the fall cone penetrometer. Houlsby & Koumoto (2001) achieved improved agreement between theoretical and experimental by introducing the concept of dynamic strength into Houlsby's analysis, and reported that the calculated values of K agreed well with the fall cone test results. Houlsby & Koumoto (2001) draw these results together and resolve the differences between theoretical and experimental findings. Also Houlsby & Koumoto (2001) compared static and dynamic analysis of the fall cone test. The effects of different cone angle (β), surface roughness, calculated values of K and heave were investigated over the results of shear strength.

Hansbo (1957) gives the following equation between the shear strength (Cu) and the cone penetration (d, depth of penetration).

$$C_u = \frac{100KW}{d^2} \qquad \text{Eq. 5.2}$$

Where; K is a constant depending mainly on the cone angle (β), C_u is shear strength (g/cm^2), W is the weight of cone for 30° (g), d is the penetration (cm).

Houlsby (1982) performed a dimensional analysis for quasi-static case, where the dimensionless factor F is a function of the cone adhesion ratio ($\alpha = a_u/c_u$) – the cone surface roughness is "α" and cone angle is "β".

$$F = \frac{W}{C_u d^2} \qquad \text{Eq. 5.3}$$

Combining Eq. 5.2 and 5.3 and replacing h by d /$3^{0.5}$;

$$K = \frac{3}{F} \qquad \text{Eq. 5.4}$$

Zreik (1991) says that "Houlsby (1982) carried out a numerical simulation of static cone penetration using a finite element model. The resulting values of F are given in the paper for various adhesion ratios and cone angles. The values of K for a smooth cone, obtained from the finite element model, lead to theoretical values of K which are listed for different cone angles (β)".

Hansbo (1957) obtained a K value for the 60^0 cone by correlation with the lab vane performed on remolded samples of clay. Karlsson (1961) obtained the values of K experimental for the 60^0 and 30^0 cones with their standard deviation (SD) by correlation with the lab vane. Wood (1985) performed test on three types of clays using a fall cone and a special vane in order to determine strength and values of K for different cone angles.

However, according to investigation of many researchers, the reason for the emergence of the different shear strength values is utilization of different angle of cones and most importantly, changed values of K according to theoretical or experimental analysis. So Houlsby (1982) concluded that the calculated shear strength values by theoretical analyses remain slightly higher than the experimental, and analytical work is necessary to reduce this difference. Zreik (1991) re-interpreted K factor (K_{rec}) using both the experimental values (K_{ex}) and theoretical values of K (K_{th}) (see Table 5.9).

Table 5.9 Experimental, theoretical and recommended K factor values (* using K factor) (Zreik, 1991)

β (^{0})	**K_{ex} (Hansbo, 1957)**	**K_{ex} (Karlsson, 1961)**	**K_{th} (Houlsby, 1982)**	**K_{ex} (Wood, 1985)**	**K_{ex}/K_{th}**	**K_{rec}**
30	-	0.79	**2.89 ***	0.83	0.29	0.83
45	-	-	1.25	0.49	0.39	-
60	0.30	0.29	0.645	0.29	0.45	0.29
75	-	-	0.36	0.19	0.53	-
90	-	-	0.205	-	0.6	0.12

In this study, the fall cone test is performed for cohesive K2-12 samples. The shear strength (C_u) of soils was defined using 30° and 80 g cone according to BS 1377 standard. The given fall cone factor K_{th} for 30° cone by Houlsby (1982) was used to determine strength value of soil samples.

Liquidity index (I_L) is defined for each penetration amount and for different water content using Eq 5.5. When the maximum value of the liquidity index (I_L) is 5.0, the minimum value of the shear strength is taken as 0.03 kg/cm^2 benefiting from the experimental studies of Zreik (1991) is given in Figure 5.4.

Eq 5.5

$$I_L = \frac{w - w_p}{w_L - w_p}$$

Where, I_L is liquidity index, w is natural water content (%), w_P is plastic limit (%), and w_L is liquid limit (%).

Also Wood (1985) denoted that the relationship between w and log (C_u) follows a straight line at water contents less than approximately 50%. In this study, the water contents of soil samples are larger than 50%. Therefore, the exponential curve is used to calculate the shear strength on I_L-log (C_u) graph.

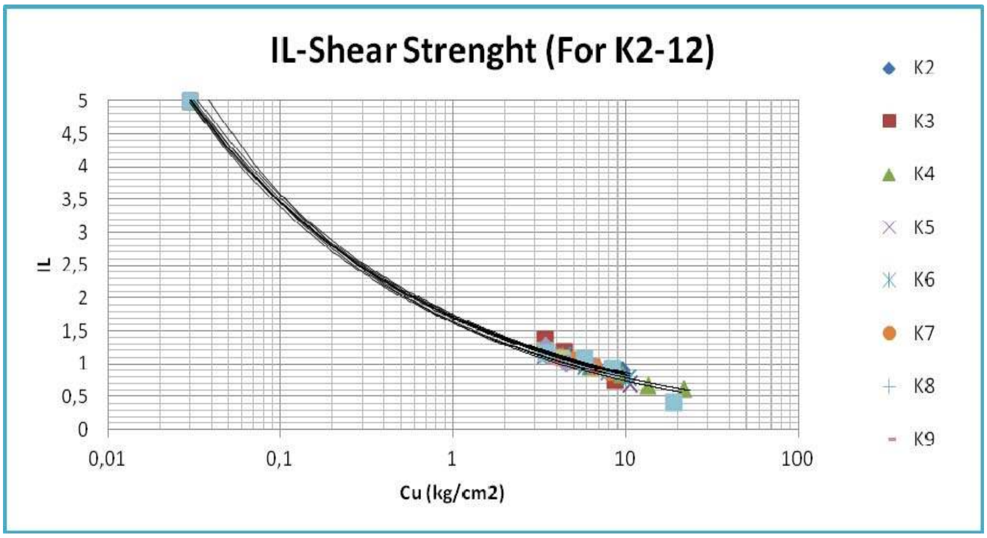

Figure 5.4 Relationship between I_L and log (C_u) for marine samples (K1-12)

Zreik (1991) showed that very soft of marine sediments have C_u value around 0.03-0.10 kg/cm^2 and liquidity index between 0.5 and 4.5. In this study, the measured values of the undrained shear strength (C_u) of marine samples are approximately between **0.04** and **0.60 kg/cm^2**, and the average values of C_u is **0.21 kg/cm^2** in Table 5.10.

Table 5.10 Relationship between I_L and C_u (kg/cm^2) for marine sediments samples

Samples	LL (%)	I_L	Cu (kg/cm^2)
K1	-	-	-
K2	38,5	2.94	0.165
K3	48	3.02	0.17
K4	63.1	3.12	0.145
K5	58.6	2.77	0.195
K6	64.3	1.95	0.6
K7	114.7	3.80	0.074
K8	116.3	4.42	0.045
K9	99.7	2.44	0.27
K10	80.5	2.11	0.55
K11	118.2	4.41	0.047
K12	91.5	4.47	0.053
Average C_u (kg/cm^2)			**0.21**

According to Table 5.10, the shear strength values of K6, K9, and K10 soil samples are observed to be very high than according to the other results. The average value of C_u of the first line is taken **12.74 kPa** and the average value of C_u of the second line is taken **17.97 kPa**.

The Shear Box Test (Unconsolide-Undrained)

The coefficient of cohesive and internal friction angle of K1 soil samples have been determined under different normal load in the shear box. This test is performed under undrained, uncohesive and unconsolide conditions following ASTM D3080 standard. Three normal stresses are applied which are σ_{n1}=1 kg/cm^2, σ_{n2}=2 kg/cm^2 and σ_{n3}=4 kg/cm^2 (Table 5.11).

Table 5.11 The obtained shear and normal stresses

Normal Direct Shear Test			
σ (kg/cm²)	1	2	4
τ (kg/cm²)	0.33	0.79	1.45

The shear stress vs. horizontal displacement graph is prepared for each loading (Figure 5.5). The shear stresses are determined by the peak values from graph and test results.

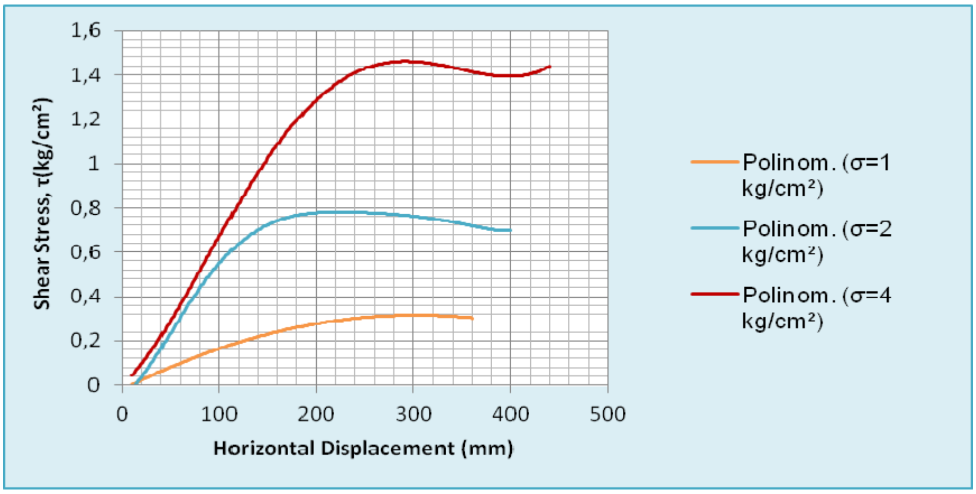

Figure 5.5 Shear stress vs. horizontal displacement graph for different normal loads

K1 soil sample consists of 4.45% shell, 90.31% sand and 5.24% silt, and there is not any cohesive sediment such as clay, as the coefficient of cohesion is assumed to be zero. In addition to this assumption, the internal friction angle (ϕ) is determined to be **23.5°** from test results as shown in Figure 5.6.

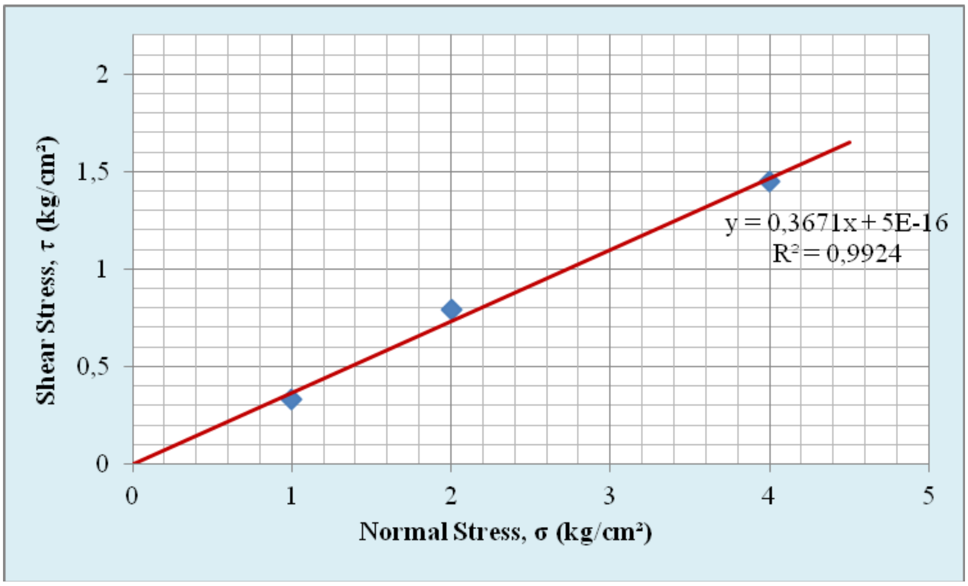

Figure 5.6 The shear stress vs. normal stress graph

5.2 Field Surveys

5.2.1 Grap Sampler

Soil samples are taken using a ***grab sampler*** (Figure 5.7) for the laboratory studies and to make the surface sediment distribution map of study area. The soil samples are taken from 12 different locations on the navigation channel and the north on side of the İzmir bay (Table 5.12). Also the locations of the samples are also shown on the map given in Figure 5.8.

Different methods have been developed for taking marine soil samples. The main types of these samplers are grab sampler and sediment corer. Feeley (2007) compares various sampling methods and lists the advantages and disadvantages of these methods. As for the advantages of grab sampler, he states that it is an inexpensive and easy-to-use method for sediment sampling applications. As for the disadvantages, he states that the samples are disturbed and leaks from the sampler in the process of sampling, hence it is applicable only to soft sediments.

Figure 5.7 a) Grab sampler, b) Soil sample taken by Grab sampler

Table 5.12 The coordinates and depth of samples

Samples	Coordinates - N	Coordinates - E	Depth (-m)
K1	38°25'38.51"	27° 1'20.80"	4.0
K2	38°25'25.98"	27° 1'26.46"	12.0
K3	38°25'16.80"	27° 1'31.68"	13.0
K4	38°25'49.50"	27° 2'9.54"	8.20
K5	38°25'38.94"	27° 2'13.86"	10.0
K6	38°25'27.06"	27° 2'19.08"	12.0
K7	38°27'0.00"	27° 7'20.46"	11.0
K8	38°26'48.36"	27° 7'24.78"	12.0
K9	38°26'37.86"	27° 7'28.20"	13.0
K10	38°26'47.94"	27° 8'10.32	11.0
K11	38°26'57.96"	27° 8'8.94"	11.0
K12	38°27'11.22"	27° 8'6.48"	10.0

Figure 5.8 The location of soil samples taken (Google Maps)

The sediment distribution map is generated using the soil type obtained by the sediment samples as given Figure 5.9.

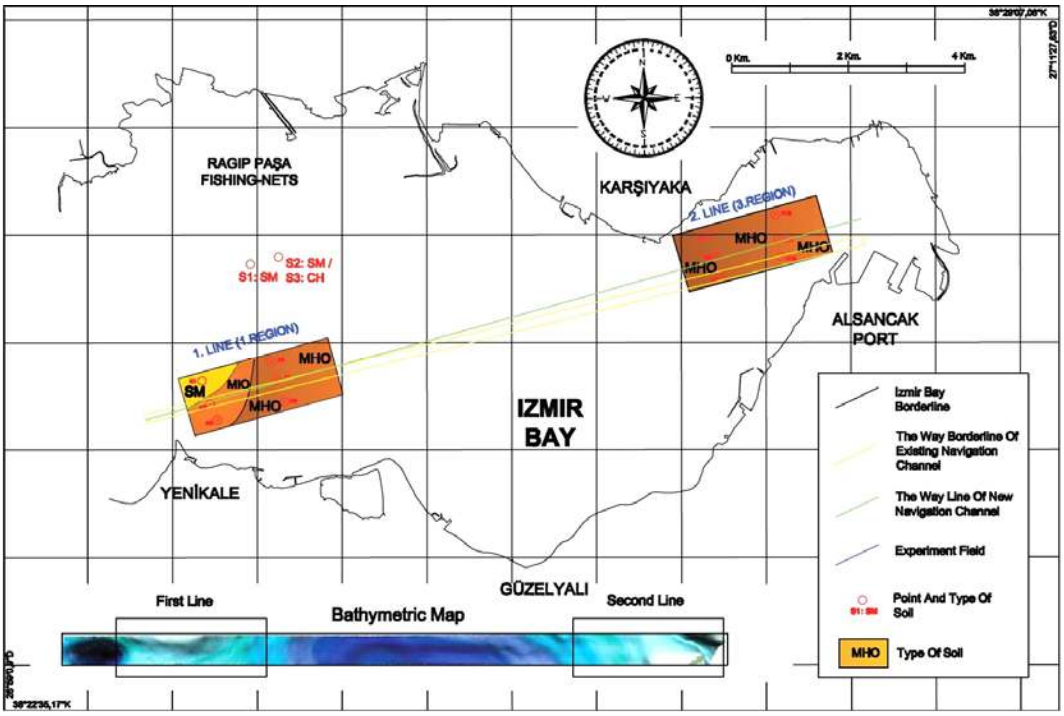

Figure 5.9 The sediment distribution map

5.2.2 Bathymetric Survey

5.2.2.1 Equipments Used

The survey equipments used in the bathymetric studies are as follows;

TopCon GB-500 RTK GPS is used to obtain the position data in the bathymetric study (Figure 5.10). Available, surveying methods of this device are static, rapid static and RTK kinematic surveying. Real-Time Kinematic (RTK) surveying method is used in this study. In this method, GPS systems use two GPS receivers as the base stations and a rover on both land and research vessel. The correction data is taken from the satellites, and then this data is transmitted from the reference station to a rover on the survey vessel via a radio system. This system can provide positions to 2-3 centimeters precision in real time, and the real-time water level changes (tide data) can be obtained within a survey area with this method.

Table 5.13 The performans and RTK specifications of Top-Con GB-500 RTK GPS

Specifications		
Performance	Static, Rapid Static	H: 3 mm+0.5 ppm (x base line length) V: 5mm+0.5 ppm (x base line length)
	RTK	H: 10mm+1ppm V: 15mm+1ppm
RTK	Ambiguity Initialization	OTF
	Communication Formats	CMR+, CMR, RTCM 2.3, TPS
	Multi Base RTK	Supported

Figure 5.10 a) TopCon GPS GB-500 and b) The installation of the reference station using tripod

Trimble HYDROPro Navigation Software (v.2.12) is used in the bathymetric survey. HydroPro is data acquisition system. The software records all the data about sea survey such as vessel dynamics, vessel offset relationships, equipment configurations, guidance information, general system parameters, timing offset. The software provides guidance to survey vessels with guidance objects such as targets, lines, or routes (Figure 5.11).

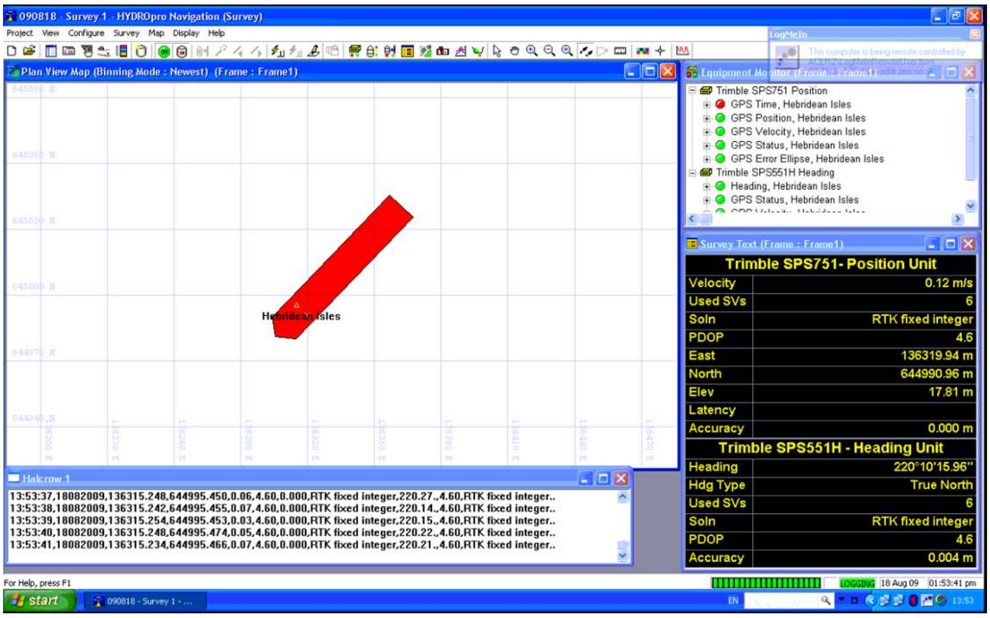

Figure 5.11 HydroPro navigation software

Within the scope of this study, the eight survey lines determined are total for both the first and the second lines on HydroPro software. These lines are taken as perpendicular to the navigation channel. The survey lines used by the HydroPro Navigation Edit software are shown in figure 5.12.

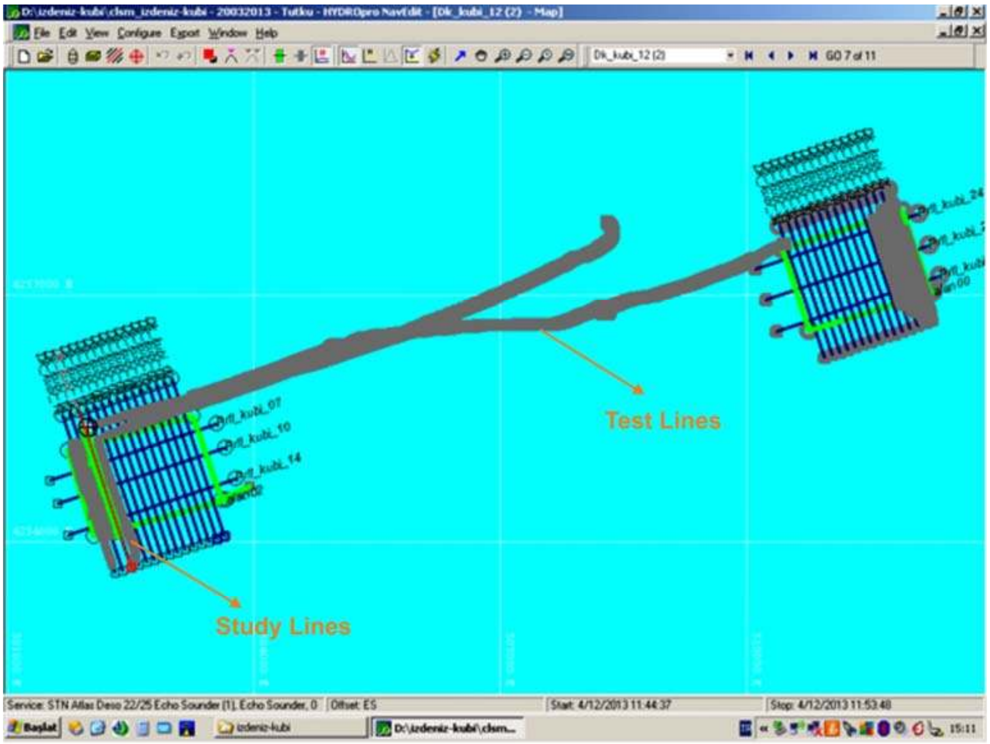

Figure 5.12 The survey lines on the Nav. Edit

<u>Hi-Target HD-370 Echo-sounder</u> is used in the bathymetric study to view the structure of the ground and to transfer data to HydroPro Navigation software (Figure 5.12). HD-370 digital Echo-Sounder is a wide range adjustable high-frequency echo-sounder. The values of frequency are between 100 and 750 kHz. Maximum transmit power: High frequency 500W. Range of speed of sound is between 1370 and 1700 m/s, and sense 1 m/s. Adjustable draft range is between 0.0 m and 15.0 m, and the draft value is taken as 0.65 m for this study. The records taken are replayed using HD-370 software as shown in Figure 5.13.

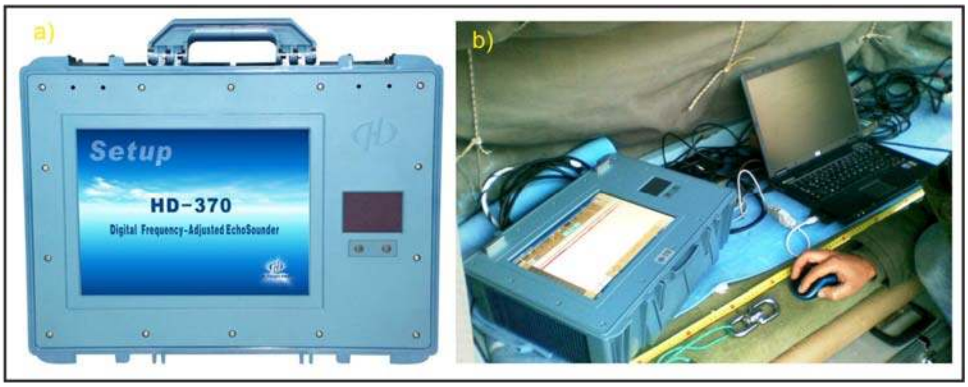

Figure 5.13 a) Hi-Target HD-370 Echo-Sounder, and b) Echo-sounder and survey computer during study

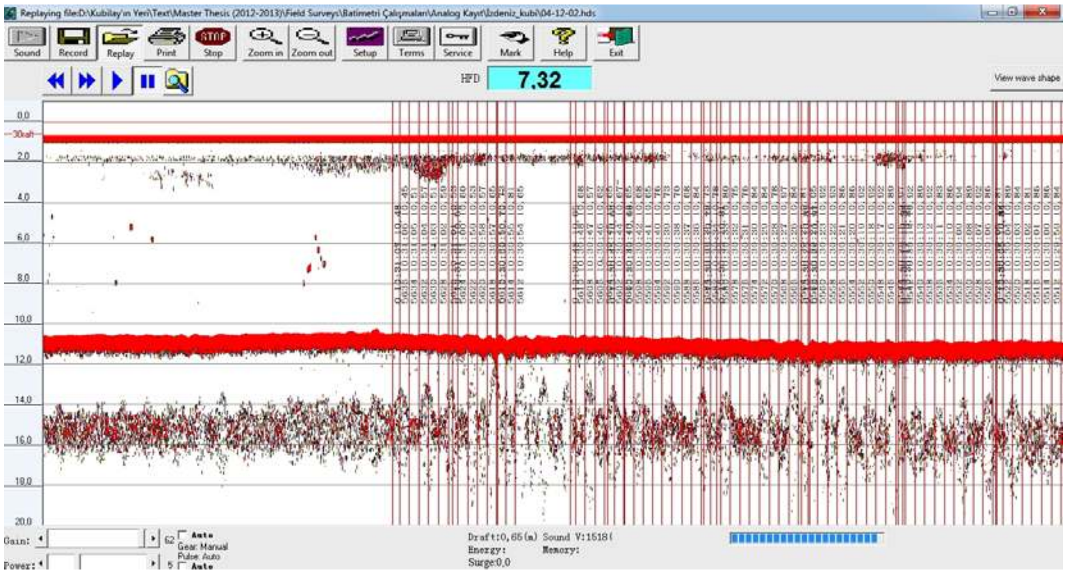

Figure 5.14 Hi-Target HD-370 software displays

Hi-Target HD-370, 200 kHz Transducer is used in this study, and the transducer is called high frequency Single-Beam bathymetric system (Figure 5.15). These systems are used to measure the water depth beneath the survey vessel. In the mapping systems, two different frequencies are used as high and low frequency according to the water depth of study area. High frequency transducer as 200 kHz is used in the water under approximately 60 meters. However, low frequency transducer is preferred for deep water as 50 kHz. High frequency transducer presents high detail information of the seabed, and show less noise and fewer undesired echoes. In this study, high frequency transducer is mounted to side mount of survey vessel (Figure 5.16).

Figure 5.15 Using 200 kHz transducer and work scheme of equipments

Figure 5.16 GPS modem antenna, GPS PG-A1 antenna, and transducer on the survey vessel

CTD RBR 620 is used to determine the properties of the sea water such as speed of sound, salinity, destiny, pressure, temperature (Figure 5.17). The data collected is displayed using Ruskin v.1.7.10 software (Figure 5.18). The speed of sound is measured as 1518 m/s, which is later used by HD-370 Echo-Sounder.

Figure 5.17 RBR 620 CTD

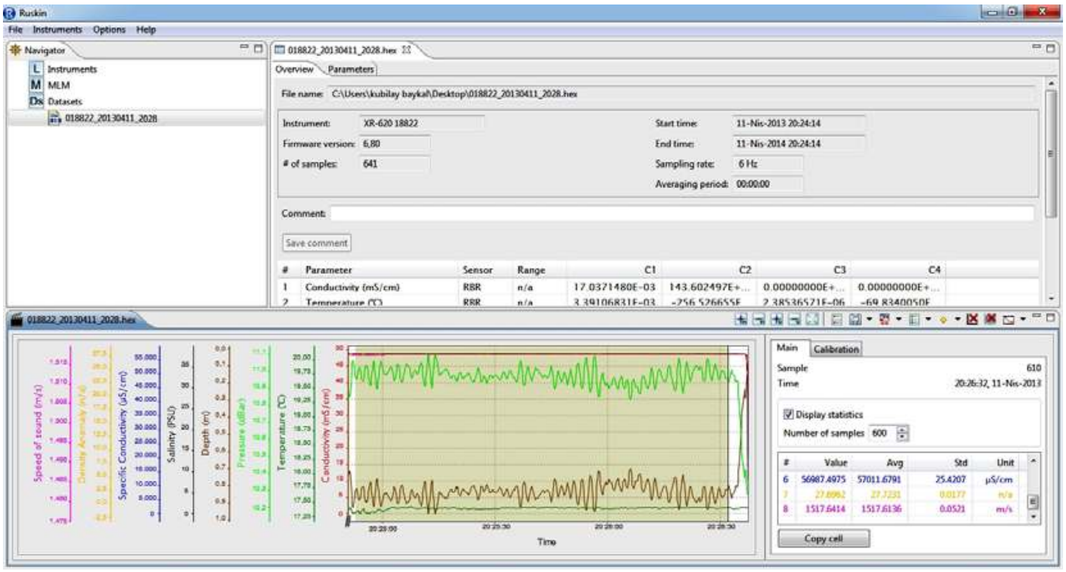

Figure 5.18 The overview of Ruskin software

HYDROPro Navigation Edit is used to edit and analyze depth, heave, tides data collected in the Navigation project. The data of all survey lines obtained are processed via Nav Edit.

HyroPro Navigation software records both the heave and depth values. However, in order to obtain the change of tide and the actual depth values, tide data should be computed from GPS height according to Turkish National Vertical Control Network

[TNVCN] Datum using RTK GPS surveying systems, or tide data should be taken from the nearest tide gauge station to the study area. Also, the tide data obtained are recorded to Navigation project database.

The connection between rover and base station is observed not being fixed in the some places during survey. Therefore, the tide data of Menteş tide gauge station is used in this study. The tide data is measured at 15 s intervals according to Universal Time [UT] and TNVCN Datum by General Command of Mapping (HGK). The tide data used in this study covers the period between 03.04.2013 and 14.04.2013 dates. The data is interpolated using HydoPro Nav. Edit. As seen in Figure 5.19 and 5.20, the maximum sea level is observed as +0.60 m, and the minimum sea level is observed as +0.05 m with respect to TNVCN datum (Figure 5.21). The average daily variation of the mean sea level is observed as 0.25 m (Figure 5.22).

For the survey line selected on the Navigation Edit software, the variation of depth, heave, tide and reduced depth data measured are shown as the depending on time and depth in Figure 5.20. The actual depth values are calculated taking into account the heave and tide data obtained. The depth values processed are defined as the Reduced Depth values. The reduced depth values are exported as x, y, z to map 2D and 3D bathymetric maps.

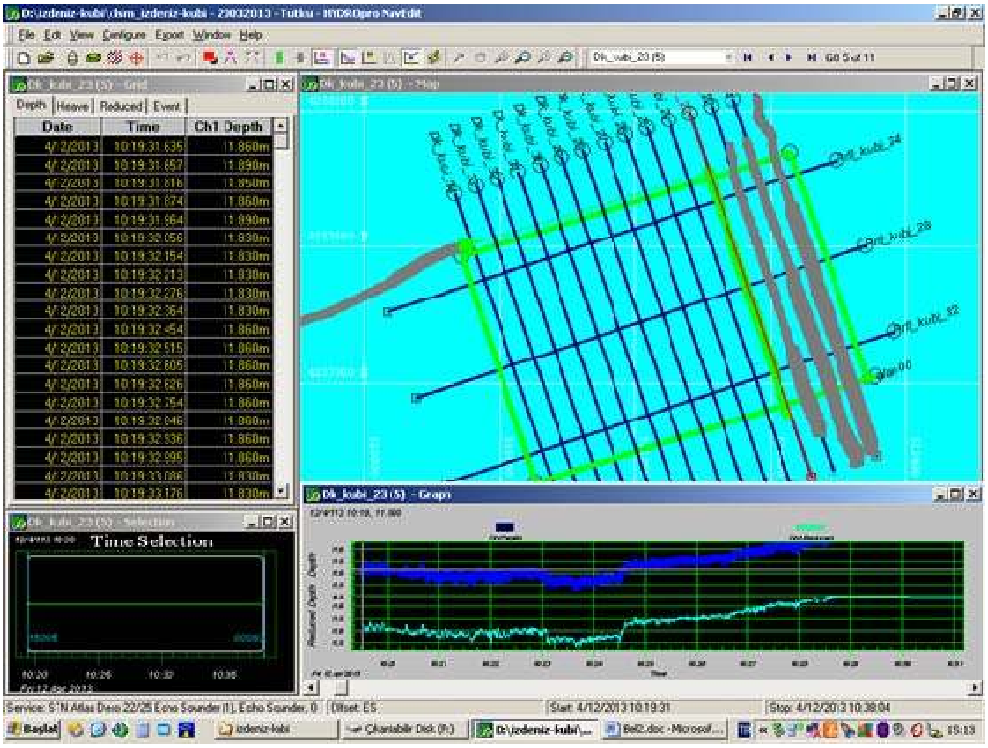

Figure 5.19 The overview of Navigation Edit software

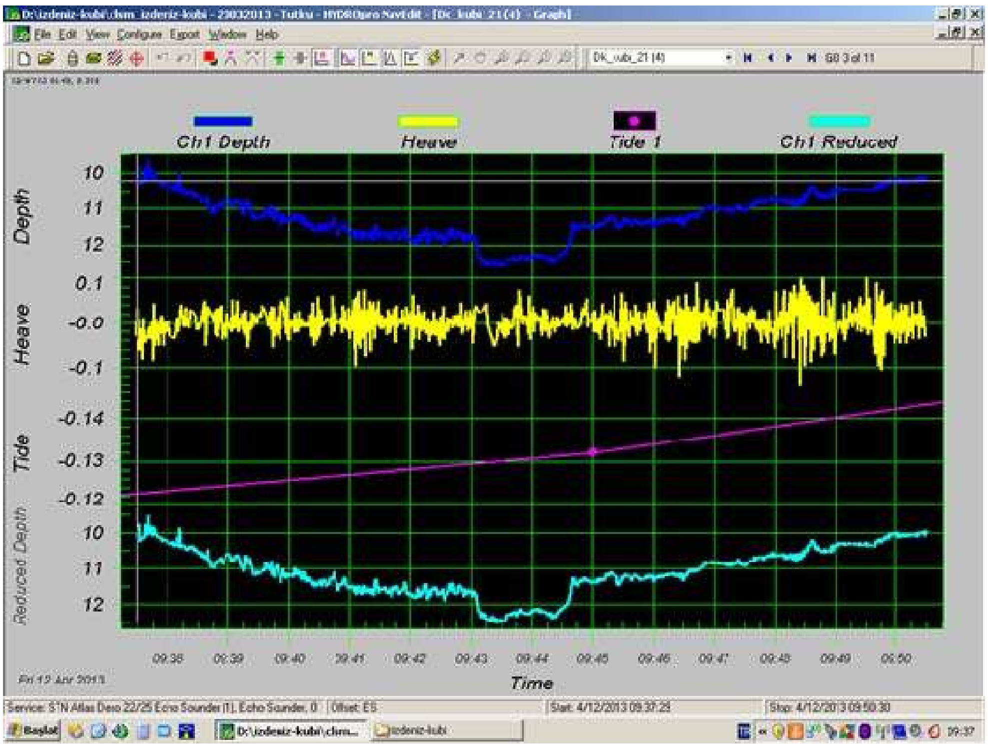

Figure 5.20 The graph of depth, heave, tide and reduced depth for the line selected

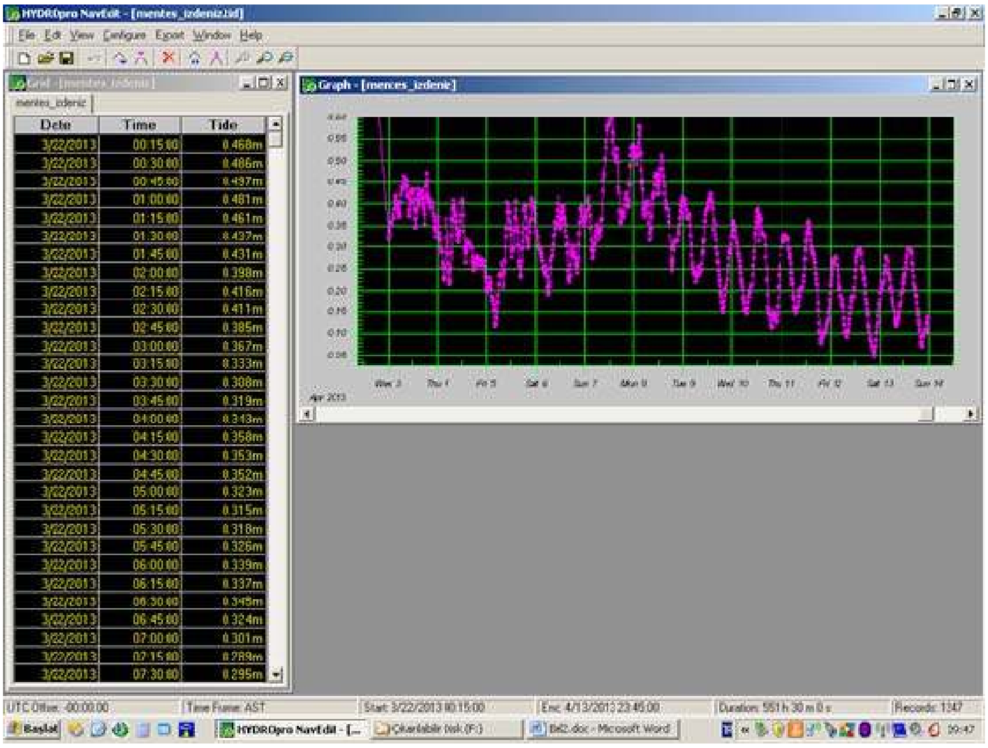

Figure 5.21 The graph and list of the tide data recorded

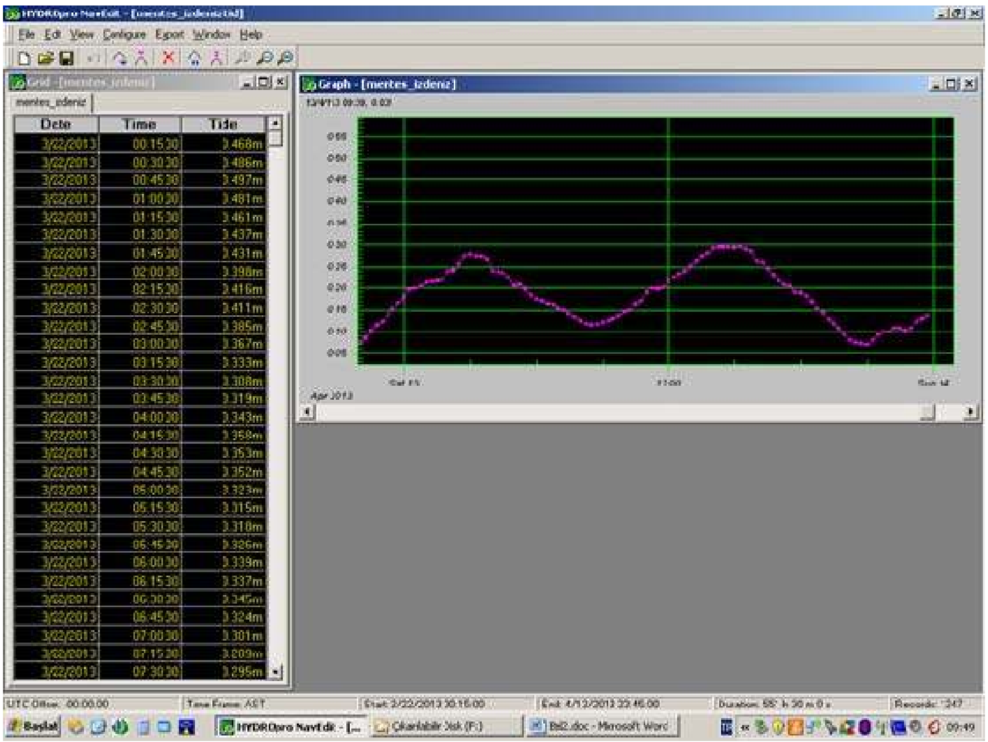

Figure 5.22 The daily changes and list of tide data recorded

Surfer v.9 Software is used to generate the bathymetric map of the first and second study line. The spacing of data is taken approximately 15 m. 48 lines are generated for X axis and 98 lines are generated for Y axis for the first study line. 50 lines for X axis and 107 lines are generated for Y axis for the second study line. The generated maps are presented at 1/1500 scale.

5.2.2.1 Assessment of The Bathymetric Survey

The locations of the navigation channel are shown on the bathymetric maps generated (Figure 5.23 and 5.24). Specially, the channel structure is very noticeable in the second line. However, the channel structure is not visible in the profile of the first study line. Because the depth values of the profile in the first study line is very high compared to the profile in the second study line. Moreover, less dredging works in the first line has been done. So the channel structure is determined using analog records obtained from Echo-Sounder.

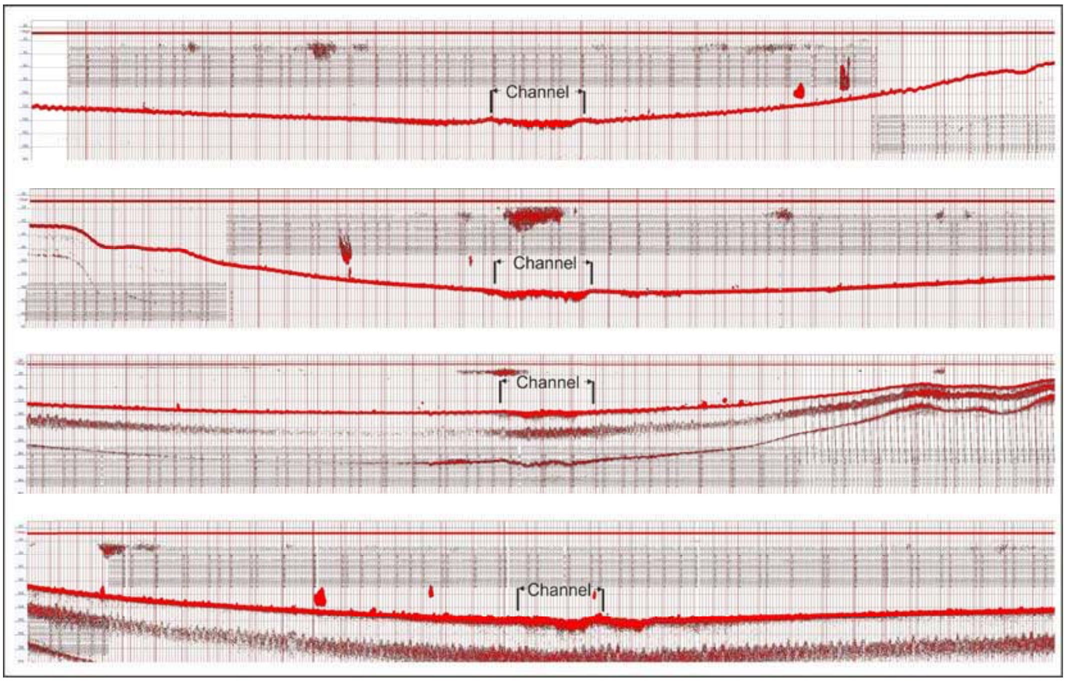

Figure 5.23 The illustration of the channel structure on the analog records taken along the profile of the first line

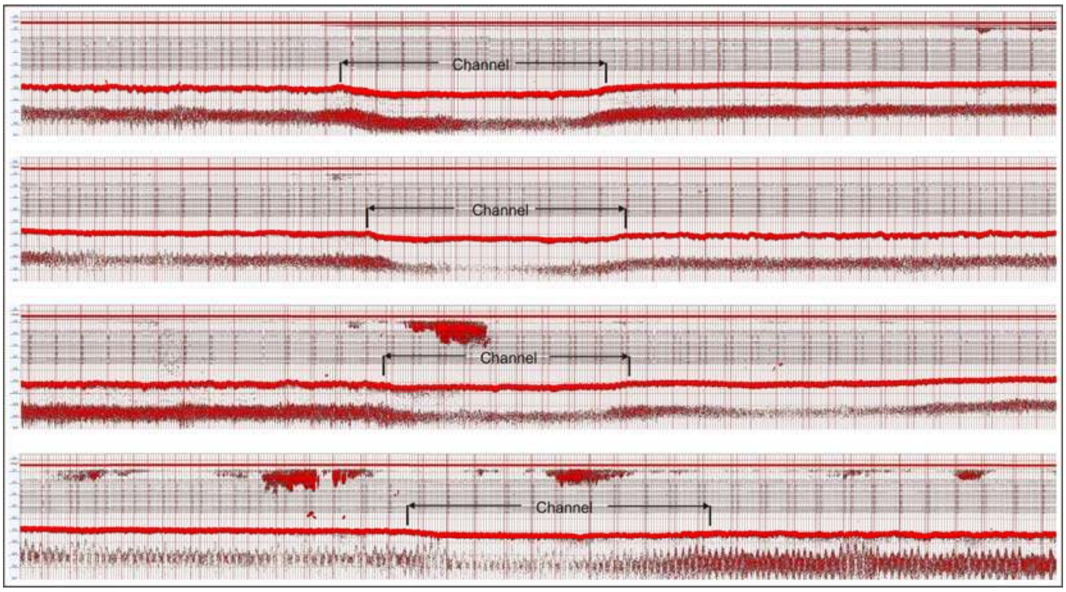

Figure 5.24 The illustration of the channel structure on the analog records taken along the profile of the second line

As seen in Figure 5.23 and 5.24, the channel structure along the profile in the second line is wider than the channel structure at the profile in the first line. The channel widths for the first and second line are measured as approximately 80.0 m and 180.0 m respectively. The decreased with of the navigation channel in the profile of the first line might be attributed to being near to the port, the traffic density of container vessels, and dense dredging works due to shallowness in this region. The channel route is shown over the bathymetric maps of the profiles in the first and second line in Figure 5.24 and 5.25.

Bathymetric maps generated are presented as 2D and 3D in Figures 5.25, 5.26, 5.27, and 5.28. In order to understand better topographical structure of the profiles in the study lines, X and Y scale are selected 45 map units, and Z scales is selected 2 map units for 1.0 cm (Figure 5.26 and 5.27).

For the profile in the first line, According to the 2D bathymetric map given in Figure 5.25, the maximum depth is approximately -16.0 m and the minimum depth is -3.50 m. Also as the depth values reduce and the density of contour lines increases towards the north side of the first line. According to the inclination map generated, the maximum inclination value is 6° and the minimum inclination value is 0.5°

(Figure 5.29). The inclination angle increases significantly to 6° towards the north side of the first line as seen in Figure 5.25 and 5.29. However, the inclination angle increases until 1.5° towards the south side of the first line. So the inclination angle values of the northern slope of the first line are much higher than the inclination angle values of the southern slope of the first line as seen Figure 5.27. Moreover, the flatter topography is observed in the northern slope of the profile in the first line. In this area, the inclination angle is under 1.5° and the maximum depth value is -3.5 m. Additionally, the inclination vectors are shown on the 2D bathymetric map (Figure 5.31). The vector directions tend towards into the channel from both north and south sides of the map. Specially, the vector magnitudes are observed to be very high in the north side of profile compared to the south side.

For the profile in the second line, according to the 2D bathymetric map given in Figure 5.26, the maximum depth is approximately -12.0 m and the minimum depth is -10.0 m. The depth values and density of contour lines changes in a similar rate for both the north and south sides of the profile in the second line. According to the inclination map generated, the maximum inclination value is 1° and the minimum inclination value is observed as close to 0° (Figure 5.30). The maximum inclination angle is observed in the slope of channel. The inclination angle is observed to be approximately 0.5° for both the north and south sides of the profile in the second line. Moreover, the profile of the second line presents much flatter topography compared to the profile in the first line (Figure 5.28 and 5.30). Additionally, the inclination vectors are shown on 2D bathymetric map as shown in Figure 5.32. The vector directions generally tend towards the channel from both north and south sides of the map, although the vector magnitudes are very low. The vector directions are observed to be unstable.

In order to generate external boundaries of the models for slope stability analysis in Slide software, the cross sections are taken as vertical to the contour lines and the channel, and parallel to the vectors from the profiles both the first and second lines.

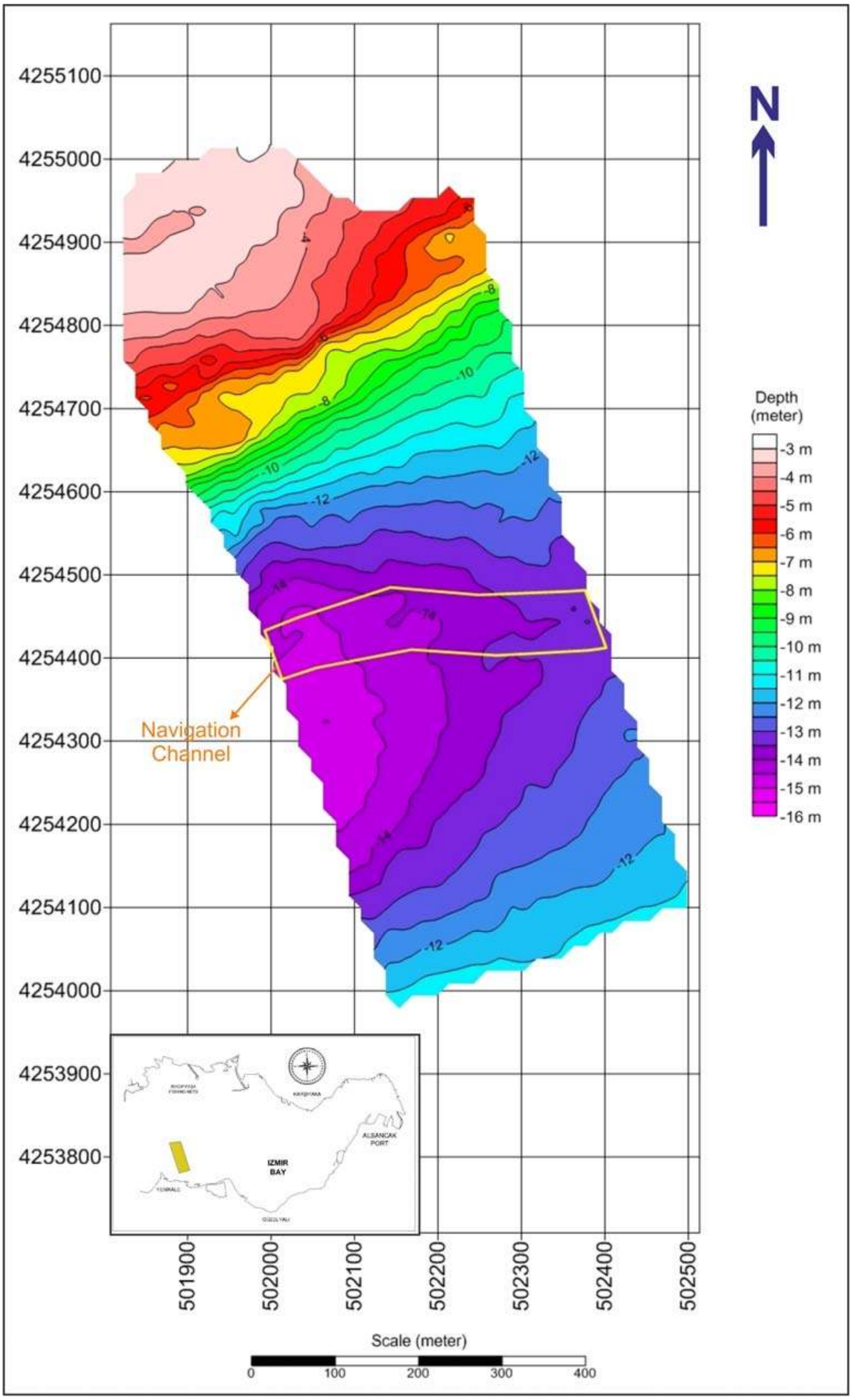

Figure 5.25 The 2D bathymetric map of the profile in the first line

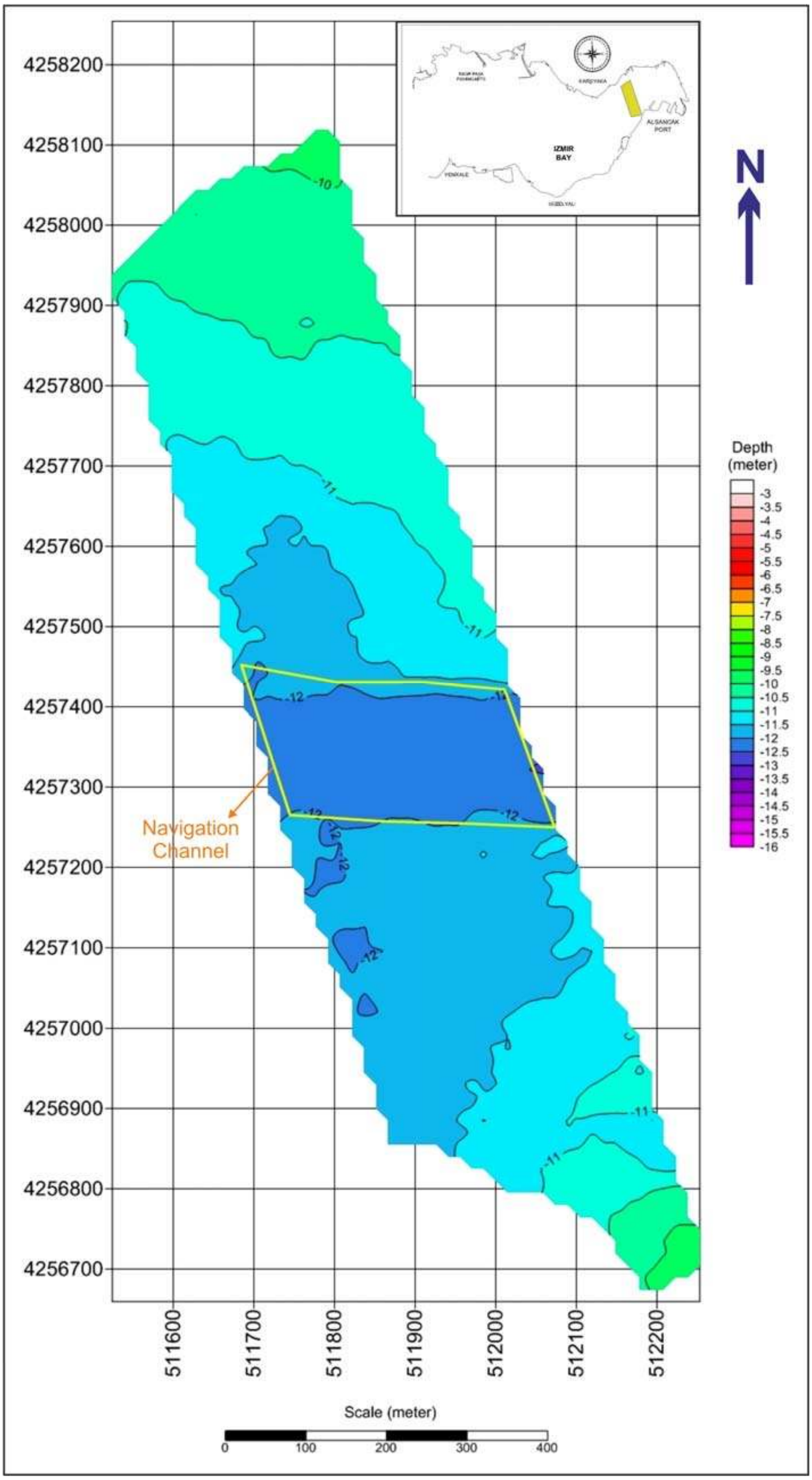

Figure 5.26 The 2D bathymetric map of the profile in the second line

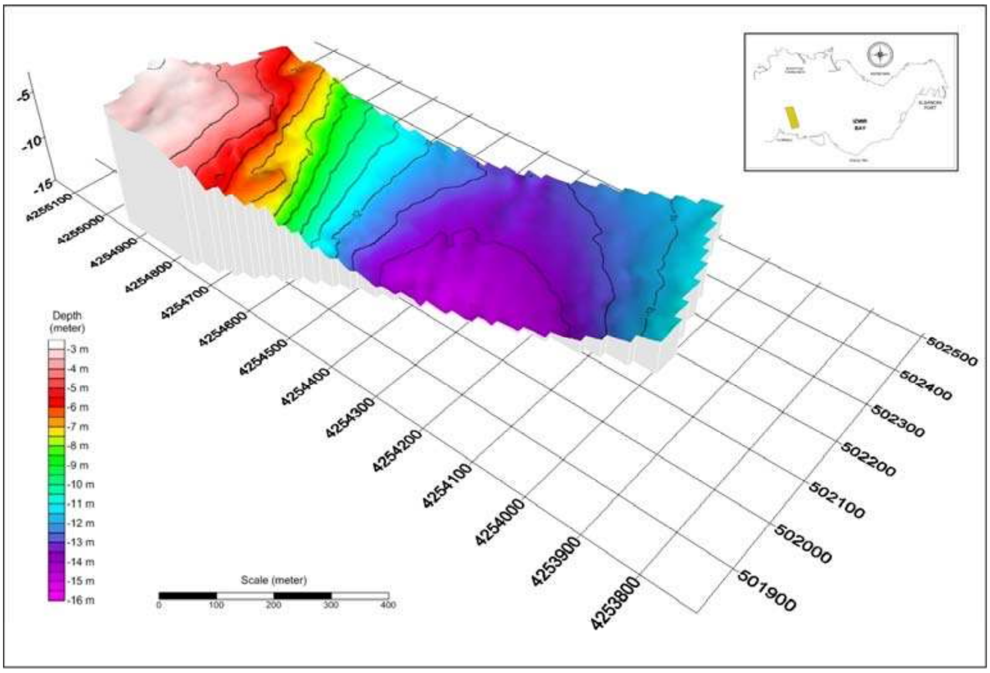

Figure 5.27 The 3D bathymetric map of the profile in the first line

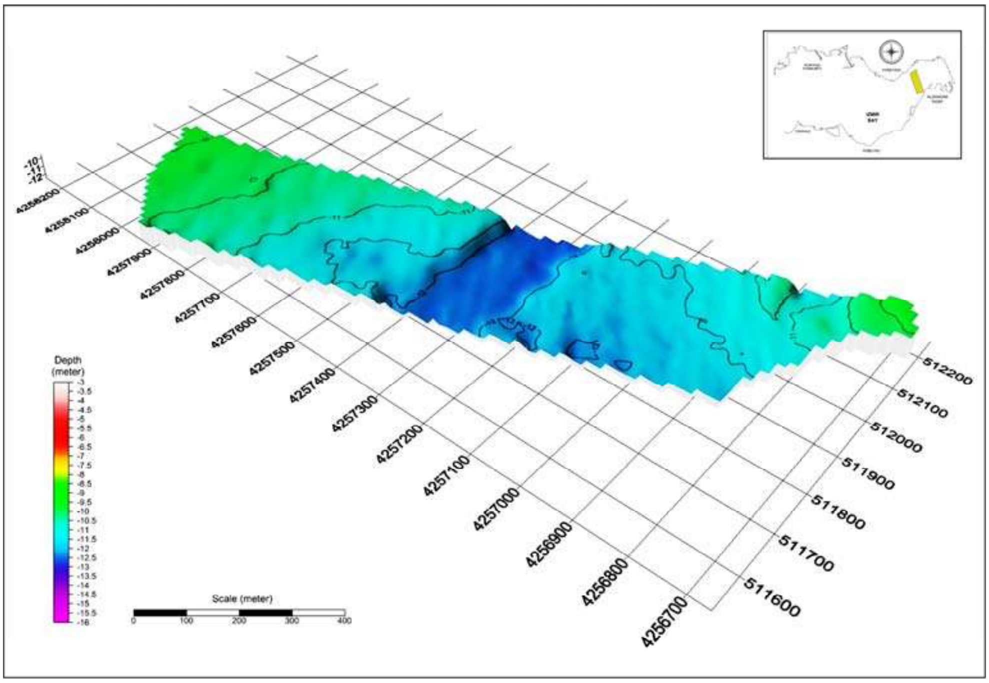

Figure 5.28 The 3D bathymetric map of the profile in the first line

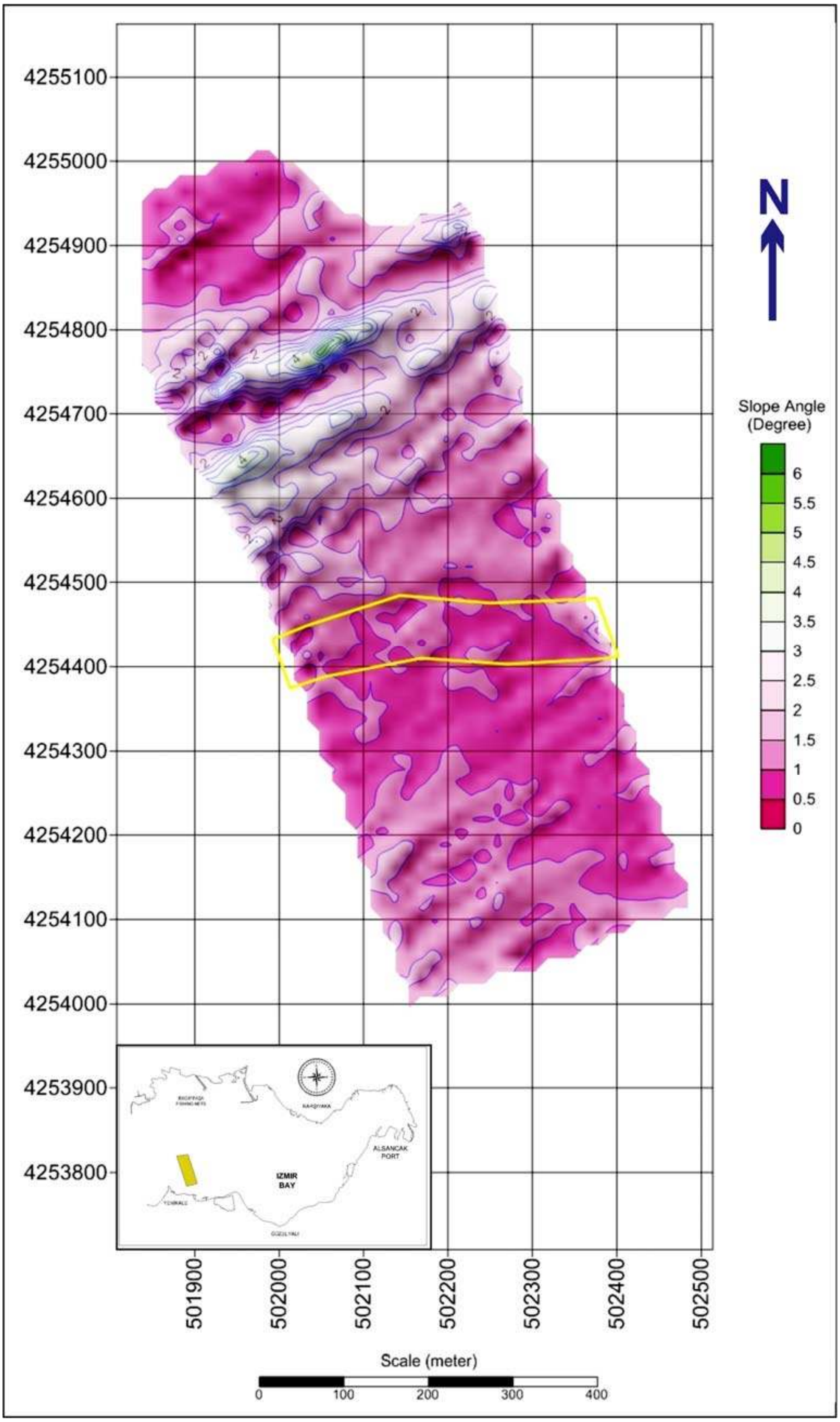

Figure 5.29 The inclination map of the profile in the first line

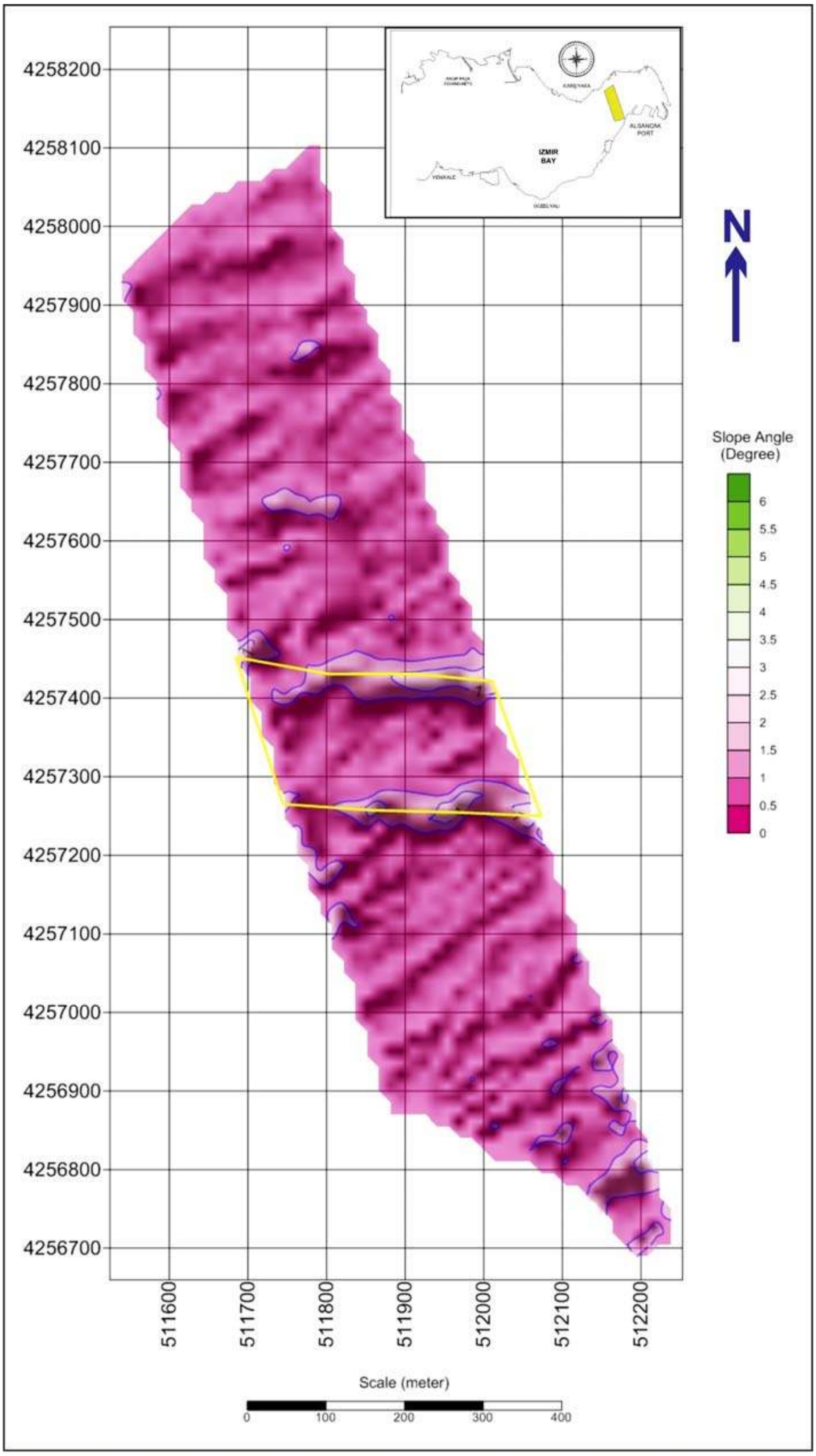

Figure 5.30 The inclination map of the profile in the second line

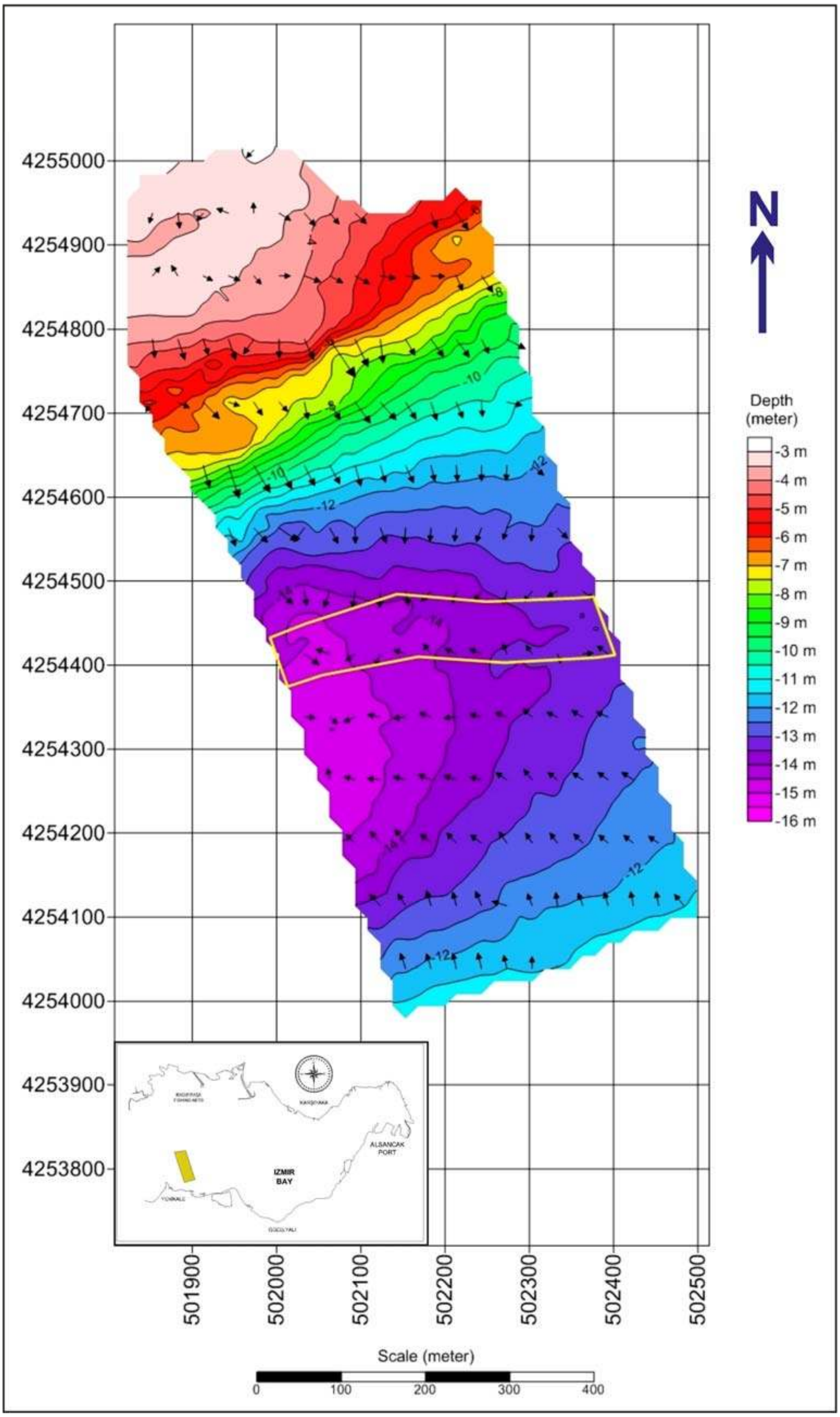

Figure 5.31 The vector map of the profile in the first line

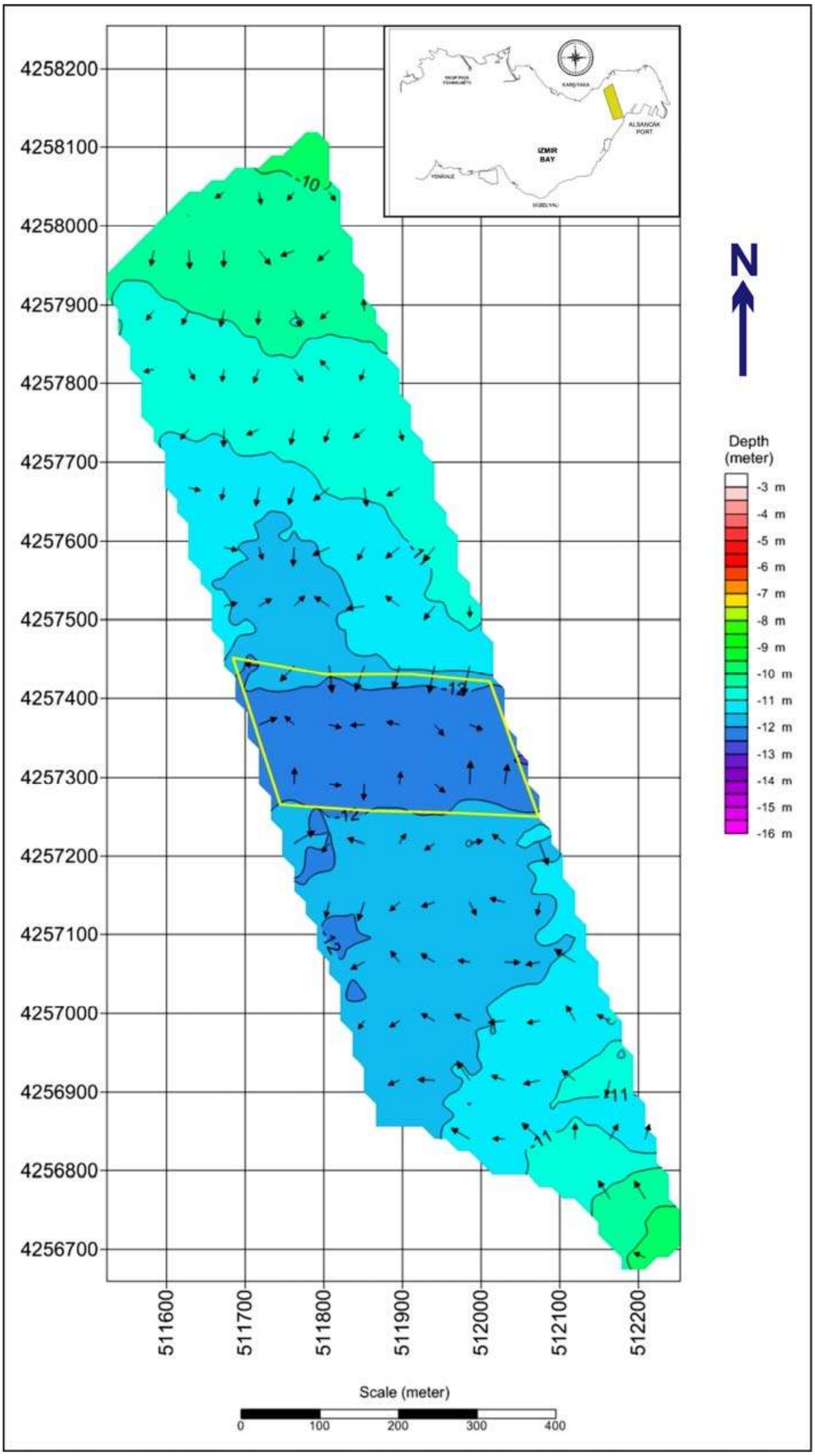

Figure 5.32 The vector map of the profile in the second line

CHAPTER SIX
SLOPE STABILTY ANALYSIS

6.1 Introduction

Slope stability is one of the most common problems in geotechnical engineering in the design of various types of construction works such as embankments, earth dams, navigation channels, and excavations which have to be safe, economic and environmentalist. Several slope stability analysis methods have been developed over many years and are still developed in order to achieve more accurate results both analytically (hand-calculations) and numerically (software).

The aims of slope stability analyses are;

- To understand the development and exchange of both natural slopes and human-made slopes under different environmental conditions,
- To determine the stability of slopes (natural or human-made) under short-term or long-term conditions,
- To examine the effect of triggering mechanisms (tsunami, earthquake, etc.) and understand failure mechanisms, and
- To study the effect of various dynamic loadings (seismic, wave, tide, etc.), qua-static or static loadings on slopes, underwater slopes, and embankments.

Numerous researchers have developed two and three dimension, and different analysis methods to resolve slope stability problems. However, two dimensional slope stability methods are the most commonly used methods among the engineers as they can be simply utilized for hand-calculations. There may be small differences in both among two dimensional slope stability methods, and between the two dimensional and three dimensional methods about the accuracy of the analysis results.

According to Albatainech (2006), the accuracy of the analysis results vary between different analysis methods is due to that these methods are based on simplifying assumptions to reduce the three dimensional problem into a two dimensional problem.

In this chapter, different slope stability analysis methods were fully reviewed, and both advantages and disadvantages of these analysis methods are denoted. Also the selection of appropriate software to determine for the slope stability analysis is discussed.

6.2 Slope Stability Analysis Methods

The calculation of global stability is commonly expressed in terms of factor of safety computed by means of *Limit Equilibrium Method* (Krahn, 2004). In the limit equilibrium method, the factor of safety is calculated using one or more of the equations of static or quasi-static equilibrium applied to the soil mass bounded by an assumed, potential slip surface and the surface of the slope. This method requires iterative techniques to obtain the lowest value for factor of safety.

Gitirana (2005) stated that Limit Equilibrium Methods of Stability Analysis are divided to three parts. These parts are Method of Slices, Finite Element Stress Methods and General Slip Surface Methods as given in Figure 6.1.

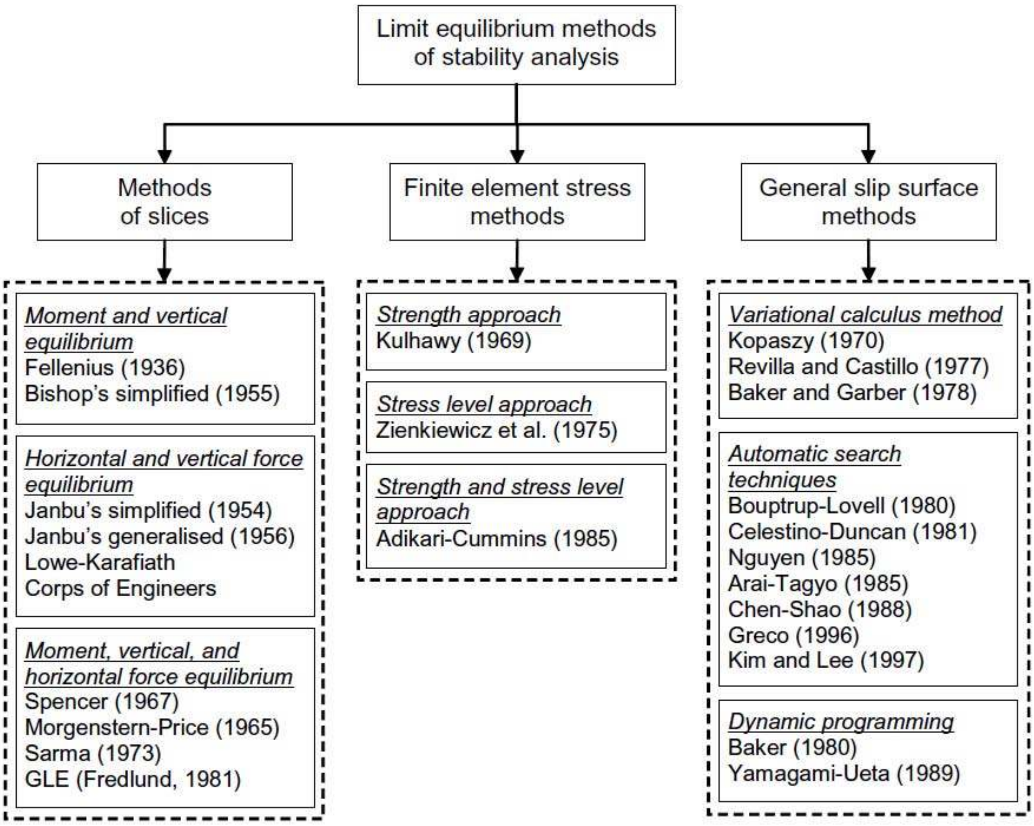

Figure 6.1 Categorisation of common limit equilibrium methods of stability analysis (Gitirana, 2005)

In Methods of Slices, the static equilibrium is applied to each of the slices and to the slipping wedge as a whole. A circular slip surface is assumed to calculate the minimum factor of safety. There are three different static equilibriums as moment, vertical and horizontal force equilibrium. According to Gitirana (2005), Fellenius (OMS) and Bishop's Simplified are used moment and vertical force equilibrium. Janbu's Simplified, Janbu's Generalized, Lowe-Karafiath and Corps of Engineers are used horizontal and vertical force equilibrium. Spencer, Morgenstern-Price and Sarma are used moment, vertical and horizontal force equilibrium.

In Finite Element Method, the Limit Equilibrium methods purpose to obtain the factor of safety under static or seismic condition on assumed critical failure surface. These slope stability analyses may need additional information such as displacement, pore water pressure, and potential complex failure mechanisms. In such cases, the stress deformation analyses should be done using software based on the finite element method (FEM) with 2D or 3D analyses. Moreover, the construction pore water pressures, the potential and possibly complex failure mechanisms may be easily provided by the finite element method.

United States Army Corps of Engineers [USACE] (2003) provide the procedure for using the FEM to compute factors of safety as follows:

- Perform an analysis using the FEM to determine the stresses for the slope
- Select a trial slip surface
- Subdivide the slip surface into segments
- Compute the normal stresses and shear stresses along an assumed slip surface. This requires interpolation of values of stress from the calculated at Gauss points in the finite element mesh to obtain values at selected points on the slip surface. If an effective stress analysis is being performed, subtract pore pressures to determine the effective normal stresses on the slip surface. Therefore the pore pressures are determined from the same finite element analysis if a coupled analysis was performed to compute stresses and deformations.
- In order to compute the factor of safety value and available shear strength at points along the shear surface, use the normal stress and the shear strength parameters as c and ϕ, or c′ and ϕ'. Use total normal stresses and total stresses shear strength parameters for total stress analysis and effective normal stresses and effective stress shear strength parameters for effective stress analysis.
- Compute an overall factor of safety using the following Equation 5.14;

$$F = \frac{\sum S_i \Delta l}{\sum \tau_i \Delta l} \qquad \text{Eq 5.14}$$

Where; S_i is available shear strength, τ_i is shear stress, Δl is length of each individual segment into which the slip surface has been subdivided.

Finite Element Method could be summarized as follows:

- This method is more efficient with soil properties determined by pre and post laboratory tests.
- The properties of soil are modeled with a non-linear function such as mesh type.
- It calculates stress, displacement, and pore water pressure.
- It controls swelling and consolidation during and after making construction
- It monitorizes cracking, hydraulic cracking, failure, and general stability.

General Slip Surface Method, The assessment of transient stability conditions requires repeated computations of *factor of safety* for several time steps. The availability of an automated search procedure becomes advantageous for such conditions (Gitirana, 2005).

6.3 Method Selection

Onalp & Arel (2004) classify the slope stability methods into two as deterministic and probabilistic.

- Deterministic methods provide absolute solutions for given particular input parameters.
- Probabilistic methods are highly dependent on the variability of the soil properties, geological and environmental conditions. Also slope stability analysis is based on the calculus of probability.

Recently, computer programs are often used for slope stability problems. These software packages are basically based on deterministic methods (Table 6.1). These deterministic methods can be divided into three main methods such as Slice Methods, Finite Element methods and General Slip Surface Method of Limit Equilibrium.

According to Onalp & Arel (2004), the limit equilibrium slice method is fast and practical. In comparison to the limit equilibrium slice methods, Janbu's Simplified and Bishop's Simplified Methods can be applied for simple slope stability analyses. Moreover Morgenstern-Price and Spencer Methods might are used under external loads condition as water, seismic etc. for more detailed investigation. However, the weak side of the slice method is that it doesn't consider displacements in environment, and when it needs additional information such as displacement, pore-water pressure, and potential complex failure mechanisms, the stress-deformation analysis should be done in environment. In this case, Limit Stress Methods are used with different methods such as Finite Element, Discrete Element, and Plasticity Theory.

Table 6.1 Software for slope stability analyses (Onalp & Arel, 2004)

Software	Method	Dimension	Author
CHASM	Hydrology, Bishop	2D, 3D	University of Bristol
CLARA 2.31	Janbu	2D, 3D	O. Hungr Geotechnical B.C
ESAU			
ESTAVEL			
GALENA	Bishop	2D	Australia
GEOSLOPE			
GGU STABILITY	Circular and Polygon Slip Failure	2D	GGU-Software, Germany
LEASE	OMS; Bishop, Morgenstern-Price	2D	M.I.T
MPROSTAB			
PCSTABL5M	Bishop, Janbu	2D	Purdue University
SLIDE 3.0	OMS, Bishop, Janbu	2D	Rocscience Inc., Toronto
SLOPE	Bishop	2D	Geosolve, London
SLOPE/W, SEEP/W	Morgenstern-Price	2D	Geosolve Inc., Calgary, Alberta
SLOPE8R, STABR	Spencer	2D	Virgina Tech
STABLE V	Bishop, Janbu	2D	University of Wisconsin
TSLOPE3		3D	TAGA Inc. California
TSTAB			

Table 6.1 Cont.

UTEXAS3	Spencer, Bishop, Swedish, Lowe&Karafiath	2D	Shinoak
WINSTABL			
FEDAM	Finite Element	2D	Univ. California-Duncan
Z-SOIL	Finite Element	2D, 3D	Lausanne, Schweizerisch
FLAC	Finite Element	2D, 3D	Itasca Consultin, Minneapolis
PLAXIS	Finite Element	2D, 3D	Netherland
$PHASE^2$	Finite Element	2D	Rocscience
UDEC	Discrete Element	2D	Itasca Consulting, MN
TRIDEC	Discrete Element	3D	Itasca Consulting, MN

Since the limit equilibrium methods are practical and fast, they are the most commonly used methods. These methods are used both in hand calculations and in the most of the software such as Slide, Slope and Slope/W etc. (Table 6.1). On the other hand, the finite element method is generally applied to much more complex engineering problems.

In this study, Rocscience Slide v.6.0 software, based on the limit equilibrium method, is used to investigate the submarine slope stability problems for Alsancak navigation channel. Slide is a limit equilibrium package to perform two-dimensional analyses in geotechnical engineering. Also Slide considers for the both static analysis and dynamic, and uses more and different soil parameters. Therefore, the material types of slopes are modeled using the different soil types obtained via the laboratory tests for slope stability analysis. Slope stability is analyzed considering the different seismic loads, sea water loads and slope angles conditions. The relationship between slope angle and factor of safety is obtained in analysis.

6.4 Using Slide Software

Slide v.6.0 is used to analyze the submarine slope stability under static conditions within the scope of this study. The detailed analysis steps of the Slide is as follow,

6.4.1 Project Settings

The Project Setting is selected to configure the main analysis parameters for the model formed. The Project Settings consist of General-Methods-Ground Water-Transient-Statistics-Random Numbers-Design Standard-Advanced-Project Summary titles.

Select: Analysis → Project Settings

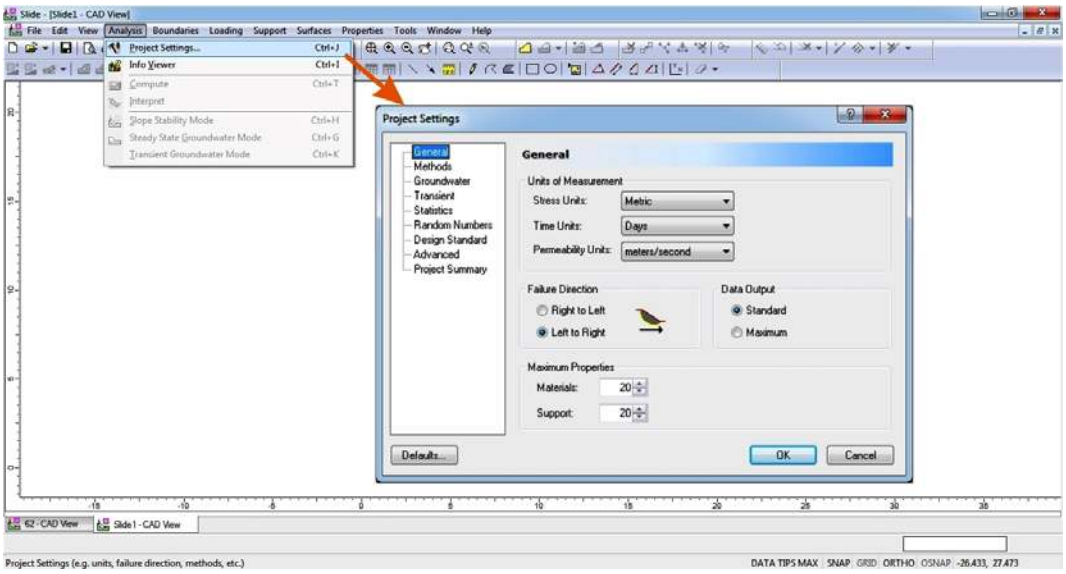

Figure 6.2 The Project Settings in Slide

For all modeling studies, the defined project properties are presented as follow;

- *General*; Units of Measurement: metric, days, meters/second, Failure Direction: Right to Left for the north slopes and Left to Rigth for the south slopes, Data Output: Standard, Maximum Materials: 2.

- *Method*; Methods: Bishop Simplified, GLE/Morgenstern-Price, Janbu Simplified, *Convergence Options*; Number of Slices: 25, Tolerance: 0.005, Maximum Iterations: 50
- *Groundwater*; Method: Steady State FEA (Finite Element Analysis), Pore Fluid Unit Weight: 10.05, *Steady State FEA Options*; Maximum Number of Iterations: 500, Tolerance: 1e-006.
- *Statistics*: Sensitivity Analysis
- Random Numbers Generation: Pseudo-random (constant seed value)
- Advanced; Initial Trial Value of FS: 1, Check malpha < 0.2, Iterate Using Steffensen's Method.

In order to determine the safety of factor (FS), Bishop Simplified, GLE/Morgenstern-Price and Janbu Simplified methods are used as methods of slice.

Different seismic coefficients are applied to slope analysis of the cross section taken from both the first and the second lines.

6.4.2 Entering Boundaries

Firstly, External Boundary is defined for each model. The coordinates of model are entered in the prompt line at the bottom right of screen in order to create the topography of study area, or the mouse's cursor is used.

Select: Boundaries → Add External
Enter Vertex: 70 0
Enter Vertex: 0 -20
Enter Vertex: [t=table, i=circle, esc=cancel, a=arc, u=undo]
Enter Vertex: c [cancel]

Moreover, "t" text command can be entered in the prompt line at the bottom right of screen in order to open coordinates table. Then the coordinates may be entered to this table, or the coordinates table prepared may be imported. Press "Enter" to confirm the entering command. Select "Zoom All" to show model to the center of the view.

In this study, in order to analyze slope stability using Slide v.6.0, two different topographies are considered from first and second study lines. These topographic models are obtained from bathymetric maps generated using Surfer v.9.0. The cross-sections are taken as A-B and C-D from the bathymetric maps generated of the first and second study line by Slice option in Surfer software. The cross-sections taken are shown over the maps in Figure 6.3.

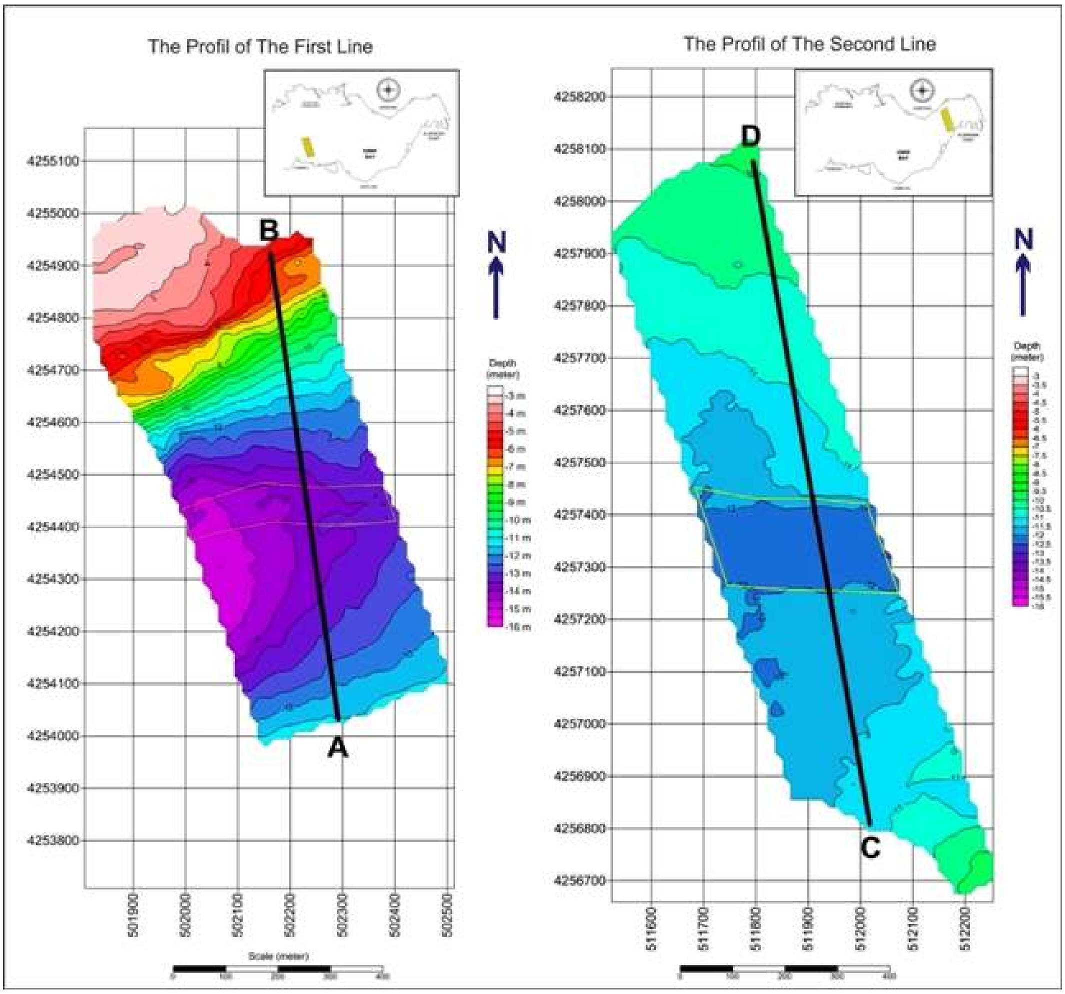

Figure 6.3 The A-B and C-D cross-sections on the bathymetric maps

The models are generated as 1:1 scaled using the coordinate and depth values (y,z) of the cross-sections in AutoCad Software. DXF file generated using AutoCad is imported as External Boundary from AutoCad to Phase2 (Figure 6.4 and 6.5). The A-B and C-D cross sections are shown in Figure 6.4 and 6.5.

Also, the soft sediment layer thickness was taken from Kayalar (1985). The thickness of soft surface layer is defined as 2.0 m for the Model_1 and Model_2 in the A-B cross-section taken along the profile in the first line. The thickness of soft surface layer is defined as 4.5 m for the Model_3 and Model_4 in the C-D cross-section taken along the profile in the second line.

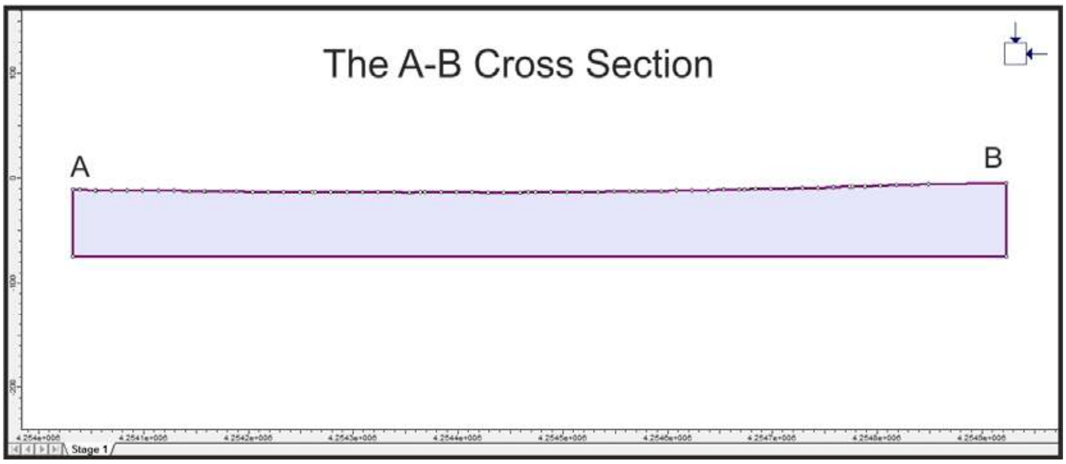

Figure 6.4 The A-B cross section in the profile of the first line

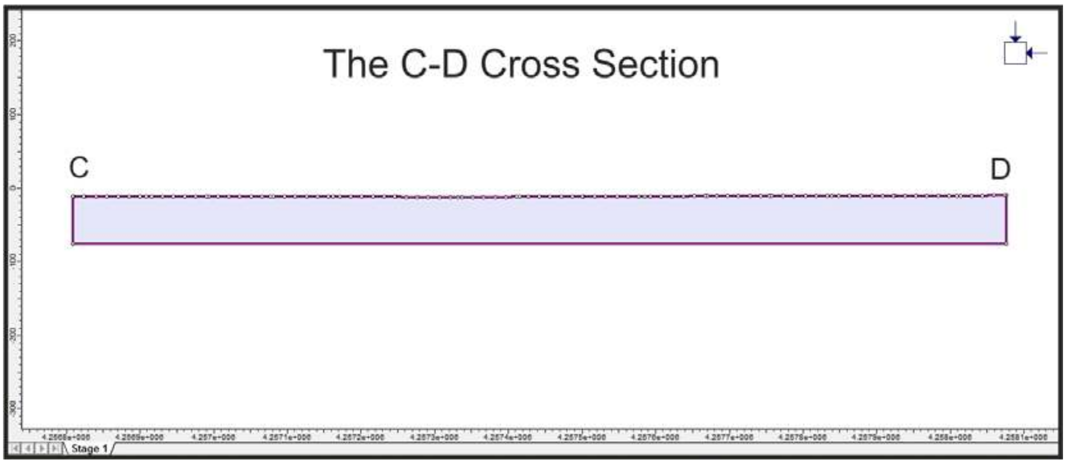

Figure 6.5 The C-D cross section in the profile of the second line

The bottom of external boundary is defined as -40.0 m, and the mean sea water level is defined 0 m for all models. Model_1 represent as the south side of channel, and Model_2 represent the north side of channel in the first line (Figure 6.6). Model_3 represent the south side of channel, and Model_4 represent the north side of channel in the second line (Figure 6.7).

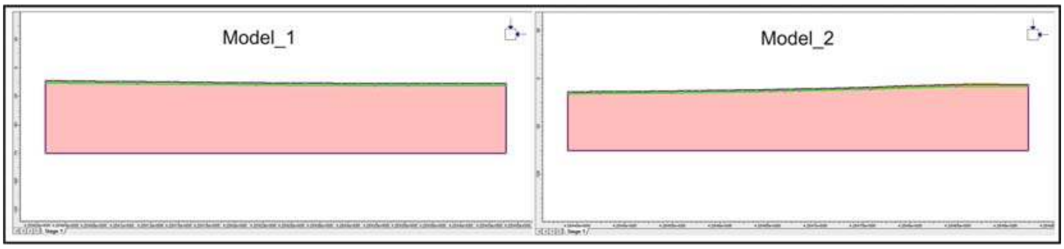

Figure 6.6 The model_1 and model_2 formed using the coordinates

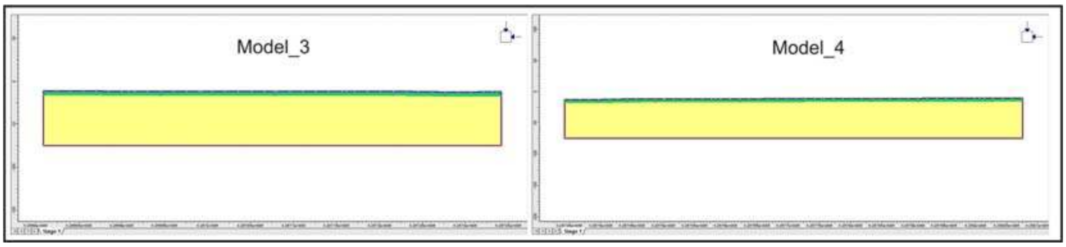

Figure 6.7 The model_3 and model_4 formed using the coordinates

6.4.3 Meshing

In Slide, meshing is selected to generate the finite element mesh, and meshing is a simple two-step process. First the boundaries must be discretize and then the mesh can be generated.

Select: Mesh → Mesh Setup → Discretize →Mesh

For all modeling studies, the defined project properties are presented as follow;

- Mesh Setup: Element Type: 6 Noded Triangles, Approximate Number of Mesh Elements: 1500.

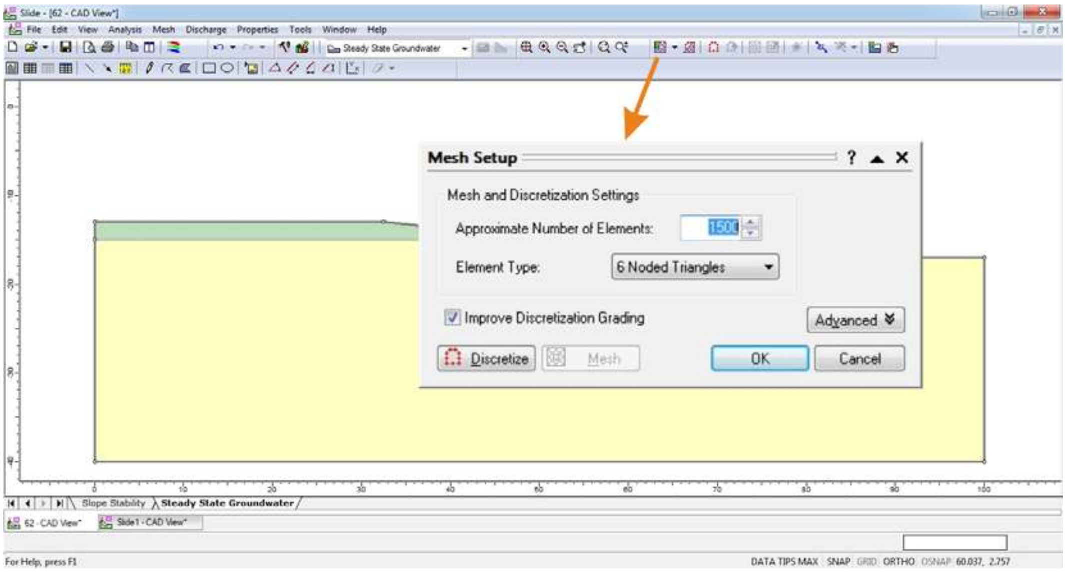

Figure 6.8 A mesh creating in Slide

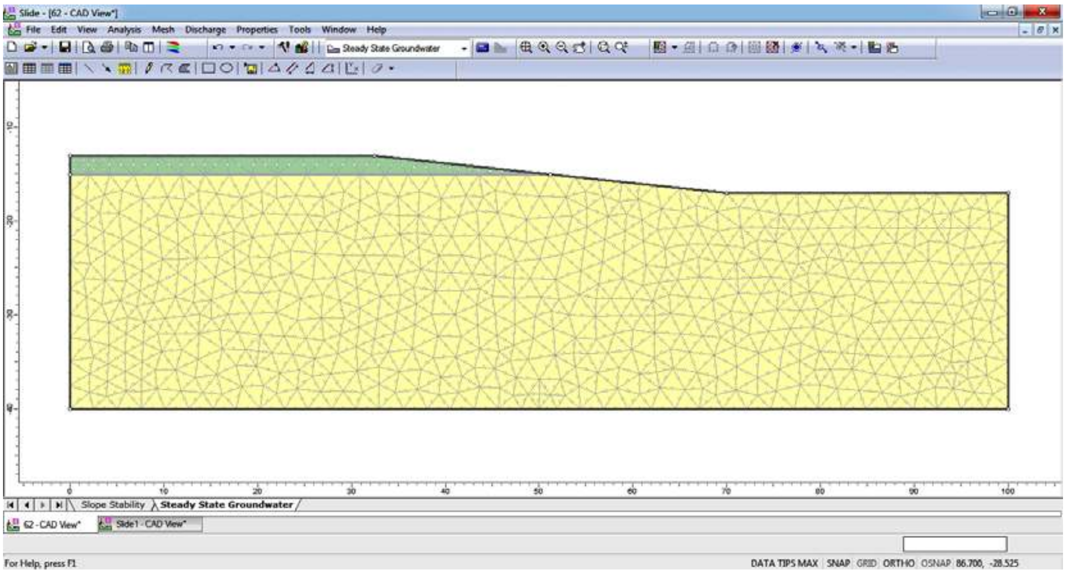

Figure 6.9 The generated mesh in Slide

6.4.4 Properties

6.4.4.1 Material Properties

The geotechnical properties of soil were determined by the laboratory tests. Material properties are defined using the parameters related to the geotechnical properties of soil in Slide.

Select: Properties → Define Materials

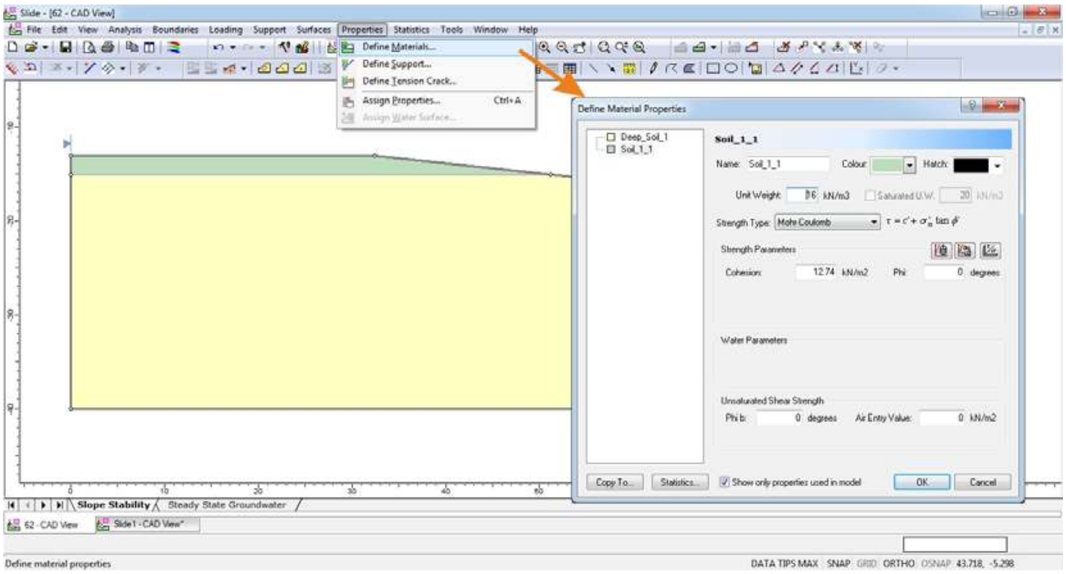

Figure 6.10 Material properties in Slide

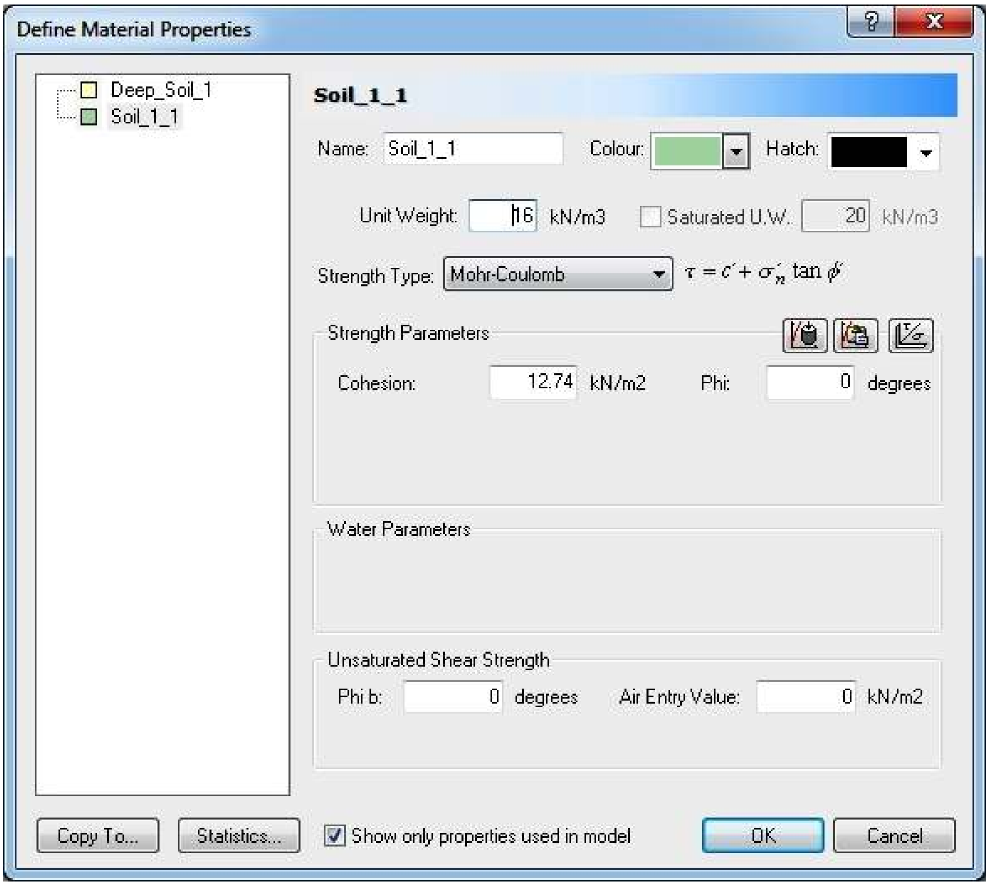

Figure 6.11 Use of the material properties in Slide

For all modeling studies, using soil types are Soil_1_1(MHO-MIO), Soil_1_2(SM), Soil_2_3(MHO), Deep_Soil_1 and Deep_Soil_2. The properties defined of these materials are presented as follow;

- Material 1: Soil_1_1(MHO-MIO) for 1.Line, Young Modules: 2000 kPa, Unit Weight (kN/m^3): 16, Poisson's Ratio: 0.3, Undrained Shear Strength (C_u) (kN/m^2): 12.74.
- Material 2: Soil_1_2(SM) for 1.Line, Young Modules: 10000 kPa, Unit Weight (kN/m^3): 19, Poisson's Ratio: 0.3, Strength Type: Mohr-Coulomb, Fric. Angle (deg): 23.5°, Cohesion (kN/m^2): 0.
- Material 3: Soil_2(MHO) for 2.Line, Young Modules: 2000 kPa, Unit Weight (kN/m^3): 16, Poisson's Ratio: 0.3, Undrained Shear Strength (C_u) (kN/m^2): 17.97.
- Material 4: Deep_Soil_1 for 1.Line, Young Modules: 3000 kPa, Unit Weight (kN/m^3): 18, Poisson's Ratio: 0.3, Undrained Shear Strength (C_u) (kN/m^2): 17.50.
- Material 5: Deep_Soil_2 for 2.Line, Young Modules: 3000, Unit Weight (kN/m^3): 18, Poisson's Ratio: 0.3, Undrained Shear Strength (C_u) (kN/m^2): 21.

The information related to Deep_Soil_1 and Deep_Soil_2 is collected from the soil laboratory report prepared by Kayalar (1985) from Civil Engineering Department, Dokuz Eylül University within the scope of Izmir Alsancak Port Extension Project-Geomorphological Surveys of Dredging Areas. Also Young Modules, Unit Weight and Poisson Ratio values of all soil materials are taken from Zhu (n.d.) of the GEOL 615 lecture note prepared by Geology Department, Bowling Green State University.

6.4.4.2 Hydraulic Properties

If the Finite Element Analysis is selected as method for Groundwater in project settings, the permeability of material need to be defined.

- A saturated permeability (K_s) must always be specified for a type of material. In this study, the permeability parameters are selected from van Genuchten Hydraulic models in Slide.
- Sand, Silty Clay and Silt materials are selected for the values of permeability from van Geneuchten Hydraulic parameters.
- Hydraulic Properties; K_s: 8.25e-5 (*Sand*-Soil_1_2), K_s: 6.95e-7 (*Silt*-Deep_Soil_1 and Deep_Soil_2), K_s: 5.5e-8 (*Silty Clay*-Soil_1_1 and Soil_2), Steps of the define hydraulic properties are as follows;

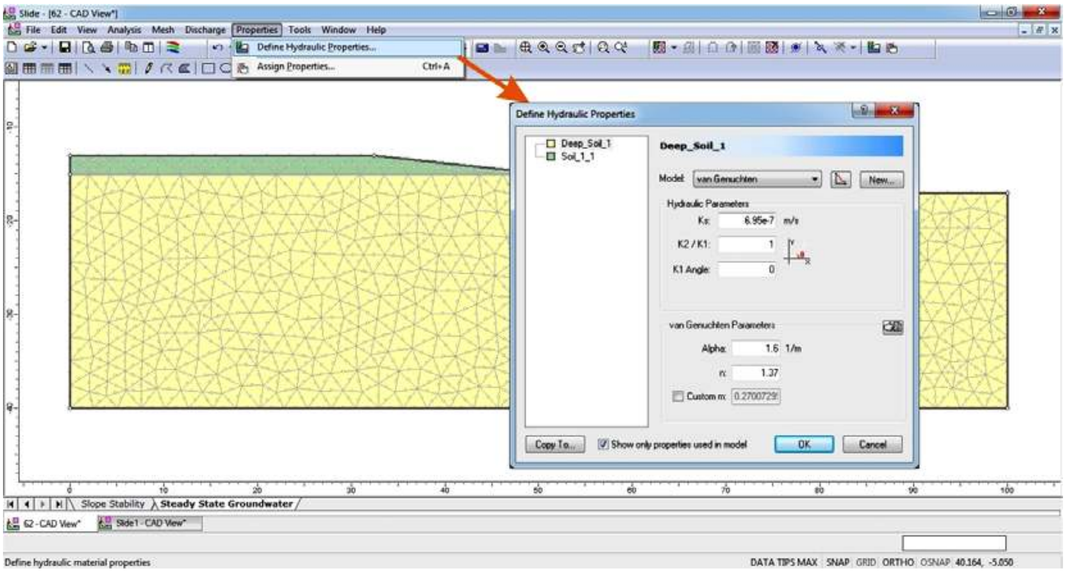

Figure 6.12 Define hydraulic properties in Slide

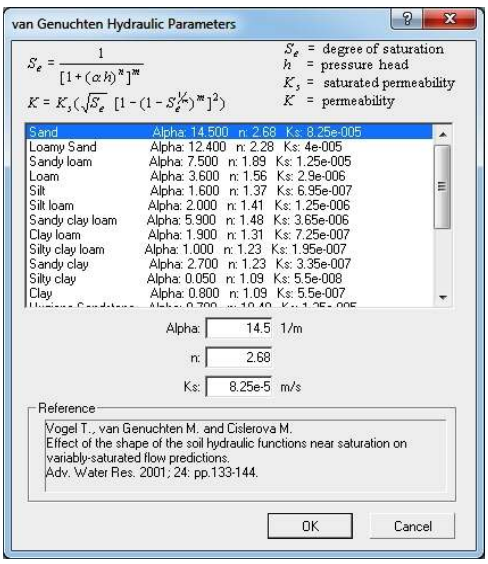

Figure 6.13 Van Genuchten hydraulic parameters

6.4.5 Loading

6.4.5.1 Water Load

In order to observe the effect of the sea water loading over slope stability, the mean sea level is taken at the depth of 0 m on the models. Then, the slope stability is investigated under the different sea water levels.

For submarine slope stability analysis, the ponded water load is used in modeling the mass of the water over the seafloor.

Select: Loading → Add Ponded Water Load

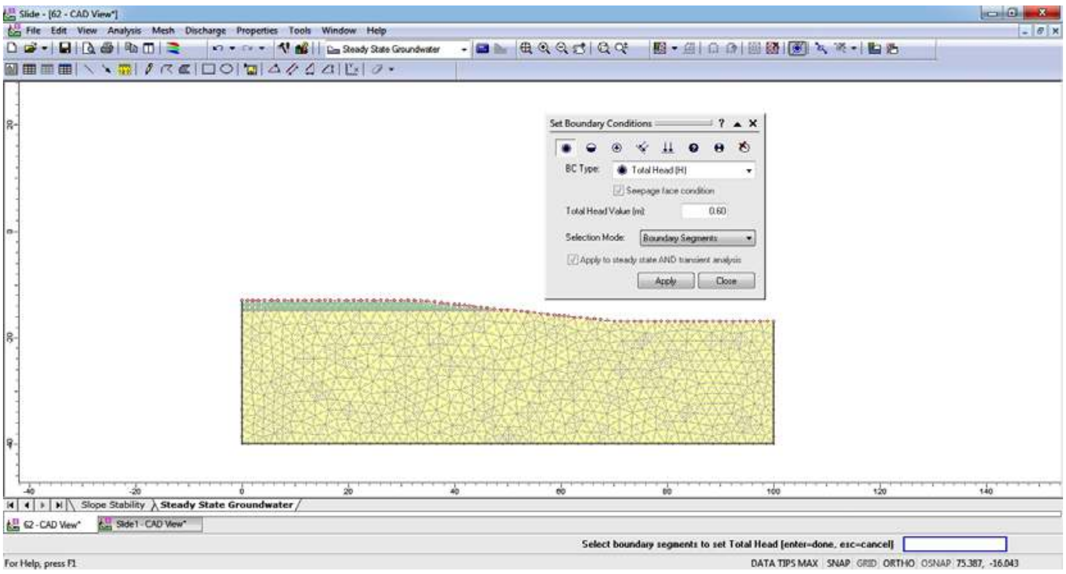

Figure 6.14 Entering total head for ponded water from set boundary conditions

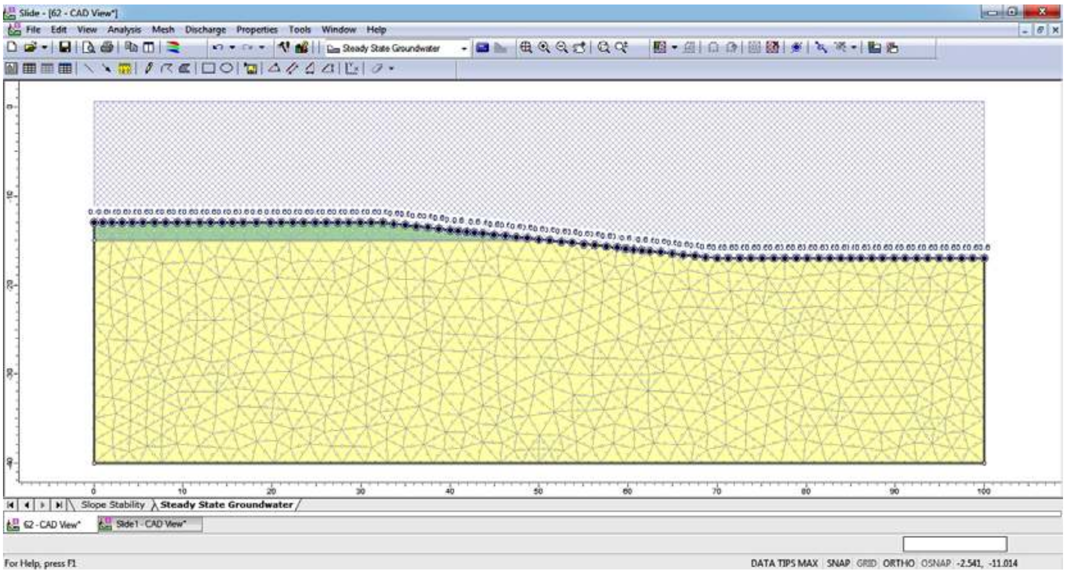

Figure 6.15 Added ponded water load to model

- Added Ponded Water Load; Orientation: Normal Boundary, Total Head: 0.

6.4.5.2 Seismic

In generally, typical values used in the slope analysis are in the range of 0.10 to 0.30 as suggested in Slide Tutorials. The seismic coefficients of **0.12 g and 0.23 g** are used for each slope analysis modeled in this study.

According to the Slide Tutorial, when a seismic coefficient is defined, an additional Body Force will be applied to each finite element mesh as follows:

Seismic Force = Seismic Coefficient * Body Force (due to gravity)
= Seismic Coefficient * (area of element * Unit Weight of element material)

Slide Tutorial stated "Body Force (due to gravity) is simply the self-weight of a finite element….The Seismic body force is vectorially added to the (downward) Body Force which exists due to gravity, to obtain the total body force acting on the element..."

Select: Loading → Seismic Loading

- Seismic Loading: Seismic Load Coefficient: * (Horizontal), Applied in Stage: 1. Seismic Loading steps are as follows;

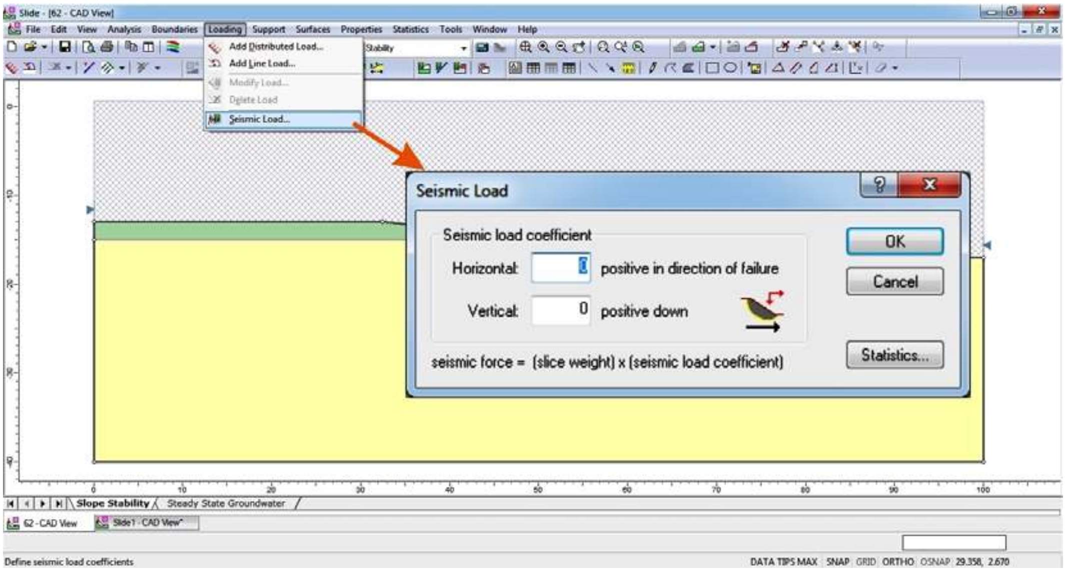

Figure 6.16 Seismic loading steps in Slide

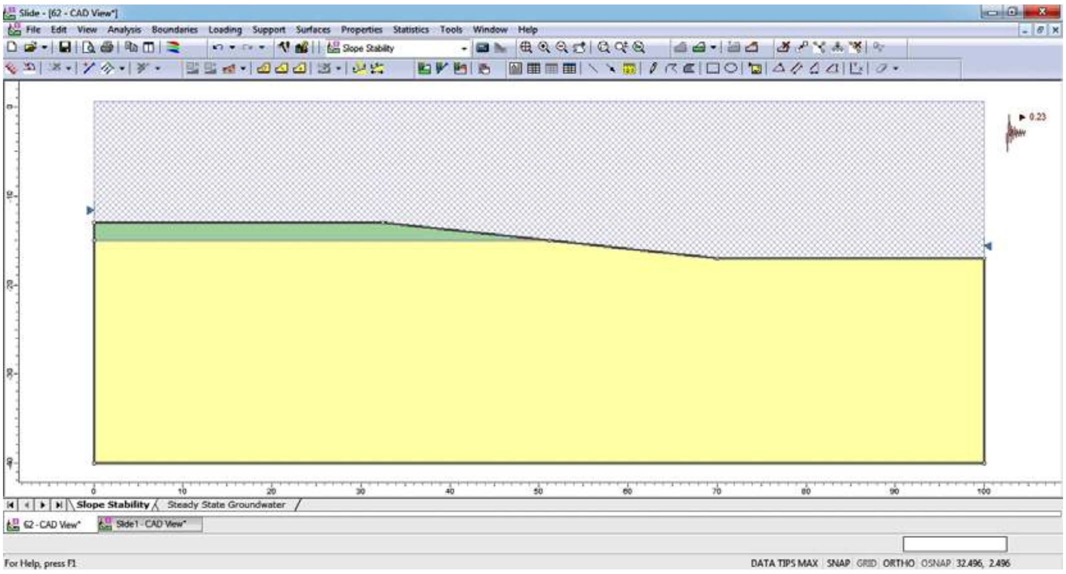

Figure 6.17 Seismic loading steps in Slide

6.4.6 Critical Slip Surface Search Methods

There are different critical slip surface search methods for circular and non-circular types of slip surfaces in Slide software. There are three search methods available for circular slip surfaces such as grid search, slope search, and auto refine search. Also there are two search methods available for non-circular slip surfaces. The manual of Slide software provides some guidelines for the selection of search method as given in Table 6.2.

Table 6.2 Guidelines for selecting a search method (Slide Tutorial, 2002)

Model	Search Methods
Homogeneous slope (1 Material)	Circular (Grid Search, Slope Search, or Auto Refine Search)
Multi-material model without well-defined weak layers	Circular Path Search Block Search
Model with well defined weak layer	Block Search Circular Search (with Composite Surfaces option turned on) Path Search

Moreover, Önalp &Arel (2004) defined three different rotational failure surface types such as slope failure, base failure and shallows failure according to slope angles, slope height and the properties of soil. In this study, rotational slip type is accepted slope failure for cohesive and soft clay.

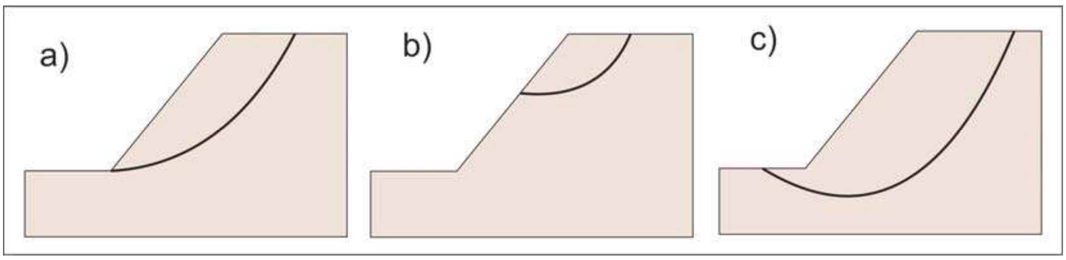

Figure 6.18 Slope failures of rotational slips; a) slope failure, b) shallow failure, c) base failure

Select: Surface Options

- Surface Options; Surface Type: Circular, Search Method: Grid Search, Grid Search Options: Composite Surfaces.

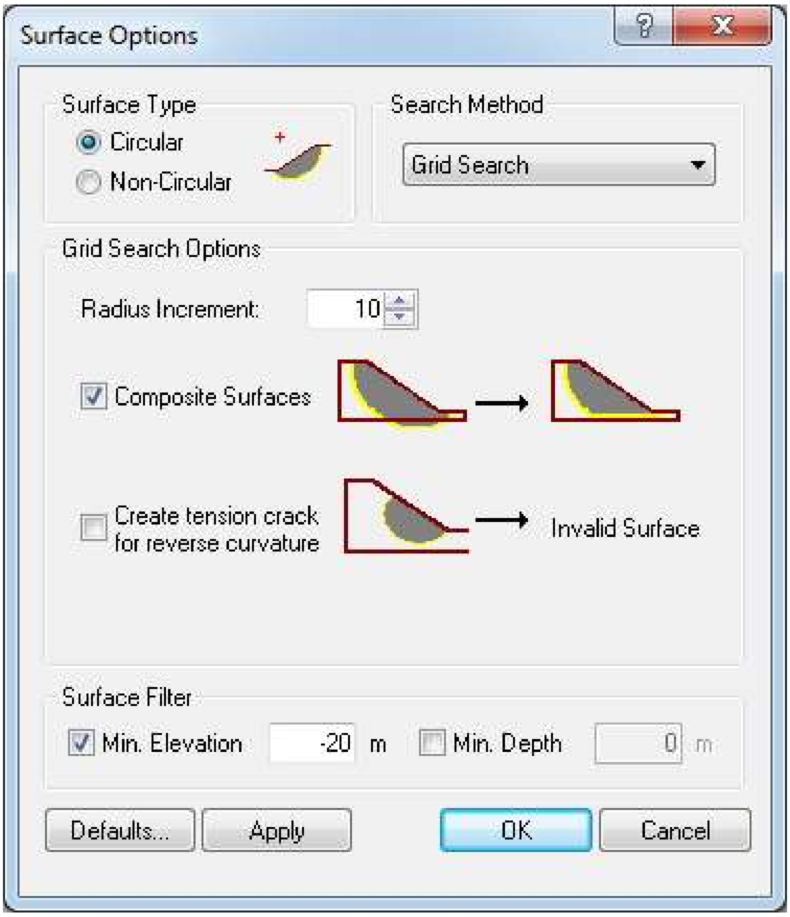

Figure 6.19 Surface options in Slide

6.5 The Results of Analysis

The safety factors obtained by hand calculation and Slide software, methods are compared using the topographic properties of Model_1 and the average soil values. Moreover, the slope stability analyses are done to investigate the relationship between with and without sea water loading using Slide software under different seismic loadings as shown in Figures 6.20 and 6.21. The analysis results are presented in Table 6.3.

Table 6.3 The results of the factor of safety obtained by software (with and without water loading) and hand (without water loading) calculation for Model_1

Calculation Methods	a=0	a=0.12	a=0.20	a=0.23
Software (With Water Loading, SWL=0 m)	6.28	1.79	1.11	0.97
Software (Without Water Loading)	2.49	1.314	0.98	0.89
Hand Calculation (Without Water Loading)	2.34	-	-	-

In order to test the accuracy of the model generated in Slide software, the hand calculation is done using analytical method. The factor of safety is calculated as **2.34** by Bishop method for Model_1 under without seismic and water loading conditions by the hand calculation. The slope angle is taken 15 degree, C_u=14.5 kPa and γ_n=17 kN/m^3 in slope stability analysis. The factor of safety (FS) value is obtained as **2.49** using the Slide software for the similar conditions and using the similar parameters.

In order to observe the effect of sea water loading over slope stability, the sea level are taken 0.0 m in the analyses. Analyses are done under the four different seismic conditions such as 0 g, 0.12 g, 0.20 g, and 0.23 g. The FS values of the analysis with sea water loading are found to be higher than the FS values of the slope analysis carried out without sea water loading. However, the FS values are observed to decrease with the increasing seismic loading. Also FS values of analysis both with and without water loading are very close to each other under a=0.23 g seismic loading.

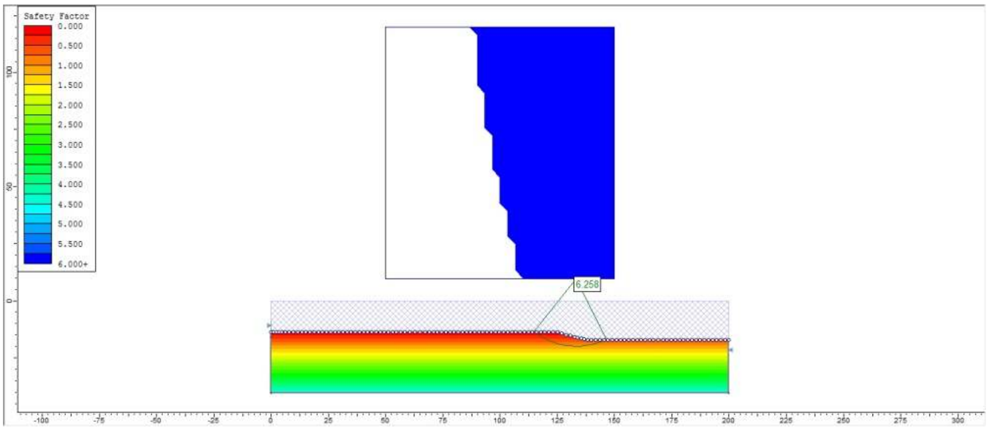

Figure 6.20 The slope stability with water loading in Slide

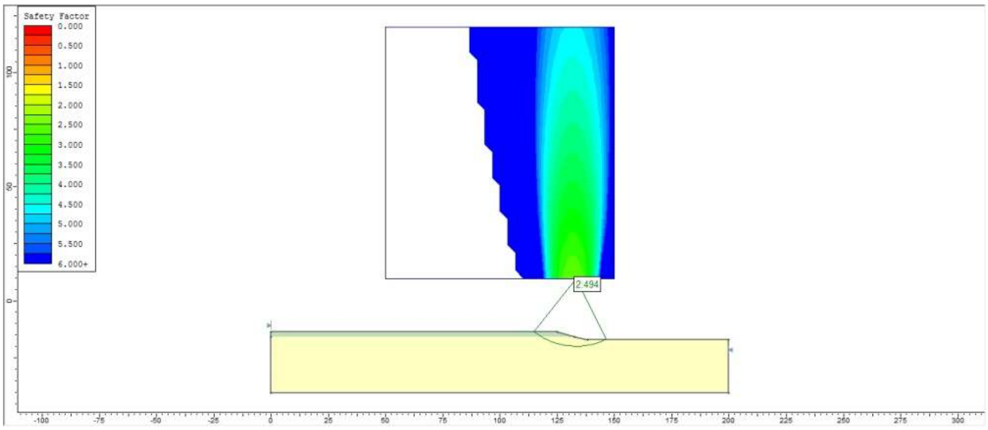

Figure 6.21 The slope stability without water loading in Slide

Additionally, slope stability analysis are also carried out taking the sea levels as -0.60, 0.0, and +0.60 m in relating the main sea level to observe the effect of sea water level changes over slope stability. Using sea level values are defined from the tide levels measured by General Command of Mapping (HGK) during the study period. For the different sea water levels, the slope stability analyses are carried out for Model_1 generated in order to investigate this balance situation. Pore-water pressure changes depending on the sea water levels are shown in Figure 23.

According to Capper & Cassine (1953), when the water loading is applied to the slope surface, the stability of slope increases. However, pore pressure also increases inside the soil depending on sea level rises, this reduces the stability of slope. As a result, there is a balance between pore pressure and water loading over slope stability as shown in Figure 6.22.

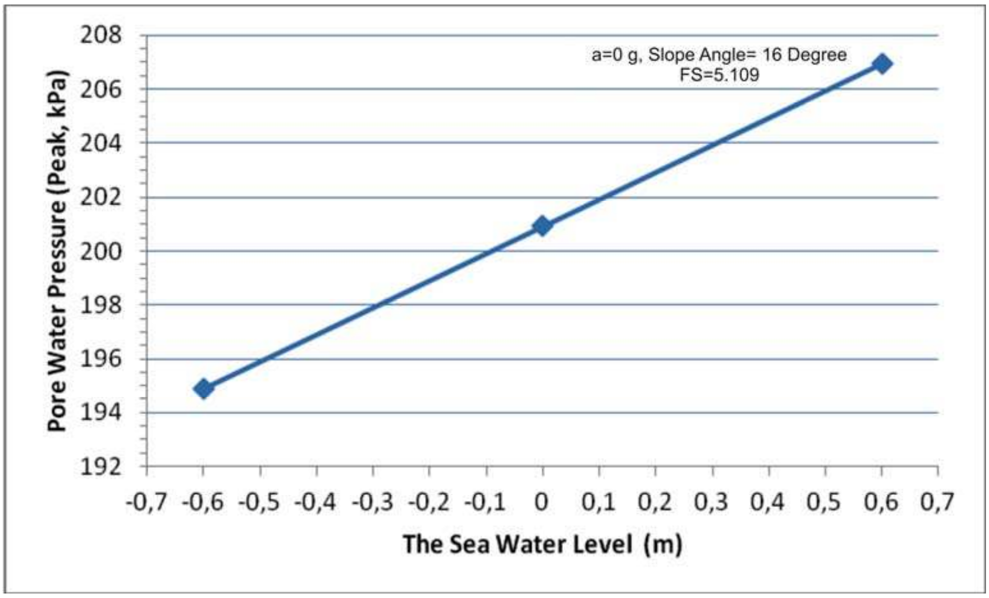

Figure 6.22 The relationship between pore water pressure and sea water level

Analysis shows that the sea water level changes are observed to be not effective over the factor of safety values. This is due to when the pore-water pressure increases when the water loading increases depending on the sea water level increase, and pore-water pressure reduces when the water loading reduces depending on the sea water level fall. Consequently, the equilibrium between the pore water pressure and the water loading remains fixed. The sea water level is taken as 0 m for the analysis of all models.

The analyses of models results

Dredging works on the navigation channel is planned to be gradually to 17 m depth in three different phases. The depth values of channel are defined as H_c=14 m, H_c=16 m, and H_c=17 m in these phases. The phases planned are shown in Figure 6.23. In this study, the slope stability analyses of the models generated are carried out for the different slope angles under the seismic loadings for last phase as H_c=17 m. The slopes are assumed to be stable when the factor of safety value is greater than or equal to 1.00 under the conditions defined.

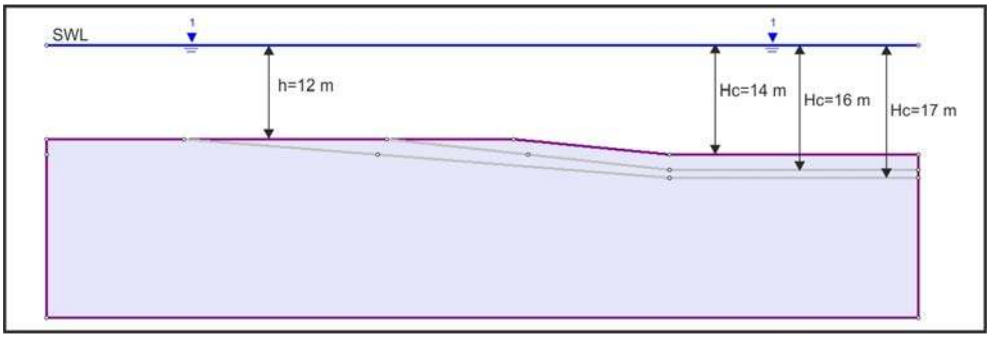

Figure 6.23 The phases of dredging works planned (Schematic)

For the Model 1, the used materials are Soil_1_1 (C_u=12.74 kPa and γ=16 kN/m^3) and Deep_Soil_1 (C_u=17.50 kPa and γ=18 kN/m^3) in the slope stability analysis. The value of critical FS and the optimum slope angle are computed as 1.001 and 13° respectively for a=0.23 g and H_c=17 m (Figure 6.24). The factor of safety values calculated by Slide is presented in Table 6.4 and 6.5. The changes in factor of safety are shown in Figure 6.32 and 6.33 with respect to the slope angles and the seismic loadings.

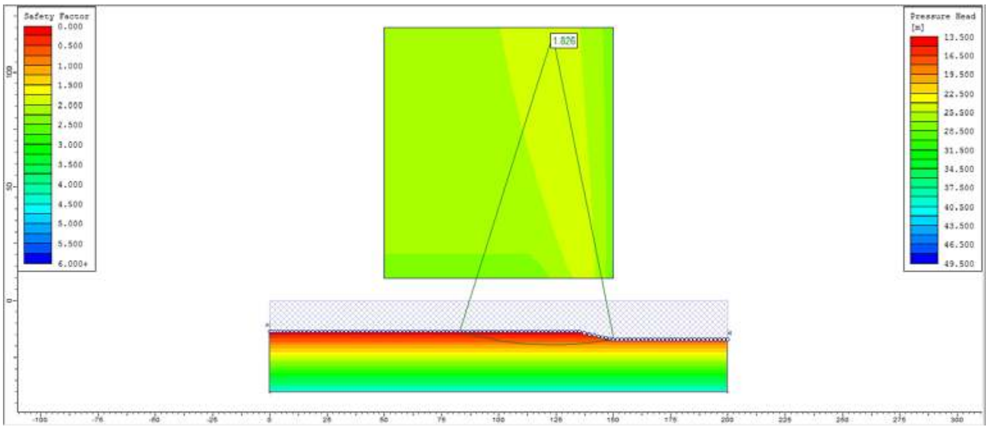

Figure 6.24 The critical slide surface of Model_1 in Slide for Hc=17 m, a=0.12 g and β=13

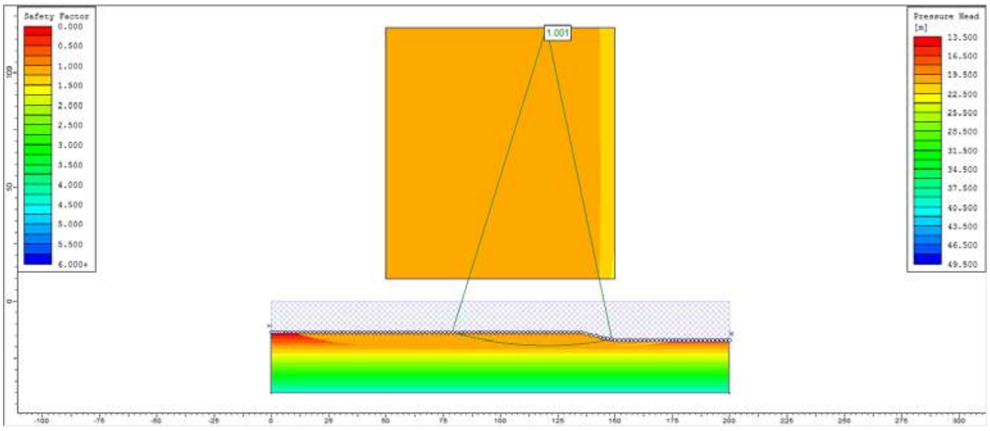

Figure 6.25 The critical slide surface of Model_1 in Slide for Hc=17 m, a=0.23 g and β=13

For the Model 2, the used materials are Soil_1_1 (C_u=12.74 kPa and γ=16 kN/m^3) and Deep_Soil_1 (C_u=17.50 kPa and γ=18 kN/m^3) in the slope stability analysis. The value of critical FS and the optimum slope angle are computed as 1.001 and 5° respectively under the conditions which is a=0.23 g and H_c=17 m (Figure 6.27). The factor of safety values calculated by Slide is presented in Table 6.4 and 6.5. The changes in factor of safety are shown in Figure 6.32 and 6.33 with respect to the slope angles and the seismic loadings.

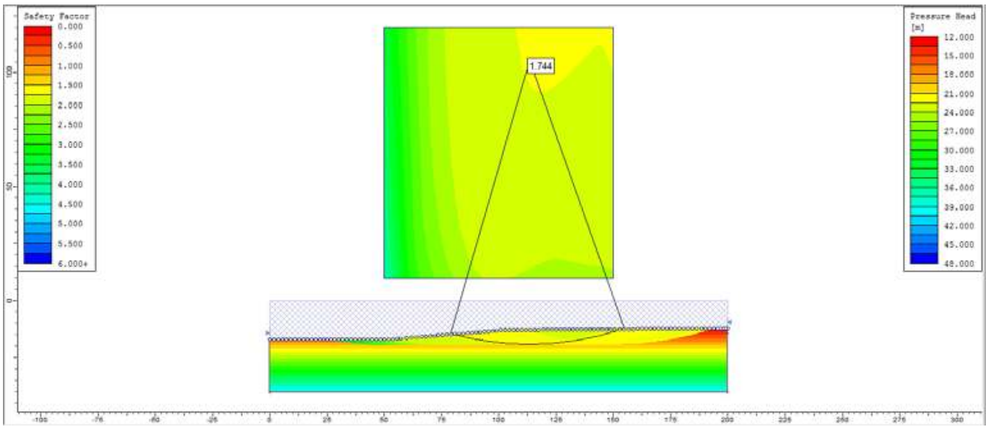

Figure 6.26 The critical slide surface of Model_2 in Slide for Hc=17 m, a=0.12 g and β=5°

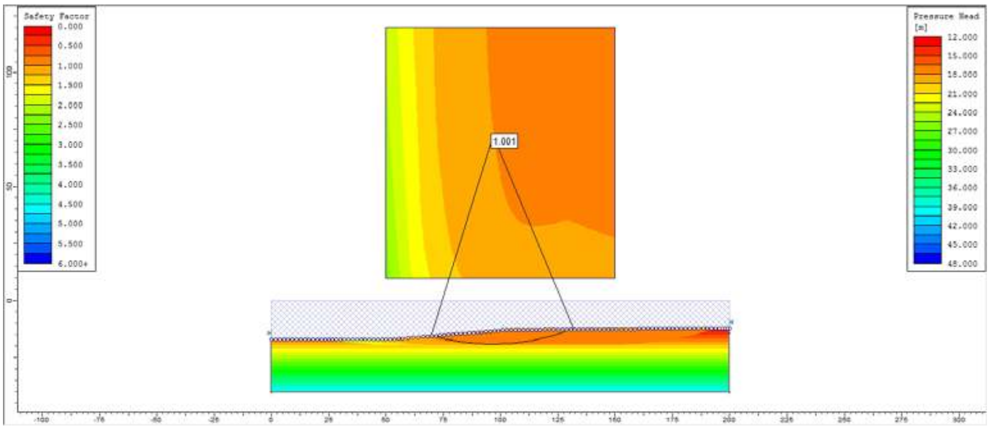

Figure 6.27 The critical slide surface of Model_2 in Slide for Hc=17 m, a=0.23 g and β=5°

For the Model 3, the used materials are Soil_2 (C_u=17.97 kPa and γ=16 kN/m^3) and Deep_Soil_2 (C_u=21 kPa and γ=18 kN/m^3) in the slope stability analysis. The value of critical FS and the optimum slope angle are computed as 1.00 and 9° respectively under the conditions which is a=0.23 g and H_c=17 m (Figure 6.29). The factor of safety values calculated by Slide is presented in Table 6.4 and 6.5. The changes in factor of safety are shown in Figure 6.32 and 6.33 with respect to the slope angles and the seismic loadings.

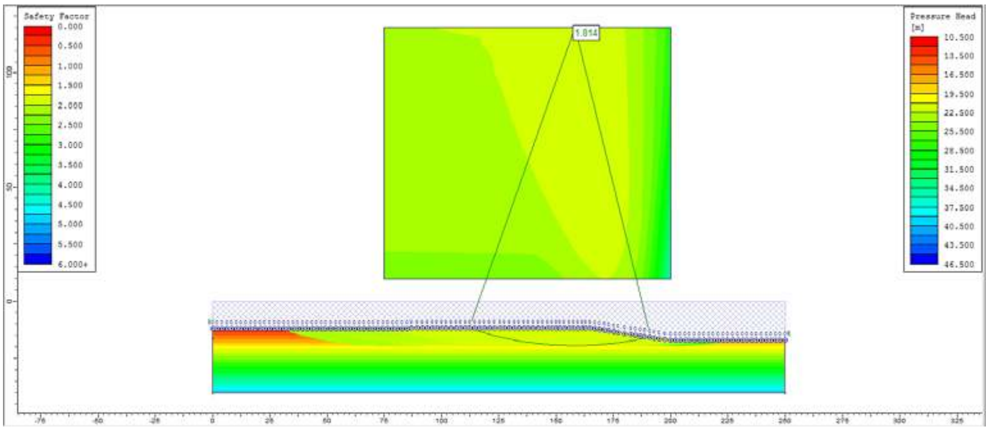

Figure 6.28 The critical slide surface of Model_3 in Slide for Hc=17 m, a=0.12 g and β=7°

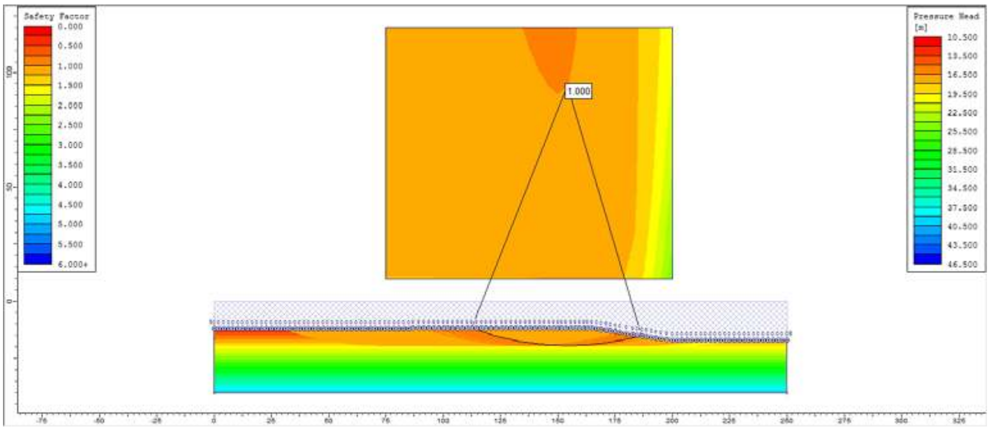

Figure 6.29 The critical slide surface of Model_3 in Slide for Hc=17 m, a=0.23 g and β=7°

For the Model 4, The used materials are Soil_2 (C_u=17.97 kPa and γ=16 kN/m^3) and Deep_Soil_2 (C_u=21 kPa and γ=18 kN/m^3) in the slope stability analysis. The value of critical FS and the optimum slope angle are computed as 1.004 and 7° respectively under the conditions which is a=0.23 g and H_c=17 m (Figure 6.31). The factor of safety values calculated is presented by Slide in Table 6.4 and 6.5. The changes in factor of safety are shown in Figure 6.32 and 6.33 with respect to the slope angles and the seismic loadings.

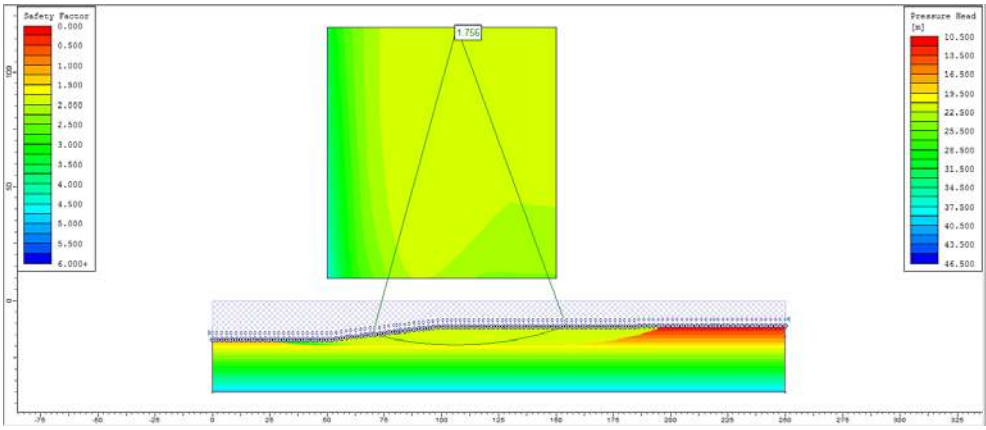

Figure 6.30 The critical slide surface of Model_4 in Slide for Hc=17 m, a=0.12 g and β=9°

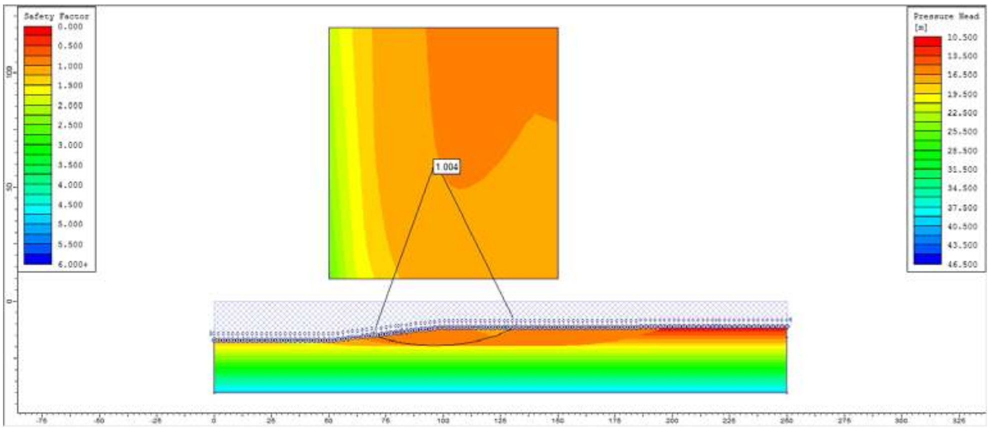

Figure 6.31 The critical slide surface of Model_4 in Slide for Hc=17 m, a=0.23 g and β=9°

Table 6.4 The factor of safety for models under seismic loading of 0.12 g

Slope Angle (β, Degree)	*For Seismic Loading of 0,12 g*			
	Model_1	**Model_2**	**Model_3**	**Model_4**
30	1,707	1,582	1,594	1,515
25	1,734	1,611	1,620	1,539
20	1,766	1,634	1,653	1,567
15	1,808	1,658	1,699	1,620
13	1,826	1,668	1,731	1,651
11	1,861	1,677	1,765	1,682
10	1,871	1,684	1,791	1,696
9	1,893	1,699	1,814	1,713
7	1,943	1,723	1,846	1,756
5	2,004	1,744	1,892	1,784
3	2,063	1,756	1,949	1,809
2	2,087	1,799	1,978	2,014

Table 6.5 The factor of safety for models under seismic loading of 0.23 g

Slope Angle (β, Degree)	*For Seismic Loading of 0,23 g*			
	Model_1	**Model_2**	**Model_3**	**Model_4**
30	0,925	0,862	0,878	0,841
25	0,941	0,873	0,898	0,865
20	0,962	0,886	0,920	0,901
15	0,989	0,908	0,948	0,937
13	**1,001**	0,920	0,960	0,952
11	1,021	0,942	0,972	0,965
10	1,026	0,956	0,988	0,973
9	1,036	0,969	**1,000**	0,985

Table 6.5 Cont.

7	1,056	0,981	1,013	**1,004**
5	1,078	**1,001**	1,027	1,018
3	1,092	1,014	1,046	1,038
2	1,109	1,039	1,077	1,075

The optimum angles of slopes are determined as 13° for Model_1, 5° for Model_2, 7° for Model_3 and 9° for Model_4 for H_c=17.0 m and a=0.23 g. The obtained safety slope positions are shown in Figure 6.37.

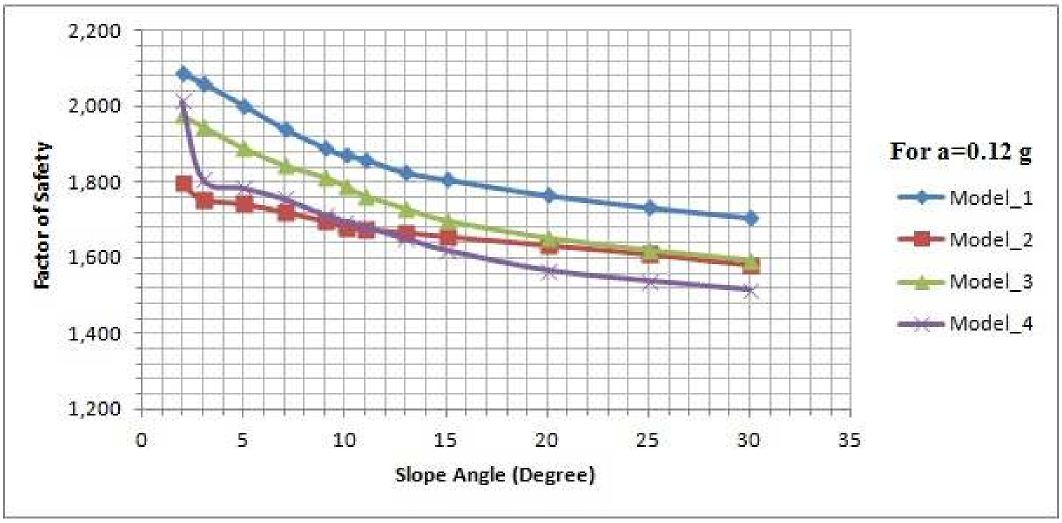

Figure 6.32 The graph of the factor of safety values calculated for all models under seismic loading of 0.12 g

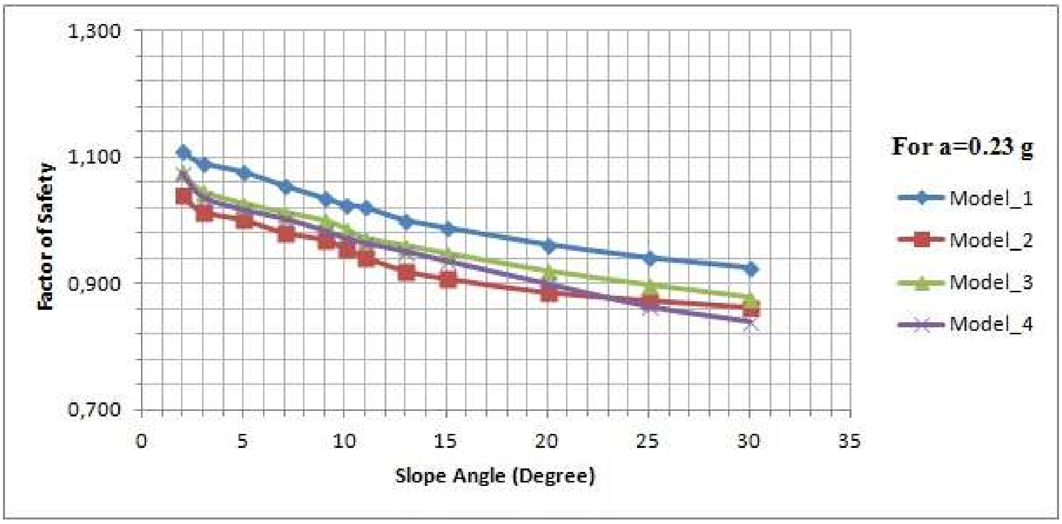

Figure 6.33 The graph of the factor of safety values calculated for all models under seismic loading of 0.23 g

As seen Figure 6.34, when the inclination of topography on the top of slope is high, the stability of slope reduces. But, when the inclination of topography on the top of slope reduces, the stability of slope increases, and the higher factor of safety values are observed.

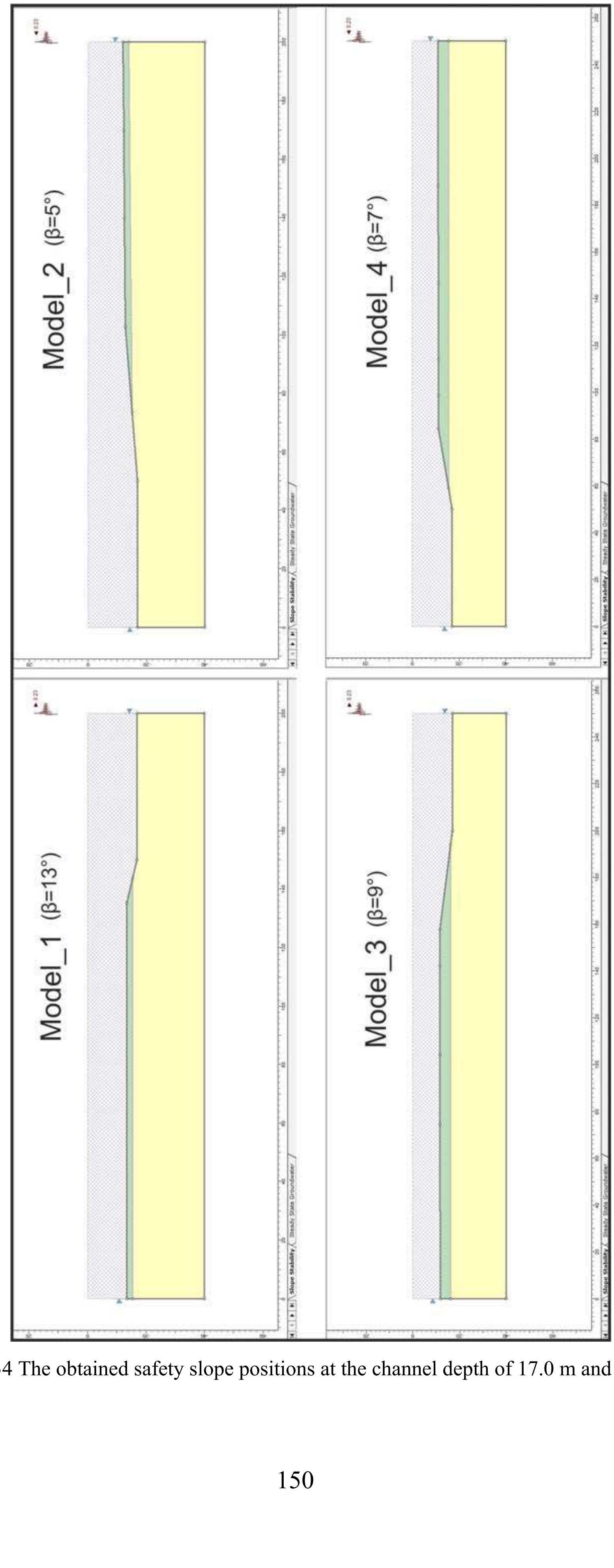

Figure 6.34 The obtained safety slope positions at the channel depth of 17.0 m and a=0.23

CHAPTER SEVEN
CONCLUSION AND RECOMMENDATIONS

This study is carried out to observe the actual situation of the navigation channel and to determine the optimum slope angles before dredging works. Within the scope of this thesis study, the survey and measurements performed, and the results of this studies are presented as follows;

1. The surface soil samples (K1-12) are taken by Grab from different twelve locations in the first and second study lines on the navigation channel. The geotechnical and geological properties of the soil samples such as water content, specific gravity, Atterberg limits and liquidity index, particle size distribution, classification of soil and unrdained shear strength are investigated.

   a) According to particle size distribution of the surface soil samples taken, K1 sample is classified as shell silty sand “SM”, K2-3 samples are classified as shell medium plasticity organic clayey silt “MIO”, and K6-12 samples are classified as shell high plastic organic clayey silt “MHO”.

   b) The sediment distribution map is generated from the test results. As seen from the sediment distribution map, clay contents and plasticity ratio of soil is observed to increase towards Alsancak port from Yenikale gateway. Also a heterogeneous distribution of the surface sediment is observed in İzmir bay.

   c) In order to determine undrained shear strength values of surface soil samples, Fall Cone for K2-12 soil samples and Shear Box test for K1 soil sample are carried out. In fall cone test, undrained shear strength values of K2-12 soil samples are defined between 0.04 and 0.60 kg/cm^2. In shear box test, the coefficient of cohesive is assumed to be zero, and internal friction angle of K1 soil sample is defined 23.5°.

d) In the slope stability analyses, two different soil layers are defined in the generated models. Undrained shear strength values of surface soil layer are defined as 12.74 kPa for the first line and 17.97 kPa for the second line. Also undrained shear strength values of deep soil layer are assumed as 17.50 kPa for the first line and 21 kPa for the second line. The shear strength values of the deep soil layers are taken from Kayalar (1985).

2. Hydrographical and Oceanographic works are carried out to reveal the actual bathymetric properties of navigation channel and to generate models in the slope stability analysis.

a) In oceanographic works, the velocity of sound value of sea water is measured as 1518 m/s which is later used by Echo-Sounder in the bathymetric work.

b) Within the scope bathymetric work, the analog records are taken from Echo-Sounder. The position of the navigation channel is aimed to determine using these analog records. According to these records, the bottom widths of the actual navigation channel are observed to be 80 m for the first line and 180 m for the second line.

c) Bathymetric maps are generated for the profiles defined in the first and second lines. In the bathymetric map of the profile in the first line, the minimum depth value is -3.50 m and the maximum depth value is -16.0 m. Also the depth values decrease and the density of contour lines increases towards the north side of the profile. In the bathymetric map of the profile in the second line, the minimum depth value is -10.0 m and the maximum depth value is -12.0 m. Also the depth values and density of contour lines changes (decrease) in a similar rate for both the north and south of the profile.

d) According to the inclination maps generated, the inclination values are found between 0.5° and 6° for the profile in the first line. The inclination values are between 0° and 1° for the profile in the second line. Moreover, the inclination maps are supported with the vector maps generated.

e) The cross sections of A-B and C-D are taken from the bathymetric maps to model in Slide software.

3. The current regime of Izmir bay is measured at two different depths such as the surface and the depth of -10.0 m by IMST (2012). The measured values are observed to be 5-7 cm/s for both two depths. However, it is also noted that the surface currents may increase up to 15 cm/s with effect of the wind. The directions of the surface currents and current at -10.0 m water depth are observed to be different from each other with modeling studies. Also the current velocities are observed to decrease towards Alsancak port, and this situation affects to the distribution of surface sediments.

4. Tide values measured by General Command of Mapping are used to determine reduced depth values in the result of the bathymetric studies. According to tide changes during the study period, the maximum sea level is +0.60 m and the minimum sea level is +0.05 m with respect TNVCN datum. Also the change of the maximum sea level is observed as 0.80 m in the previous tide measurement studies.

5. The seismic accelerations are calculated depending on the earthquake magnitudes (M) and the distances (R) of the important earthquakes occurred in the past. The calculated seismic accelerations are defined as 0.12 g and 0.23 g in the analysis. In the result of the analyses show that, the stability of slopes are observed to decrease depending on the increased seismic accelerations.

6. The slope stability analyses are carried out for four different models called as Model_1, Model_2, Model_3 and Model_4.

a) In the submarine slope stability analysis, the effect of sea water level changes due to tidal is considered for Model_1. Analysis shown that the sea water level changes are observed to be not effective over the factor of safety values.

b) The slope stability analysis of navigation channel are carried out for the depth of channel as H_c=17, and two seismic loadings as a=0.12 g and a=0.23 g using Slide software. The methods used are Bishop Simplified, GLE-Morgenstern-Price and Spencer in Slide.

c) When the seismic loading is 0.12 g, the slopes of channel is stable for whole the depths of channel. However, when the seismic loading increases, the stability of slopes fall. According to the results of analysis under the seismic loading of a=0.23 g,

At the depth of channel of H_c=17 m, the safe slope situations are presented as follows;

For Model_1, FS=1.001, β=13°
For Model_2, FS=1.001, β=5°
For Model_3, FS=1.000, β=9°
For Model_4, FS=1.004, β=7°

d) The inclination of topography on the top of slope is observed to negatively affect to the slope stability.

Finally, the stability of slopes of navigation channel is analyzed, and the optimum slope angles are defined under seismic loads. In the future studies, the modeling studies are supported with drillings and seismic cross-sections to increase the precision of the models generated, and the slope analysis should be carried out using numerical solutions taking into account dynamic conditions as sea water wave load and seismic load for the more detailed works.

REFERENCES

Aksu, A. E., Yaşar, D., & Uslu, O. (1998). Assessment of marine pollution in İzmir Bay: Heavy metal and organic compound concentrations in surface sediments, *Turkish Journal of Engineering and Environment Science, 22*, 387-415.

Albataineh, N. (2006). *Slope stability analysis using 2D and 3D methods*, M.Sc. Thesis, The Graduate Faculty of The University of Akron, United State America.

American Society for Testing and Materials, [ASTM], (2004). Annual Book of ASTM Standards Construction: Soil and Rock, 4, American Society of Testing and Materials Publication.

Bayraktar, S. (2000). *Improving of materials dredged from İzmir Alsancak port-navigation channel*, Final Thesis, Graduate School of Natural and Applied Sciences, Dokuz Eylül University, Izmir.

Bowditch, LL. D. N. (2002). *The American practical navigator* (2002 ed.). United Stated America: National Imagery And Mapping Agency.

British Standards, [BS], (1990). Methods of test of soils for civil engineering purposes, *British Standard: BS 1377*.

Capper, P. L., & Cassine W. F. (1953). *The mechanics of engineerings*, England: E. & F. N. Spon Limited

Chaney R. C., & Demars K. R. (1985). *Strength testing of marine sediments*, San Diego: American Society of Testing and Materials Publication.

Coşkun, S. (2009). *The investigation of multi-beam three dimensional bathymetry map and shallow sedimentary structures of İzmir bay*, M.Sc. Thesis, Institute of Marine Sciences and Technology, Graduate School of Natural and Applied Sciences, Dokuz Eylül University, Izmir.

Çalımcı, M. (1996). *Within the scope of the sea fills, laboratory research of lime stabilization geotechnics of the bottom soils in the front of İzmir port*, M.Sc. Thesis, Institute of Marine Science and Technology, Dokuz Eylül University, İzmir.

Dean, R.G., & Dalrymple R.A. (1984). *Water wave mechanics for engineers and scientists*, London: World Scientific Publishing.

Dokay Engineering. (2013). *Gulf of İzmir and İzmir port rehabilitation project, environmental impact assessment report*, Ankara.

Ekiz, T. (2005). *The meaning of seismological and earthquake source properties of İzmir*, M.Sc. Thesis, Graduate School of Natural and Applied Sciences, Dokuz Eylül University, Izmir.

Ergin, A. (2009). *Coastal engineering,* Ankara, Turkey: Middle East Technical University Press.

Feeley, K. (2007). *Triggering mechanisms of submarine landslides*, Research Report, Department of Civil and Environmental Engineering, Northeastern University, Massachusetts, Boston.

Giardini, D., Grünthal, G.,Sheldlock, K. M., & Zhang, P. (1999). The GSHAP global seismic hazard map, *Annali Di Geofisica, 42, (6).*

Gitirana, Jr. G. F. N. (2005). *Weather-related geo-hazard assessment model for railway embankment stability*, P.hD. Thesis. University of Saskatchewan, Saskatoon, SK, Canada.

Global warming. (n.d.). Retrieved March 5, 2013, from http://hyperphysics.phy-astr.gsu.edu/hbase/thermo/grnhse.html#c5

Göktürkler, G. (2002). *Three-dimensional simulation of seismic wave propagation in the metropolitan area of İzmir*, P.hD. Thesis, Graduate School of Natural and Applied Sciences, Dokuz Eylül University, Izmir.

Hance, J. J. (2003). *Development of a database and assessment of seafloor slope stability based on published literature*. M.Sc. Thesis, Department of Civil Engineering, The University of Texas at Austin, United State America.

Hansbo, S. (1957). A new approach to the determination of the shear strength of clay by the fall-cone test, *Proceeding of The Royal Swedish Geotechnical Institute, 14*

Hendersen, S. M. (2002). *Surf beat forcing and dissipation*, P.hD. Thesis, Department of Oceanograph, Dalhouse University, Halifax, Nova Scotia.

Houlsby, G. T. (1982). Theoretical analysis of the fall-cone test, *Geotechnical, 32*, (2), 111-118.

Institute of Marine Sciences and Technology. [IMST], (1985). *Bathymetry and geology sites of oceanography and marine discharge survey of İzmir bay*, Institute of Marine Sciences and Technology, Dokuz Eylül University, İzmir, Turkey.

Introduction to storm surge. (n.d.). Retrieved March 11, 2013, from http://www.nhc.noaa.gov/ssurge/surge_intro.pdf

Karahan, H. (1988) *Modelling the current of coast and bay, and an application for İzmir bay,* P.hD. Thesis, The Department of Environment Engineering, Graduate School of Natural and Applied Sciences, Dokuz Eylül University, Izmir.

Kayalar, A. Ş., Yılmaz, R., Duman, Ş., Erdemirci, M., Arısoy, Y., & Özer, Y. (1985). *İzmir Alsancak port extension project-Geomorphological surveys of dredging areas*, The Report of Soil Tests, Civil Engineering Department, Dokuz Eylül University, İzmir.

Kaya, O. (1999). Ground structure of İzmir and environment*, Geotechnical Problems of İzmir and Environment Symposium Papers,* 1-4.

Koca, M. Y., & Yılmaz, H. R. (1999). Statistical assessment of basic parameters of beach road ground soil and the actual soil profile on the sea bottom between Gümrük-Üçkuyular (İzmir), *Dokuz Eylül University, Faculty of Engineering, Journal of Science and Engineering, 1*, (3), 29-46. İzmir.

Koumoto, T., & Houlsby, G. T. (2001). Theory and practice of the fall cone test, *Geotechnique, 51*, (8), 701-712.

Krahn, J. (2004). *Stability modelling with Slope/W* (1th ed.), Canada: GEO-SLOPE/W International Ltd.

Natarajan, M., Mohan, K., & Balasubramanian. (n.d.). *Waves and tides*. Retrieved March 5, 2013, from http://ocw.unu.edu/international-network-on-water-environment-and-health

Nave, C. R. (2012). *HyperPhysics*, Georgia State University, Retrived March 18, 2013 from http://hyperphysics.phy-astr.gsu.edu/hbase/hframe.html

Ocakoğlu, N., Demirdağ, E., & Kuşcu, İ. (2004). Neotectonic structures in the area offshore of Alaçatı, Doğanbey and Kuşadası (western of Turkey): Evidence of strike–slip faulting in the Aegean extensional province. *Tectonophysics, (391)*. 67-83.

Okşan, E. (2001). *Improving of materials dredged from İzmir Alsancak port-navigation channel*, M.Sc. Thesis, Graduate School of Natural and Applied Sciences, Dokuz Eylül University, Izmir.

Önalp, A. (2002). *Geotechnical information-1:Soils and mechanism with solvable problems*, (2th ed.), İstanbul: Birsen Press.

Önalp, A., & Arel, E. (2004). *Geotechnical information-II: Engineering of slopes*, İstanbul: Birsen Press.

Öncel, A. O. (2007). *Marmara and tsunami*. Retrieved March 11, 2013, from http://faculty.kfupm.edu.sa/ES/oncel/marmaratsunami.htm

Prentiss, D. (n.d.) *A map showing the distribution of volcanic structures on the earth's surface*. Retrieved March 20, 2013 from http://www.geog.ucsb.edu/~dylan/mtpe/geosphere/wh/vol/volcanoes.html

Raaijmakers, T. (2005). *Submarine slope development of dredging trenches and channels*, Final Thesis Report, Delft University of Technology.

Sawaragi, T. (1995). *Coastal engineering-waves, beaches, wave-structure iteractions*, Amsterdam, New York: Elsevier.

Slide Tutorial (n.d.). Retrived July 12, 2013, from http://www.rocscience.com/help/slide/webhelp/tutorials/Slide_Tutorials.htm

Sonuvar, B. (2004). *The engineering geology and the ground improvement studies of İzmir bay approaching channel and Konak-Halkapınar coast*, M.Sc. Thesis, Graduate School of Natural and Applied Sciences, Dokuz Eylül University, Izmir.

Storm surge overview. (n.d.). Retrieved March 11, 2013, from http://www.nhc.noaa.gov/surge

The millennium ecosystem assessment overview. (n.d.). Retrieved March 12, 2013, from http://www.millenniumassessment.org/en/GraphicResources.aspx

The Ministry of Transportion, Navigation and Communication, [MTNC], (1992). *The report related to dredging works of İzmir port*.

Turkish Standards Institution, [TSI], (2000). *Classification of soil for civil engineering purposes*, Ankara:TSI Publication.

Ulu, A. (2006). *The importance of bathymetrical and seismic surveys in dredging works*, M.Sc. Thesis, Institute of Marine Science and Technology, Graduate School of Natural and Applied Sciences, Dokuz Eylül University, İzmir.

United State Army Corps of Engineers. [USACE], (2003). *Engineering and design slope stability, engineer manual*, Department of The Army, United State Army Corps of Engineers Washington.

Uslu, O., & Saner, E. (1987). Modelling of pollutant transport and dispersion in the marine environment, The Ministry of Environment and Urbanism of The Republic of Turkey, *Environment*, (3), 9-14.

Wood, D. M. (1985). Some fall-cone tests, *Geotechnique, 35*, (1), 64-68.

Yalçın, İ. A. (2008). *A geotechnical earthquake engineering investigation for soils of south eastern coast of İzmir bay*, M.Sc. Thesis, Graduate School of Natural and Applied Sciences, Dokuz Eylül University, Izmir.

Yıldız, B. (2004). *Historical backround of İzmir port's approaching channel problem propositions to its solution to make more efficient the port*, M.Sc. Thesis, Graduate School of Natural and Applied Sciences, Dokuz Eylül University, Izmir.

Yıldız, H., Demir, C., Gürdal, M. A., Akabalı, O. A., Demirkol, E. Ö., Ayhan, M. E., & Türkoğlu, Y. (2003). Analysis of sea level and geodetic measurements of Antalya-II, Bodrum II, Erdek and Menteş tide gauges in the period of 1984-2002, *Map Bulletin*, Retrieved June, 2012, from General Command of Mapping.

Yüksel Project. (2012). *Gulf of İzmir and İzmir port rehabilitation project and geotechnical report of port navigation channel, maneuver division, port basin, II. part container ground and circulating channel*, Ankara, Turkey.

Zhu, T. (n.d.). *Some useful numbers on the engineering properties of materials (geologic and otherwise)*, GEOL 615 Lecture Notes, Department of Geophysics, Stanford University, United State America. Retrieved July 18, 2013, from http://www.stanford.edu/~tyzhu/Documents/Some%20Useful%20Numbers.pdf

Zreik, D. A. (1991). *Determination of the undreined shear strength of very soft cohesive soils by a new fall cone apparatus*, M.Sc. Thesis, Department of Civil Engineering, Massachusetts Institute of Technology, United State America.